博士√/ 硕士□研究生成果佐证材料

培养单位：生物与农业工程学院

学　　号：2018451033

姓　　名：苑恒轶

导师姓名：任露泉

学　　科：仿　生

（一）发表学术论文：

1. **Hengyi Yuan**, Yi Li, Zhihui Qian*, Lei Ren* and Luquan Ren. A Piezoresistive Sensor with High Sensitivity and Flexibility Based on Porous Sponge. Nanomaterials, 2022, 12: 3833. (SCI 检索，IF：5.719，Q1)

2. Chi Ma, Bing Zhu, Zhihui Qian, Lei Ren, **Hengyi Yuan**, Yunbao Meng. 3D-printing of conductive inks based flexible tactile sensor for monitoring of temperature, strain and pressure. Journal of Manufacuring Processes, 2023,87:1-10.（SCI 检索，IF：6.1，Q1）

3. Bing Zhu, Chi Ma, Zhihui Qian, Lei Ren, **Hengyi Yuan**. Highly stretchable and sensitive multimodal tactile sensor based on conductive rubber composites to monitor pressure and temperature, Polymers, 2022,14,1294.（SCI 检索，IF：4.7，Q1）

（二）已授权专利：

1. 发明专利

1.**苑恒轶**，邢进，吕恕位等. 一种新型仿生机械的行走机构. 中国：ZL201910245645.4，2024.03.08

2.**苑恒轶**，邢进，张庆芳等. 一种仿生捕鱼器及其控制方法. 中国：ZL201910043907.9，2021.11.05

2. 实用新型专利

苑恒轶，邢进，于海跃等. 一种可调节的仿生微纳柔性触觉传感器用固定装置. 中国：ZL201922165259.2，2020.05.22

报告编号：**L24U2022-670**

检　索　报　告

一、检索要求

1. 委 托 人：苑恒轶
2. 委托单位：吉林大学
3. 检索目的：论文被 SCI-E 数据库收录及所在期刊影响因子、分区情况

二、检索范围

Science Citation Index Expanded (SCI-EXPANDED)	1975-present	网络版
Web of Science	1975-present	网络版
JCR-(Journal of Citation Report)	2021	网络版

三、检索结果

委托人提供的 1 篇论文被 SCI-E 数据库收录，收录及所在期刊影响因子、分区情况见附件一。

特此证明！

东北师范大学科技查新咨询中心

教育部科技查新工作站（L24）

（盖　章）

检索报告人：李海斌

2022 年 12 月 7 日

附件一：论文被 SCI-E 数据库收录及所在期刊影响因子、分区情况

标题: A Piezoresistive Sensor with High Sensitivity and Flexibility Based on Porous Sponge

作者: Yuan, HY (Yuan, Hengyi); Li, Y (Li, Yi); Qian, ZH (Qian, Zhihui); Ren, L (Ren, Lei); Ren, LQ (Ren, Luquan)

来源出版物: NANOMATERIALS **卷:** 12 **期:** 21 **文献号:** 3833 **DOI:** 10.3390/nano12213833 **出版年:** NOV 2022

Web of Science 核心合集中的 "被引频次": 0

被引频次合计: 0

摘要: Chemical plating has recently been employed for the preparation of flexible piezoresistive sensors; however, plating solutions and processes that affect the sensitivity still need further exploration. In the study, a sponge-based flexible sensor with copper as its conductive material is prepared using electroless plating. The variation in sponge resistance and sensitivity changes with different plating times are studied. It is found that, with the increasing plating time, the conductivity increases and the resistance of sample will decrease. Moreover, the range of resistance difference will decrease under compression, thus the sensitivity decreases. Furthermore, the sensor's applications were assessed, verifying the practicability of the developed preparation method. This study may bring ideas for the new development of flexible pressure sensors.

入藏号: WOS:000881497400001

PubMed ID: 36364609

语言: English

文献类型: Article

作者关键词: flexible piezoresistive sensor; porous structure; high sensitivity; electroless plating process

KeyWords Plus: STRETCHABLE CONDUCTORS; POLYURETHANE SPONGE; CARBON NANOTUBES; COPPER NANOWIRES; TRANSPARENT; FABRICATION; COMPOSITE; FOAMS

地址: [Yuan, Hengyi; Qian, Zhihui; Ren, Lei; Ren, Luquan] Jilin Univ, Key Lab Bion Engn, Changchun 130022, Peoples R China.

[Yuan, Hengyi; Li, Yi] Jilin Engn Normal Univ, Sch Mech & Vehicle Engn, Changchun 130052, Peoples R China.

[Ren, Lei] Univ Manchester, Sch Mech Aerosp & Civil Engn, Manchester M13 9PL, Lancs, England.

通讯作者地址: Qian, ZH; Ren, L (通讯作者), Jilin Univ, Key Lab Bion Engn, Changchun 130022, Peoples R China.

Ren, L (通讯作者), Univ Manchester, Sch Mech Aerosp & Civil Engn, Manchester M13 9PL, Lancs, England.

电子邮件地址: zhqian@jlu.edu.cn; lei.ren@manchester.ac.uk

Affiliations: Jilin University; Jilin Engineering Normal University; University of Manchester

出版商: MDPI

出版商地址: ST ALBAN-ANLAGE 66, CH-4052 BASEL, SWITZERLAND

Web of Science Index: Science Citation Index Expanded (SCI-EXPANDED)

Web of Science 类别: Chemistry, Multidisciplinary; Nanoscience & Nanotechnology; Materials Science, Multidisciplinary; Physics, Applied

研究方向: Chemistry; Science & Technology - Other Topics; Materials Science; Physics

IDS 号: 6B7GN

eISSN: 2079-4991

29 字符的来源出版物名称缩写: NANOMATERIALS-BASEL

ISO 来源出版物缩写: Nanomaterials

来源出版物页码计数: 13

基金资助致谢:

基金资助机构	授权号
National Natural Science Foundation of China	52175270
Project of Scientific and Technological Development Plan of Jilin Province	20220508130RC

This research was supported by the project of National Natural Science Foundation of China (No. 52175270, Zhihui Qian) and the Project of Scientific and Technological Development Plan of Jilin Province (No.20220508130RC, Zhihui Qian).

开放获取: Green Published, gold

Impact factor & JCR分区(2021):

NANOMATERIALS

期刊影响因子™

2021	五年
5.719	5.81

JCR 学科类别	类别排序	类别分区
CHEMISTRY, MULTIDISCIPLINARY *其中SCIE 版本*	55/179	Q2
MATERIALS SCIENCE, MULTIDISCIPLINARY *其中SCIE 版本*	109/345	Q2
NANOSCIENCE & NANOTECHNOLOGY *其中SCIE 版本*	53/109	Q2
PHYSICS, APPLIED *其中SCIE 版本*	37/161	Q1

来源: Journal Citation Reports 2021. 进一步了解

The End

nanomaterials

MDPI

Article

A Piezoresistive Sensor with High Sensitivity and Flexibility Based on Porous Sponge

Hengyi Yuan [1,2], Yi Li [2], Zhihui Qian [1,*], Lei Ren [1,3,*] and Luquan Ren [1]

[1] Key Laboratory of Bionic Engineering, Jilin University, Changchun 130022, China
[2] School of Mechanical and Vehicle Engineering, Jilin Engineering Normal University, Changchun 130052, China
[3] School of Mechanical, Aerospace and Civil Engineering, University of Manchester, Manchester M13 9PL, UK
* Correspondence: zhqian@jlu.edu.cn (Z.Q.); lei.ren@manchester.ac.uk (L.R.)

Abstract: Chemical plating has recently been employed for the preparation of flexible piezoresistive sensors; however, plating solutions and processes that affect the sensitivity still need further exploration. In the study, a sponge-based flexible sensor with copper as its conductive material is prepared using electroless plating. The variation in sponge resistance and sensitivity changes with different plating times are studied. It is found that, with the increasing plating time, the conductivity increases and the resistance of sample will decrease. Moreover, the range of resistance difference will decrease under compression, thus the sensitivity decreases. Furthermore, the sensor's applications were assessed, verifying the practicability of the developed preparation method. This study may bring ideas for the new development of flexible pressure sensors.

Keywords: flexible piezoresistive sensor; porous structure; high sensitivity; electroless plating process

Citation: Yuan, H.; Li, Y.; Qian, Z.; Ren, L.; Ren, L. A Piezoresistive Sensor with High Sensitivity and Flexibility Based on Porous Sponge. *Nanomaterials* **2022**, *12*, 3833. https://doi.org/10.3390/nano12213833

Academic Editor: Camelia Bala

Received: 20 September 2022
Accepted: 27 October 2022
Published: 30 October 2022

1. Introduction

In recent years, with the development of wearable gadgets used in health monitoring, research on sensors has greatly deepened and expanded, with aims of high quality, flexibility, sensitivity, and response speed [1–5]. Flexible sensors can easily attach to individuals' skin, solving the mismatch between rigid planar sensors and human body curves. Based on their working mechanism, flexible sensors are divided into capacitive, piezoelectric, and piezoresistive sensors used for monitoring pressure, temperature, humidity, and so on [6–11].

Flexible piezoresistive sensors have attracted significant attention and are widely used in electronic skin, soft robotics, health monitoring, and so on [12,13]. There were many attempts in the applied magnetism and engineering to create flexible pressure sensors of different types. Melzer fabricated [Co/Cu] multilayers revealing a giant magnetoresistance (GMR) effect on free-standing elastic poly (dimethylsiloxane) (PDMS) membranes [14]. A series of multilayer thin-film structures based on Fe20Ni80 and Fe11Ni89 with Cu or Ta spacers were designed, prepared, and investigated [15]. Flexible magnetoimpedance (MI) sensors fabricated using a NiFe/Cu/NiFe tri-layer on Kapton substrate have been studied by Li [16]. Many methods have been developed for preparing high-performance flexible piezoresistive sensors [17–19]. Conductive nanomaterials, such as graphene, carbon nanotubes, and metal nanomaterials, with elastomeric material, such as PDMS, PU, SBS, and Ecoflex, are integrated to form composites [20–28]; however, for the sensors to perform well, conductive fillers and elastomeric materials must be controlled. For example, the composite conductive thin film was prepared with a spraying method by shadow masks [29]. This preparation method is simple and low-cost, but the electrical property is largely affected by material deformation and the sliding between conductive nanomaterials. To solve the problems, the sensor structure is designed with regard to the wave structure, effectively decreasing the influence of material deformation [30,31]. Other sensor structures, such as

spring and net-shaped, have been developed [32–34]. Although the preparation methods, such as template and electrospinning, coupled with the designed sensor structures have further applications [35,36], the requirements of material stretchability and stability are still difficult to meet, along with mass production challenges [37].

In recent years, materials with three-dimensional (3D) network structures have been widely used in every field thanks to their simple and economical production along with excellent stretchability and stability [38–40]. Graphene with 3D networks has been extensively studied for its great electrical conductivity and mechanical performance. Nevertheless, some preparation methods, such as CVD and hydrothermal reduction, are complicated [41–44]. For instance, three-dimensional porous polymer composites with graphene networks prepared by CVD and PEDOT/PSS coating showed high conductivity [38]. However, their complicated and costly preparation methods make mass production and wide application difficult. In a recent report, 3D graphene sponge flexible sensors with great performance are prepared by the electrodeposition method, but the derived microcracks significantly influence the resistance variations when stretched [45]. In further research, the chemical plating method is applied in the preparation of 3D graphene sponge flexible sensors; compared with the electrode position method, there are no microcracks in the preparation process, making it suitable for good conductivity and uniform coating. Although chemical plating is appropriate for preparing flexible piezoresistive sensors, plating solutions and other experimental processes affect the sensitivity [46], requiring further exploration.

In this paper, the chemical plating method is applied for preparing high-sensitivity and flexible piezoresistive sensors based on the porous sponge, the experiment cost is low, and finite element analysis is employed to demonstrate the flexible piezoresistive sensors' mechanism. The sensitivity is raised to 98.5% and the application of wearable gadgets is verified by flexible circuit.

2. Materials and Methods

2.1. Materials

Materials: Sponge (polyurethane, 5 mm thickness) was produced by Nanjing Saneduo Sponge (Nanjing, China); $CuSO_4$ $5H_2O$ (99 wt%) and HCl (37.5 wt%) were purchased from Beijing Chemical Works (Beijing, China); $NaKC_4H_4O_6$ (99 wt%), $Na_3PO_4{\cdot}12H_2O$ (98 wt%), SDBS (90 wt%), and Na_2CO_3 (99.8 wt%) were from Tianjin Guangfu Technology Development Co., Ltd. (Tianjin, China); NaOH (96 wt%) was from Tianjin Beichen Founder Reagent Factory (Tianjin, China; $NiCl_2{\cdot}6H_2O$ (98 wt%) and $SnCl_2{\cdot}2H_2O$ (98 wt%) were from Tianjin Yongsheng Fine Chemicals Co., Ltd. (Tianjin, China); HCHO (36 wt%) was from Liaoning Quan Rui Reagent Co., Ltd. (Liaoning, China); Op-10 emulsifier (99 wt%) was from Tianjin Zhiyuan Chemical Reagent Co., Ltd. (Tianjin, China); and $PdCl_2$ (99.9 wt%) was from Tianjin Chemical Reagent Third Factory (Tianjin, China).

2.2. Preparation Methods

A 5 mm thick low-density sponge was cut to 70 mm × 50 mm. There are no special requirements for the type and size of sponges. The types of sponges are common in the market. Other types of sponges are also operable. Sponge size is also important for the purpose of uniform specifications, and different sizes of sponges also have this feature. An electroless copper plating sponge composite mainly includes six steps: cleaning, sensitization, activation, reduction, plating, and post-treatment, as shown in Figure 1.

① Cleaning

The purpose of the substrate and, consequently, the sponge cleaning is to ensure obtaining the ideal catalytic activity, mainly including alkaline and ultrasonic cleaning.

A. Alkaline cleaning. Ingredients of alkaline cleaning solution: 20–40 g/L NaOH, 20–30 g/L Na_2CO_3, 5–10 g/L $Na_3PO_4{\cdot}12H_2O$, and 1–3 g/L OP-10 emulsifier. Alkaline cleaning process: 10 min at 70 °C.

B. Ultrasonic cleaning. After alkaline cleaning, the sample is immersed in CH_3COCH_3 solution, followed by ultrasonic cleaning for 2 min with an ultrasonic instrument, and then immersed in deionized water for 1 min.

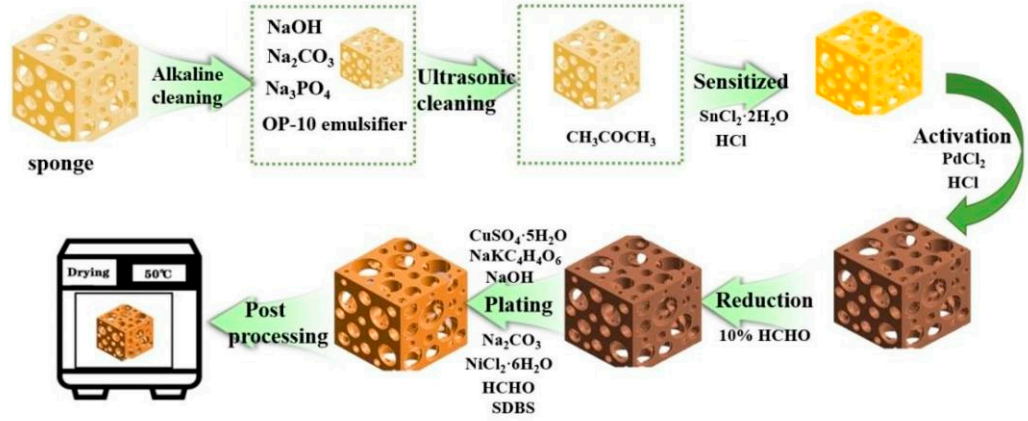

Figure 1. Schematic diagram of the flexible piezoresistive sensor preparation process.

② Sensitization

The purpose of the sensitization is to adsorb a layer of easily oxidized material inside and on the sponge's surface as a reducing agent for catalytic metal ions during the subsequent activation treatment. The sensitizing solution comprises 20 g/L $SnCl_2·2H_2O$ and 40 mL/L HCl. The sensitization process is carried out at room temperature for 6 min. During the sensitization process, the sponge must be pressed to ensure the sensitization liquid is fully in contact with the inner space support of the sponge. Finally, it is cleaned with a deionized water press for 30 s.

③ Activation

The purpose of activation is to generate a catalytic metal layer inside and outside of the sponge as a catalyst for the REDOX reaction during the following electroless plating. The activation solution comprises 1 g/L $PdCl_2$ and 10 mL/L HCl. The activation process takes 6 min at room temperature and requires the sponge to be pressed to ensure that the activation fluid can make full contact with the inner space of the sponge. Finally, it is cleaned with a deionized water press for 30 s.

④ Reduction

The purpose of reduction is to improve the catalytic activity of the substrate's surface, accelerate the deposition rate of the electroless copper plating solution, and prevent contamination of the electroless copper plating solution. The reducing solution comprises 10% HCHO. The reduction process involves stirring at room temperature for 3 min. During the reduction process, the sponge must be pressed to ensure the sensitization liquid is fully in contact with the inner space support of the sponge.

⑤ Plating

The purpose of plating is to reduce the metal ions in the electroless plating solution to their metal state and deposit them on the surface of the plated parts to form a copper film. The plating solution consists of 10 g/L $CuSO_4·5H_2O$, 40 g/L $NaKC_4H_4O_6$, 8 g/L NaOH, 2 g/L Na_2CO_3, 1 g/L $NiCl_2·6H_2O$, 20 mL/L HCHO(36%), and 0.5 g/L SDBS. The plating process takes 30 s of being pressured in a 40 °C water bath box.

⑥ Post-processing

The purpose of post-treatment is to remove the residual liquid and means processing in a drying oven at 50 °C for 30 min after thoroughly cleaning with deionized water.

2.3. Testing Methods

Scanning electron microscopy (SEM, SU3500, HITACHI, Tokyo, Japan) was employed to observe the samples' morphologies. The accelerating voltage of the SEM microscope was 15 kV, measuring the distance at 58 mm, and the magnification was 50.

An energy-dispersive spectrometer (EDS, 550i, IXRF, Austin, TX, USA) was used to determine the samples' elemental composition. The EDS's accelerating voltage was 15 kV, with a take-off angle of 35.0°.

A universal testing machine (ZQ-990B, Dongguan Zhigu Precision Instrument Co., Ltd., Dongguan, Guangdong, China) and a digital multimeter (KEYSIGHT-34465A, KEYSIGHT Technologies, Springs, CO, USA) (as shown in Figure 2) were used to analyze the performance of the attained sensor. During the measurement, two pieces of copper foil were placed on the upper and lower surfaces of the sensor to act as conductors and the measuring surface (as shown in the inset of Figure 2). As the indenter moves up and down, it can better fit the surface of the sample, which is more accurate than the point measurement. Here, 0–100 N force was dynamically applied, with the pressure speed set as 1 mm/min. The press exerts a force of 0 N–100 N on the sponge during the compression process, gradually compressing and deforming the sponge and thinning the pores. When the loading force reaches 100 N, the compression process stops. Under the deformation state of the 100 N force applied by the press, it gradually decreases, and the sponge's pores recover during the recovery process. When the pressing force on the sponge measures at zero N, the sponge recovers partial deformation before the cyclic compression. The press repeatedly applies a force of 0–100 N, taking 20 cycles as an example.

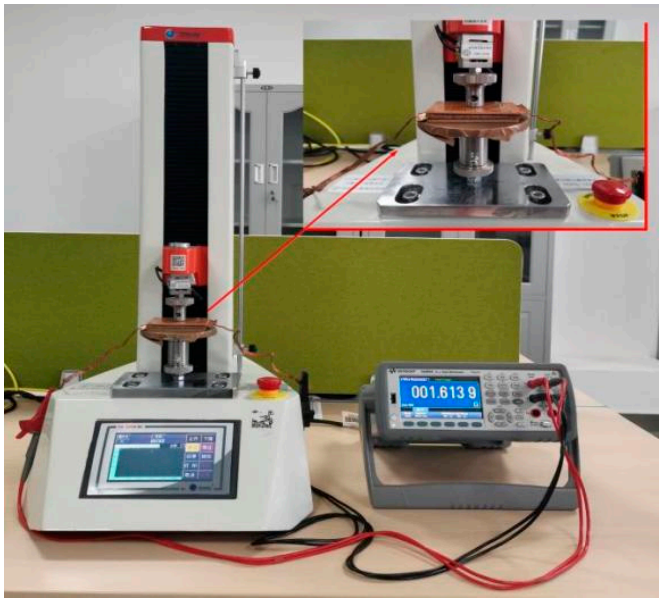

Figure 2. Sensor performance test system ((**left**): press, (**right**): multimeter, (**inset**): resistance measuring point).

2.4. Finite Element Analysis

Finite element analysis was employed to analyze the performance improvement mechanism of the attained flexible sensor. The finite element software ANSYS (Version 2021, ANSYS, Canonsburg, PA, USA) was used to simulate the feasibility of the material as a flexible sensor. The sponge compression process was simplified as only one porous material and the press was simplified as an applied displacement. In the static analysis, the density of the sponge is 40 kg/m^3, Poisson's ratio is 0.38, and the modulus of elasticity is 0.9 Gpa; the material was assumed as a flexible body owing to its deformation under pressure. The porous material is meshed using 36,073 tetrahedral elements, determined through a convergence analysis by gradually increasing the mesh density until the deviations in

the estimated stress reach <5%. In order to control the sponge's deformation accurately, displacement was applied at the top of the material and fixed constraints were applied at the bottom. The finite element analysis was divided into two steps. At first, the flexible material was not deformed, followed by 5%, 10%, 15%, 20%, and 25% deformations. Secondly, a 12 V voltage to the top of the undeformed and deformed material and a 0 V voltage at the bottom were applied, obtaining the resistance variation trends by averaging the current density at the bottom of the material.

3. Results and Discussions

3.1. Structural Analysis

In this study, electroless plating was used for the first time to attach the copper to the sponge's surface and to its pores to functionalize the material. Many studies ignored the high possibility of nanoparticles separating from the matrix material and causing severe health problems to users when used as a wearable gadget for motion detection; therefore, this study used harmless copper as the conductive filler material of the sponge.

Figure 3 shows the SEM images of sponges with different plating times. Figure 3a shows the SEM images of sponges without copper plating. As can be seen from the sample cross section, the sponge has a network structure inside without any attachments. Figure 3b–g show samples with different plating times ranging from 1 to 10 min. It can be deduced that the sample's surface changes and the sponge is covered with a layer of dense copper with folds evenly distributed. The copper film uniformly covers the surface and the sponge's pores and forms a network. The sponge's pores fill up with the increasing plating time and the copper film of the sample thickens, demonstrating that copper is successfully deposited on the sponge's surface. The reduced copper is coated on the sponge during preparation and penetrates the interconnecting holes. The SEM images show the microstructure of the copper-coated sponge and the interconnecting pores covered by the copper.

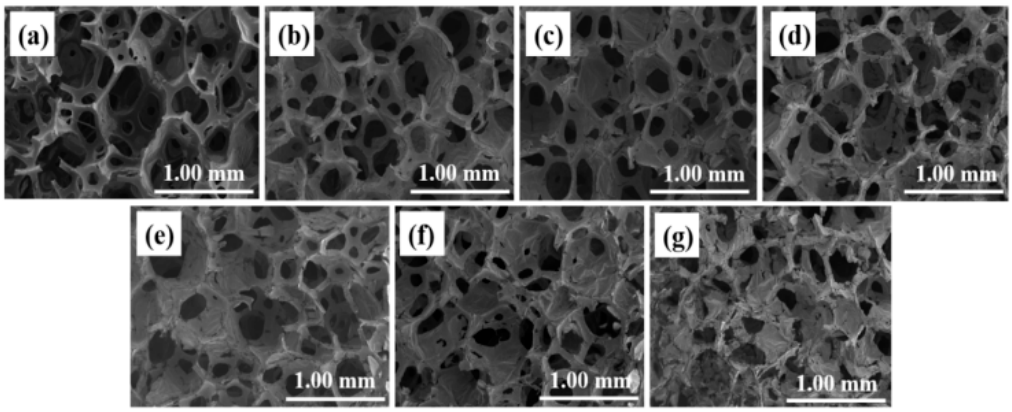

Figure 3. Scanning electron microscopy images of samples with different plating times: (**a**) unplated, (**b**) 1 min, (**c**) 1.5 min, (**d**) 2 min, (**e**) 4 min, (**f**) 8 min, and (**g**) 10 min.

3.2. Elemental Analysis

Based on the electroless plating method, the copper mass fraction in the sponge's pores is controlled by the plating time in the study. Figure 4 shows the energy spectrum of sponge samples before and after plating. As shown, the elements in the sample without plating are mainly carbon and oxygen, with the carbon content being the largest. After plating, a tiny amount of palladium, tin, and a large amount of copper appeared, while the proportion of copper increased significantly to about 95%.

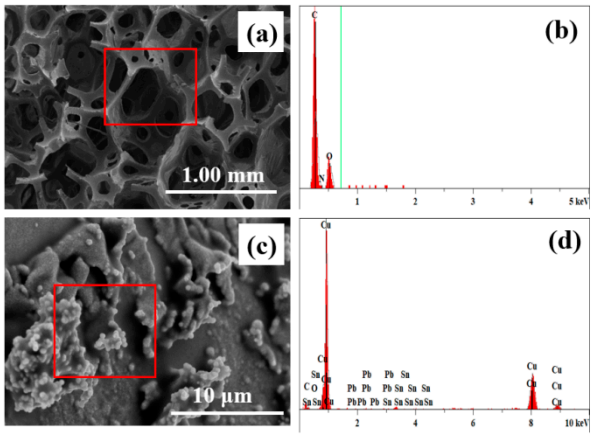

Figure 4. (**a**) The SEM and (**b**) energy spectrum of the sample before copper plating; (**c**) the SEM and (**d**) energy spectrum of the sample after copper plating.

3.3. Mechanical Property Analysis

Sponge is a kind of material with a porous structure; it is insulated, soft, elastic, and does not easily undergo plastic deformation. Based on the above characteristics, the sponge is analyzed after copper plating. Figure 5 shows the deformation of the sponge-based sensor subjected to cyclic compression load, divided into two phases of compression and recovery. Figure 5a,b show the load and sponge's deformation during the first hour of testing. The load is cycled with the test time changes. When the maximum peak value force (100 N) is applied, the deformation of the sponge is the largest, and it is the least when applying the minimum peak value (0 N). Increasing the test time brings the sponge deformation closer to stability at the tenth cycle (at minute 15). Figure 5c shows the stress–strain curve, demonstrating that the sponge can still be nearly restored to its initial state under many load cycles, thus indicating that the compressibility of a sponge-based material is a feasible flexible sensor.

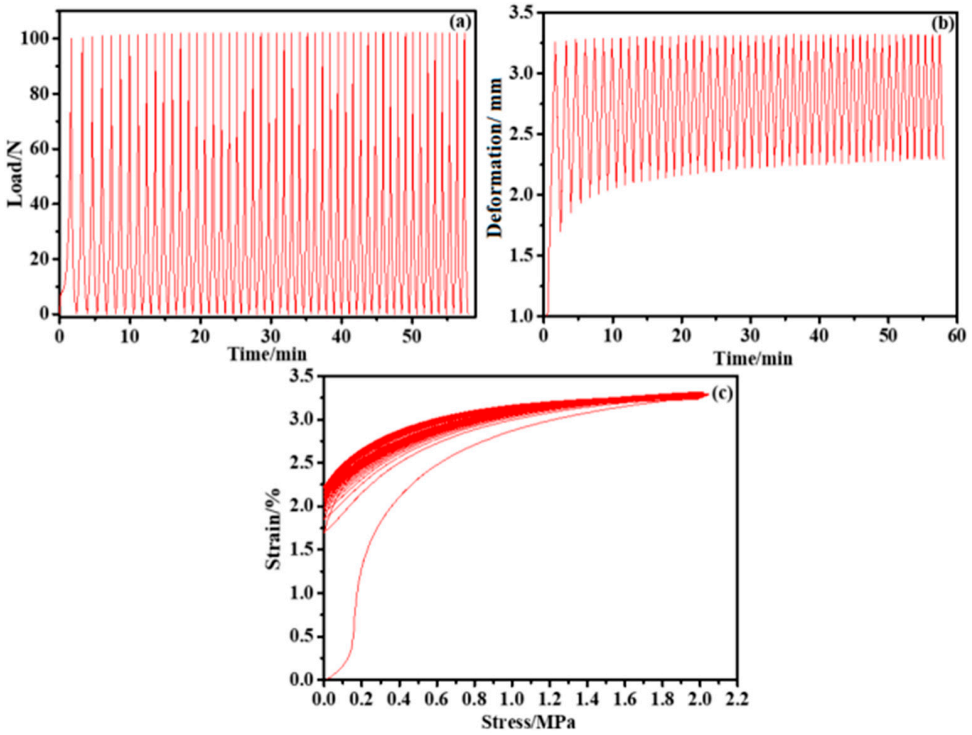

Figure 5. (**a**) Cyclic force curve applied by the press, (**b**) cyclic compression deformation curve of the sample, and (**c**) the stress–strain curve of the sample.

3.4. Finite Element Analysis

As shown in Figures 6 and 7, in the finite element model, the variation law of resistance can be obtained by measuring the current/current density at the same voltage. The voltage of the upper surface of the sample is set to 12 V, the voltage of the lower surface is set to 0 V, and the meshes are unchanged. The average current density is obtained by solving the model. The average current density of the undeformed sponge is 142,260 mA/mm^2, the average current density of 5% deformation is 176,070 mA/mm^2, the average current density of 10% deformation is 192,460 mA/mm^2, the average current density of 15% deformation is 208,800 mA/mm^2, the average current density of 20% deformation is 223,320 mA/mm^2, and the average current density of 25% deformation is 230,590 mA/mm^2. It can be seen that increasing the deformation increases the current density and decreases the resistance against a constant voltage. Among the prepared materials, the copper-coated sponge has relatively high conductivity. This is because of the fact that a large amount of deformation under compression will directly increase the effective cross-section area and decrease the length of the sponge pore unit, thus decreasing the electrical resistance, leading to the resistance variations according to different deformations. In addition, the deposition thickness of copper increases with the increasing plating time within the study (as shown in Figure 3), indicating the copper content deposited in sponge pore is improved. Under this condition, the electrical resistivity will decrease, and it can be inferred the copper-coated sponge has better conductivity. However, in this study, when the reaction time is too long, the prepared plating solution will be out of work at the temperature of the water bath, so this effect is not observed with a long plating time. Therefore, the copper-coated sponge has advantages to be selected as a flexible piezoresistive sensor material.

3.5. Sensor Performance Analysis

The process used in this study can produce sensors with different sensitivities. Therefore, it is necessary to characterize and compare their sensitivities by various methods to determine their performance, benefits, and potential applications. Through the electroless plating of copper on the surface of the sponge, it can conduct electricity. The copper-plated sponge is equivalent to a flexible sensor and shows good electrical conductivity. $\Delta R/R_0$ represents the sensitivity, where $\Delta R = R_n - R_0$, R_n represents the sensor's resistance against a particular stimulus, and R_0 represents its initial resistance.

Figure 8 shows the resistance distribution fitting curve of the sample sponge under one cyclic loading pressure. As demonstrated by the figure, the left half section of the horizontal axis is force unloading while the right half is force loading. It can be deduced from the results that the maximum value of the resistance fitting curve is when the pressure is equal to 0 N and the sponge porosity is at a maximum. The sponge's minimum volume is achieved, the pressure is 100 N, and the sponge's pores are completely closed, equivalent to a conductor with a constant resistance value. Under cyclic loading pressure, the resistance presents a periodic distribution.

As shown in Figure 9, within the plating time range of 1 to 10 min, the sensor's conductivity increases with the increasing plating time. The sensor's conductivity with a 10 min duration is the highest, with its resistance measured at 0.128 Ω under 0 N and 0.015 Ω under 100 N, respectively. In comparison, it is the lowest with a one-minute duration, with its resistance measured at 355,828 Ω at 0 N and 4369 Ω at 100 N. This difference is due to the increase in plating time, the actual coverage of the copper on the unit area of the sensor, and the decrease in the sensor's equivalent resistance. If the plating time is infinite, theoretically, the copper will completely cover the sponge and fill every pore.

The piezoresistive sensitivities of sponges with different plating times were compared to determine the sensor with the best performance parameters. The results are shown in Figure 10. In this study, the sensor prepared within one minute of plating time shows the highest sensitivity, at around 99%, while the one prepared with 10 min of plating time has the lowest sensitivity, measured at around 88%. This is due to the porous sponge's pores

being filled with more conductive materials and becoming smaller with the increasing plating time. Therefore, the conductivity is enhanced and the sponge's resistance to pressure is reduced. It is proven that the sensor's sensitivity prepared by this process is tunable and has a potential application.

To evaluate the sensor's performance further, they were compared to the same types of sensors developed in previous literature [47] (as shown in Table 1).

Table 1. Comparisons of the sensors' performance.

Materials	Maximum Compression Deformation	Carbon Nano Tube (CNT) Capacity	Carbohydrate Content	Max $\Delta R/R_0$ (%)
Sponge	50.0%	1.5–3.0%	70.0%	<90.0%
Sponge	50.0%	3.0%	70.0–85.0%	<90.0%
Sponge (this paper)	85.0%	0%	0%	98.8%

The comparison shows that the sensor developed in this study has higher sensitivity, more stability, and compression recovery properties, and the preparation process is more straightforward and with lower costs compared with others.

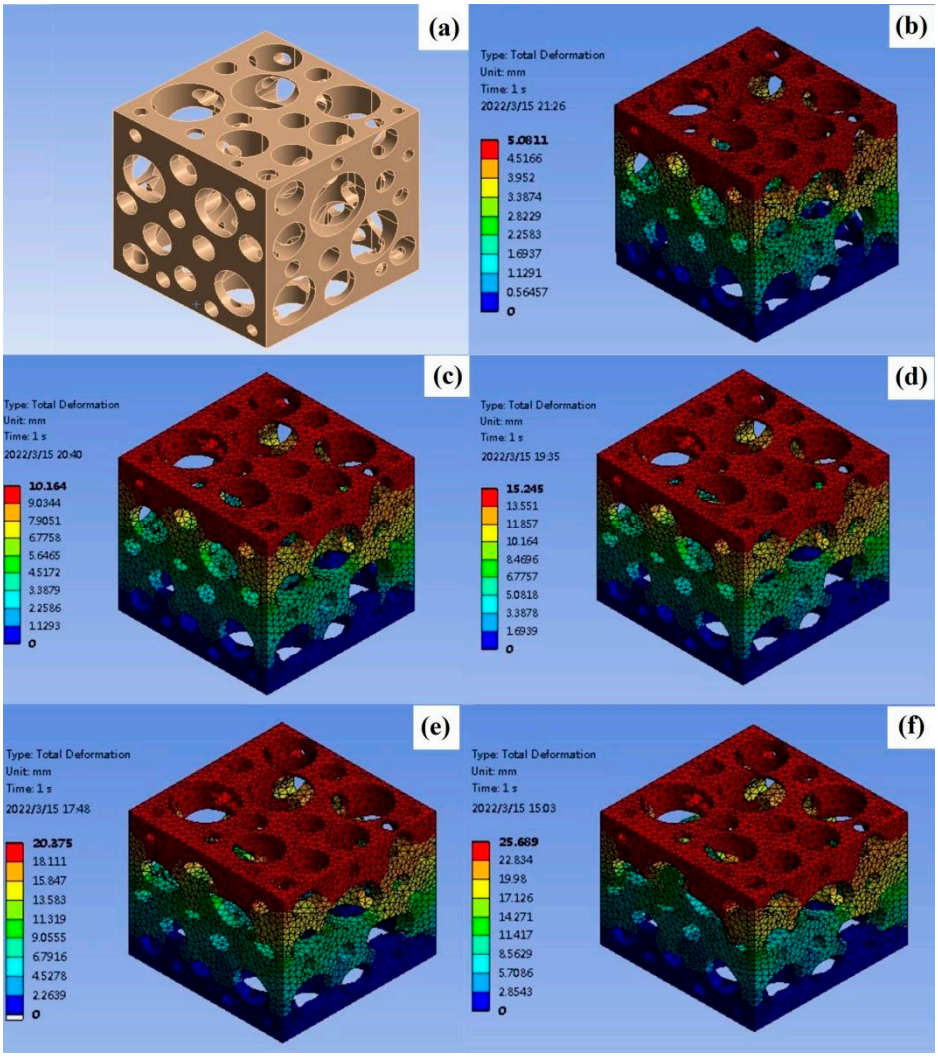

Figure 6. Deformation of sponge with different displacement constraints: (**a**) no deformation, (**b**) 5%, (**c**) 10%, (**d**) 15%, (**e**) 20%, and (**f**) 25%.

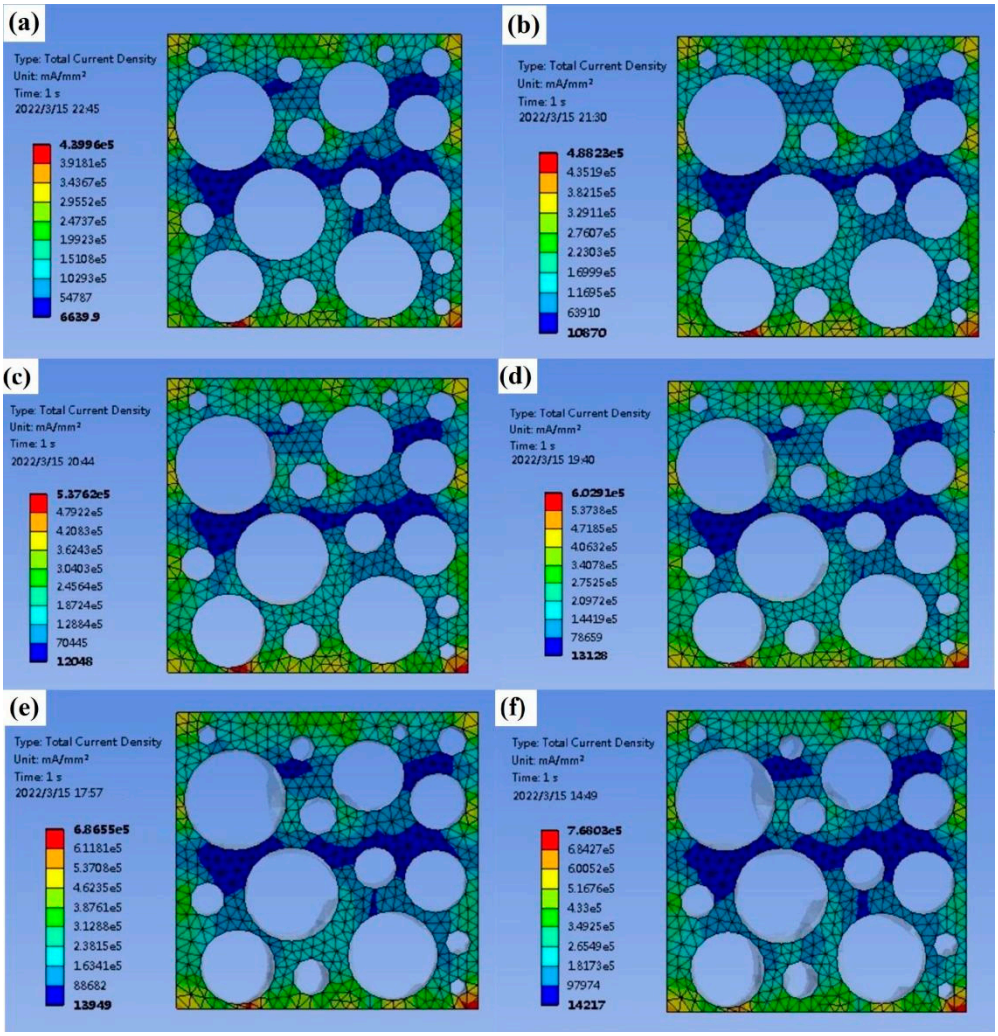

Figure 7. Current density of sponges with different deformations: (**a**) no deformation, (**b**) 5%, (**c**) 10%, (**d**) 15%, (**e**) 20%, and (**f**) 25%.

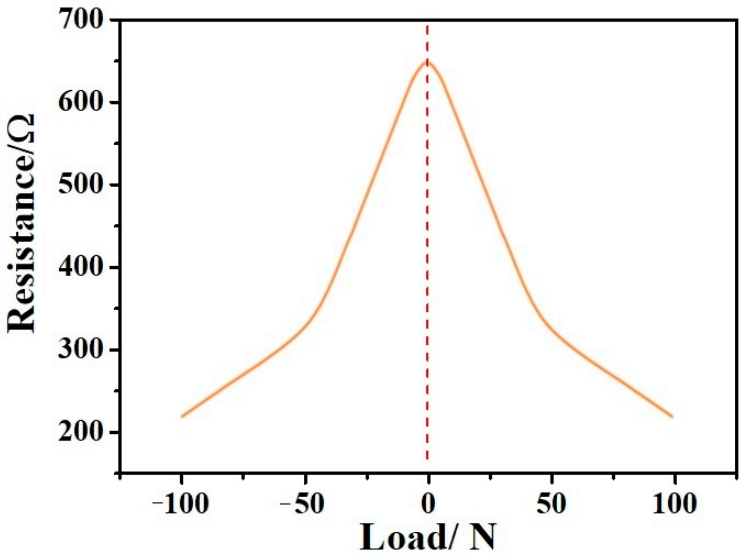

Figure 8. Resistance distribution fitting curve of the sample sponge under one cyclic loading pressure.

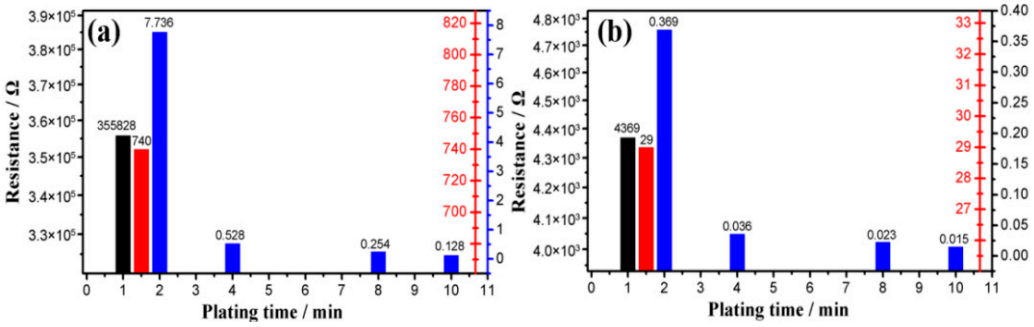

Figure 9. The resistance of sponge with different plating times: (**a**) before compression and (**b**) after compression.

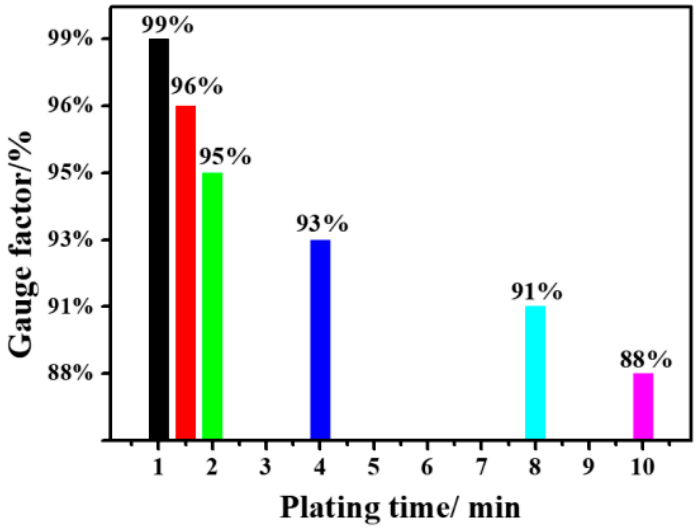

Figure 10. Sponge sensitivity at different plating times.

3.6. Sensor's Application Analysis

Biocompatibility has to be considered when developing sensors that are usually attached to individuals' skin and can cause health issues. In this study, copper is attached to the sponge's pores' walls. When used for human motion detection, the manufacturing process developed in the study would avoid the possibility that nanoparticles separate from the surface of the elastomer as a result of repeated circulation. It is safe for the user and suitable for commercial human motion detection products. In this study, copper was embedded into the sponge's pores to significantly reduce the possibility of tearing during use. This advantage makes the sensors developed in this study suitable for wearing.

In order to visually characterize the sensor's performance, LED lamps and a power supply were connected to form a series circuit. As shown in Figure 11, the LED lamp is lit when the switch is off, indicating the sensor's good conductivity. The LED lamp's brightness is significantly enhanced when pressure is applied to the sensor. Similarly, as shown in Figure 12, by increasing the bending angle, the fitting surface of different shapes is simulated and the LED lamp's brightness is significantly enhanced. The sensor's resistance gradually reducing with the compression load can explain this.

The sponge, with its porous structure prepared by electroless plating, has potential applications for monitoring a wide range of pressure stimuli in wearable, flexible electronic gadgets and other related fields.

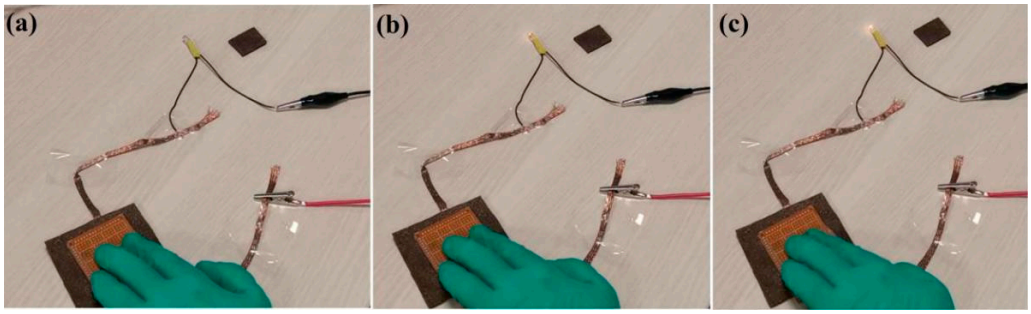

Figure 11. Flexible switch applications: (**a**) unpressed, (**b**) partly pressed, and (**c**) completely pressed.

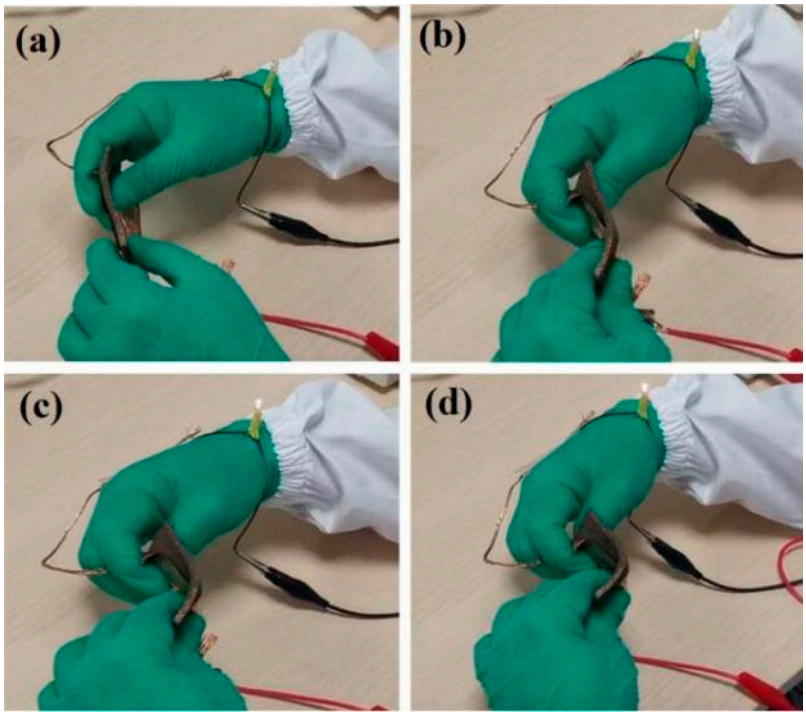

Figure 12. Flexible switch applications: (**a**) 180°, (**b**) 150°, (**c**) 120°, and (**d**) 90°.

4. Conclusions

Flexible pressure sensors constitute an important part of the applications of flexible electronic sensing systems and have been widely used in biomedical engineering, robotics, and other fields. In the study, a sponge-based flexible sensor with copper as its conductive material is prepared using electroless plating. The sponge's resistance and sensitivity changes with different plating times are studied. We found that increasing the plating time decreases the resistance value, and sensitivity gradually decreases while the conductivity increases. In this study, the sensor prepared within one minute of plating time shows the highest sensitivity, at around 99%, while the one prepared with 10 min of plating time has the lowest sensitivity, measured at around 88%. Furthermore, the sensor's applications were assessed, verifying the practicability of the developed preparation method for flexible sensors. This study brings forth new ideas, simplifies the preparation process, and reduces production expenses for flexible pressure sensors.

There are still limitations to this paper, which could be further investigated in future studies: (1) more materials with better conductivity should be considered as sensors' conductive materials; (2) further improvement in the preparation method and process of the sensors is necessary to advance their overall performance.

Author Contributions: Conceptualization, H.Y. and Z.Q.; methodology, H.Y.; software, Y.L.; validation, H.Y., Z.Q., L.R. (Lei Ren) and L.R. (Luquan Ren); formal analysis, Z.Q.; investigation, H.Y.; resources, Z.Q.; data curation, H.Y.; writing—original draft preparation, H.Y.; writing—review and editing, H.Y.; visualization, Y.L.; supervision, L.R. (Lei Ren); project administration, Z.Q.; funding acquisition, Z.Q. All authors have read and agreed to the published version of the manuscript.

Funding: This research was supported by the project of National Natural Science Foundation of China (No. 52175270, Zhihui Qian) and the Project of Scientific and Technological Development Plan of Jilin Province (No.20220508130RC, Zhihui Qian).

Data Availability Statement: Not applicable.

Conflicts of Interest: The authors declare no conflict of interest.

References

1. Trung, T.-Q.; Lee, N.-E. Flexible and Stretchable Physical Sensor Integrated Platforms for Wearable Human-Activity Monitoring and Personal Healthcare. *Adv. Mater.* **2016**, *28*, 4338–4372. [CrossRef] [PubMed]
2. Mukundan, A.; Feng, S.-W.; Weng, Y.-H.; Tsao, Y.-M.; Artemkina, S.-B.; Fedorov, V.-E.; Lin, Y.-S.; Huang, Y.-C.; Wang, H.-C. Optical and Material Characteristics of MoS_2/Cu_2O Sensor for Detection of Lung Cancer Cell Types in Hydroplegia. *Int. J. Mol. Sci.* **2022**, *23*, 4745. [CrossRef] [PubMed]
3. Hua, Q.-L.; Sun, J.-L.; Liu, H.-T.; Bao, R.-R.; Yu, R.-M.; Zhai, J.-Y.; Pan, C.-F.; Wang, Z.-L. Skin-inspired Highly Stretchable and Conformable Matrix Networks for Multifunctional Sensing. *Nat. Commun.* **2018**, *9*, 244. [CrossRef] [PubMed]
4. Laskowska, M.; Nowak, A.; Dulski, M.; Weigl, P.; Blochowicz, T.; Laskowski, L. Spherical Silica Functionalized by 2-Naphthalene Methanol Luminophores as a Phosphorescence Sensor. *Int. J. Mol. Sci.* **2021**, *22*, 13289. [CrossRef] [PubMed]
5. Munteanu, I.-G.; Apetrei, C. Electrochemical Determination of Chlorogenic Acid in Nutraceuticals Using Voltammetric Sensors Based on Screen-Printed Carbon Electrode Modified with Graphene and Gold Nanoparticles. *Int. J. Mol. Sci.* **2021**, *22*, 8897. [CrossRef]
6. Mannsfeld, S.; Tee, B.; Stoltenberg, R.; Chen, C.; Barman, S.; Muir, B.; Sokolov, A.; Reese, C.; Bao, Z.-N. Highly Sensitive Flexible Pressure Sensors with Microstructured Rubber Dielectric Layers. *Nat. Mater.* **2010**, *9*, 859–864. [CrossRef]
7. Konishi, S.; Hirata, A. Flexible Temperature Sensor Integrated with Soft Pneumatic Microactuators for Functional Microfingers. *Sci. Rep.* **2019**, *9*, 15634. [CrossRef]
8. Jeon, J.; Lee, H.-B.; Bao, Z. Flexible Wireless Temperature Sensors Based on Ni Microparticle-Filled Binary Polymer Composites. *Adv. Mater.* **2013**, *25*, 850–855. [CrossRef]
9. Han, Z.-W.; Liu, L.-P.; Zhang, J.-Q.; Han, Q.-G.; Wang, K.-J.; Song, H.-L.; Wang, Z.; Jiao, Z.-B.; Niu, S.-C.; Ren, L.-Q. High-performance Flexible Strain Sensor with Bio-inspired Crack Arrays. *Nanoscale* **2018**, *10*, 15178–15186. [CrossRef]
10. Guo, H.-Y.; Lan, C.-Y.; Zhou, Z.-F.; Sun, P.; Wei, D.; Li, C. Transparent, Flexible, and Stretchable WS2 Based Humidity Sensors for Electronic Skin. *Nanoscale* **2017**, *9*, 6246–6253. [CrossRef]
11. Ma, L.; Wu, R.; Patil, A.; Zhu, S.; Meng, Z.; Meng, H.; Hou, C.; Zhang, Y.; Liu, Q.; Yu, R.; et al. Full-Textile Wireless Flexible Humidity Sensor for Human Physiological Monitoring. *Adv. Funct. Mater.* **2019**, *29*, 1904549. [CrossRef]
12. Huang, Y.; Fan, X.-Y.; Chen, S.-C.; Zhao, N. Emerging Technologies of Flexible Pressure Sensors: Materials, Modeling, Devices, and Manufacturing. *Adv. Funct. Mater.* **2019**, *29*, 1808509. [CrossRef]
13. Nela, L.; Tang, J.-S.; Cao, Q.; Tulevski, G.; Han, S.-J. Large-Area High-Performance Flexible Pressure Sensor with Carbon Nanotube Active Matrix for Electronic Skin. *Nano Lett.* **2018**, *18*, 2054–2059. [CrossRef] [PubMed]
14. Melzer, M.; Makarov, D.; Calvimontes, A.; Karnaushenko, D.; Baunack, S.; Kaltofen, R.; Mei, Y.; Schmidt, O. Stretchable Magnetoelectronics. *Nano Lett.* **2011**, *11*, 2522–2526. [CrossRef] [PubMed]
15. Chlenova, A.; Lepalovsky, V.; Vas'kovskiy, V.; Svalov, A.; Kurlyandskaya, G. Magnetoimpedance effect in multilayered permalloy structure with different magnetostriction: Small-pressure sensor. *AIP Conf. Proc.* **2017**, *1886*, 020005.
16. Li, B.; Kavaldzhiev, M.; Kosel, J. Flexible Magnetoimpedance Sensor. *J. Magn. Magn. Mater.* **2015**, *378*, 499. [CrossRef]
17. Yao, S.; Zhu, Y. Nanomaterial-Enabled Stretchable Conductors: Strategies, Materials and Devices. *Adv. Mater.* **2015**, *27*, 1480–1511. [CrossRef]
18. Zhao, S.-F.; Li, J.-H.; Cao, D.-X.; Zhang, G.-P.; Li, J.; Li, K.; Yang, Y.; Wang, W.; Jin, Y.-F.; Sun, R.; et al. Recent Advancements in Flexible and Stretchable Electrodes for Electromechanical Sensors: Strategies, Materials, and Features. *ACS Appl. Mater. Interfaces* **2017**, *9*, 12147–12164. [CrossRef]
19. Langley, D.; Giusti, G.; Mayousse, C.; Celle, C.; Bellet, D.; Simonato, J.-P. Flexible Transparent Conductive Materials Based on Silver Nanowire Networks: A Review. *Nanotechnology* **2013**, *24*, 452001. [CrossRef]
20. Geim, A.-K. Graphene: Status and prospects. *Science* **2009**, *324*, 1530–1534. [CrossRef]
21. Kim, K.S.; Zhao, Y.; Jang, H.; Lee, S.Y.; Kim, J.M.; Kim, K.S.; Ahn, J.-H.; Kim, P.; Choi, J.-Y.; Hong, B.H. Large-Scale Pattern Growth of Graphene Films for Stretchable Transparent Electrodes. *Nature* **2009**, *457*, 706–710. [CrossRef] [PubMed]
22. Sekitani, T.; Nakajima, H.; Maeda, H.; Fukushima, T.; Aida, T.; Hata, K.; Someya, T. Stretchable Active-Matrix Organic Light-Emitting Diode Display Using Printable Elastic Conductors. *Nat. Mater.* **2009**, *8*, 494–499. [CrossRef] [PubMed]

23. Sekitani, T.; Noguchi, Y.; Hata, K.; Fukushima, T.; Aida, T.; Someya, T. A Rubberlike Stretchable Active Matrix Using Elastic Conductors. *Science* **2008**, *321*, 1468–1472. [CrossRef]
24. Han, T.; Wang, G. Peroxidase-like Activity of Acetylcholine-Based Colorimetric Detection of Acetylcholinesterase Activity and an Organophosphorus Inhibitor. *J. Mater. Chem. B* **2019**, *7*, 2613–2618. [CrossRef]
25. Huang, W.-P.; Li, J.-H.; Zhao, S.-F.; Han, F.; Zhang, G.-P.; Sun, R.; Wong, C.-P. Highly Electrically Conductive and Stretchable Copper Nanowires-Based Composite for Flexible and Printable Electronics. *Compos. Sci. Technol.* **2017**, *146*, 169–176. [CrossRef]
26. Xu, F.; Wang, X.; Zhu, Y.-T.; Zhu, Y. Wavy Ribbons of Carbon Nanotubes for Stretchable Conductors. *Adv. Funct. Mater.* **2012**, *22*, 1279–1283. [CrossRef]
27. Hu, W.-L.; Wang, R.-R.; Lu, Y.-F.; Pei, Q.-B. An Elastomeric Transparent Composite Electrode Based on Copper Nanowires and Polyurethane. *J. Mater. Chem. C* **2014**, *2*, 1298–1305. [CrossRef]
28. Lee, P.; Ham, J.; Lee, J.; Hong, S.; Han, S.; Suh, Y.D.; Lee, S.E.; Yeo, J.; Lee, S.S.; Lee, D.; et al. Highly Stretchable or Transparent Conductor Fabrication by a Hierarchical Multiscale Hybrid Nanocomposite. *Adv. Funct. Mater.* **2014**, *24*, 5671–5678. [CrossRef]
29. Hu, L.-B.; Wei, Y.; Brochu, P.; Gruner, G.; Pei, Q.-B. Highly Stretchable, Conductive, and Transparent Nanotube Thin Films. *Appl. Phys. Lett.* **2009**, *94*, 161108. [CrossRef]
30. Zhu, Y.; Xu, F. Buckling of Aligned Carbon Nanotubes as Stretchable Conductors: A New Manufacturing Strategy. *Adv. Mater.* **2012**, *24*, 1073–1077. [CrossRef]
31. Bowden, N.; Brittain, S.; Evans, A.-G.; Hutchinson, J.W.; Whitesides, G.-M. Spontaneous Formation of Ordered Structures in Thin Films of Metals Supported on an Elastomeric Polymer. *Nature* **1998**, *393*, 146–149. [CrossRef]
32. Shang, Y.-Y.; He, X.-D.; Li, Y.-B.; Zhang, L.-H.; Li, Z.; Ji, C.-Y.; Shi, E.-Z.; Li, P.-X.; Zhu, K.; Peng, Q.-Y.; et al. Super-Stretchable Spring-Like Carbon Nanotube Ropes. *Adv. Mater.* **2012**, *24*, 2896–2900. [CrossRef] [PubMed]
33. Liang, H.-W.; Guan, Q.-F.; Zhu, Z.; Song, L.-T.; Yao, H.-B.; Lei, X.; Yu, S.-Y. Highly Conductive and Stretchable Conductors Fabricated from Bacterial Cellulose. *NPG Asia. Mater.* **2012**, *4*, e19. [CrossRef]
34. Chen, Z.-P.; Ren, W.-C.; Gao, L.-B.; Liu, B.-L.; Pei, S.-F.; Cheng, H.-M. Three-Dimensional Flexible and Conductive Interconnected Graphene Networks Grown by Chemical Vapour Deposition. *Nat. Mater.* **2011**, *10*, 424–428. [CrossRef] [PubMed]
35. Yu, C.-J.; Masampu, C.; Rong, J.; Wei, B.-Q.; Jiang, H. Stretchable Supercapacitors Based on Buckled Single-Walled Carbon-Nanotube Macrofilms. *Adv. Mater.* **2010**, *21*, 4793–4797. [CrossRef] [PubMed]
36. Wu, C.; Fang, L.-J.; Huang, X.-Y.; Jiang, P.-K. Three-Dimensional Highly Conductive Graphene–Silver Nanowire Hybrid Foams for Flexible and Stretchable Conductors. *ACS Appl. Mater. Interfaces.* **2014**, *6*, 21026–21034. [CrossRef] [PubMed]
37. Wu, H.; Hu, L.; Rowell, M.W.; Kong, D.; Cha, J.J.; McDonough, J.R.; Zhu, J.; Yang, Y.; McGehee, M.D.; Cui, Y. Electrospun Metal Nanofiber Webs as High-Performance Transparent Electrode. *Nano. Lett.* **2010**, *10*, 4242–4248. [CrossRef]
38. Zhang, Y.; Sheehan, C.-J.; Zhai, J.; Zou, G.; Luo, H.; Xiong, J.; Zhu, Y.; Jia, Q. Polymer-Embedded Carbon Nanotube Ribbons for Stretchable Conductors. *Adv. Mater.* **2010**, *22*, 3027–3031. [CrossRef]
39. Chen, M.; Zhang, L.; Li, C. Three-Dimensional Porous Stretchable and Conductive Polymer Composites Based on Graphene Network Grown by Chemical Vapour Deposition and PEDOT: PSS Coating. *Chem. Commun.* **2015**, *51*, 3169–3172. [CrossRef]
40. Yu, Y.; Zeng, J.-F.; Chen, C.-J.; Xie, Z.; Guo, R.-S.; Liu, Z.-L.; Zhou, X.-C.; Yang, Y.; Zheng, Z.-J. Composite Materials: Three-Dimensional Compressible and Stretchable Conductive Composites. *Adv. Mater.* **2014**, *26*, 666. [CrossRef]
41. Park, J.; Wang, S.; Li, M.; Ahn, C.-G.; Hyun, J.-K.; Dong, S.-K.; Kim, D.-K.; Rogers, J.-A.; Huang, Y.-G.; Jeon, S.-K. Three-Dimensional Nanonetworks for Giant Stretchability in Dielectrics and Conductors. *Nat. Commun.* **2012**, *3*, 916. [CrossRef] [PubMed]
42. Chen, M.-T.; Zhang, L.; Duan, S.-S.; Jing, S.-L.; Jiang, H.; Li, C.-Z. Highly Stretchable Conductors Integrated with a Conductive Carbon Nanotube/Graphene Network and 3D Porous Poly(dimethylsiloxane). *Adv. Funct. Mater.* **2015**, *24*, 7548–7556. [CrossRef]
43. Wei, W.; Yang, S.; Zhou, H.; Lieberwirth, I.; Feng, X.-L.; Müllen, K. 3D Graphene Foams Cross-Linked with Pre-Encapsulated Fe_3O_4 Nanospheres for Enhanced Lithium Storage. *Adv. Mater.* **2013**, *25*, 2909–2914. [CrossRef]
44. Xu, Y.-X.; Sheng, K.-X.; Li, C.; Shi, G.-Q. Self-Assembled Graphene Hydrogel via a One-Step Hydrothermal Process. *ACS Nano* **2010**, *4*, 4324–4330. [CrossRef] [PubMed]
45. Fei, H.; Li, J.-H.; Zhao, S.-F.; Yuan, Z.; Huang, W.-P.; Zhang, G.-P.; Rong, S.; Wong, C.-P. A Crack-based Nickel@Graphene Wrapped Polyurethane Sponge Ternary Hybrid Obtained by Electrodeposition for Highly Sensitive Wearable Strain Sensors. *J. Mater. Chem. C* **2017**, *5*, 10167–10175.
46. Fei, H.; Su, X.-Y.; Huang, M.-Q.; Li, J.-H.; Zhang, Y.; Zhao, S.; Liu, F.; Zhang, B.; Wang, Y.; Zhang, G.; et al. Fabrication of a Flexible and Stretchable Three-Dimensional Conductor Based on Au–Ni@Graphene Coated Polyurethane Sponge by Electroless Plating. *J. Mater. Chem. C* **2018**, *6*, 8135–8143.
47. Herren, B.; Webster, V.; Davidson, E.; Saha, M.-C.; Altan, M.-C.; Liu, Y. PDMS Sponges with Embedded Carbon Nanotubes as Piezoresistive Sensors for Human Motion Detection. *Nano Mater.* **2021**, *11*, 1740. [CrossRef] [PubMed]

polymers

MDPI

Article

Highly Stretchable and Sensitive Multimodal Tactile Sensor Based on Conductive Rubber Composites to Monitor Pressure and Temperature

Bing Zhu [1,†], Chi Ma [1,†], Zhihui Qian [2,*], Lei Ren [2,3,*] and Hengyi Yuan [2]

[1] State Key Laboratory of Automotive Simulation and Control, Jilin University, Changchun 130025, China; zhubing@jlu.edu.cn (B.Z.); machi20@mails.jlu.edu.cn (C.M.)
[2] Key Laboratory of Bionic Engineering, Jilin University, Changchun 130025, China; yuanhy18@mails.jlu.edu.cn
[3] School of Mechanical, Aerospace and Civil Engineering, University of Manchester, Manchester M13 9PL, UK
* Correspondence: zhqian@jlu.edu.cn (Z.Q.); lei.ren@manchester.ac.uk (L.R.)
† These authors contributed equally to this work.

Abstract: Stretchable and flexible tactile sensors have been extensively investigated for a variety of applications due to their outstanding sensitivity, flexibility, and biocompatibility compared with conventional tactile sensors. However, implementing stretchable multimodal sensors with high performance is still a challenge. In this study, a stretchable multimodal tactile sensor based on conductive rubber composites was fabricated. Because of the pressure-sensitive and temperature-sensitive effects of the conductive rubber composites, the developed sensor can simultaneously measure pressure and temperature, and the sensor presented high sensitivity (0.01171 kPa^{-1} and 2.46–30.56%/°C) over a wide sensing range (0–110 kPa and 30–90 °C). The sensor also exhibited outstanding performance in terms of processability, stretchability, and repeatability. Furthermore, the fabricated stretchable multimodal tactile sensor did not require complex signal processing or a transmission circuit system. The strategy for stacking and layering conductive rubber composites of this work may supply a new idea for building multifunctional sensor-based electronics.

Keywords: multimodal sensors; stretchable tactile sensors; resistance-type sensors; conductive rubber; carbon nanomaterials

Citation: Zhu, B.; Ma, C.; Qian, Z.; Ren, L.; Yuan, H. Highly Stretchable and Sensitive Multimodal Tactile Sensor Based on Conductive Rubber Composites to Monitor Pressure and Temperature. *Polymers* **2022**, *14*, 1294. https://doi.org/10.3390/polym14071294

Academic Editor: Marcin Masłowski

Received: 18 February 2022
Accepted: 21 March 2022
Published: 23 March 2022

1. Introduction

Stretchable and flexible tactile sensors for direct human body contact applications are attracting increasing interest in academic and industry fields. With the development of stretchable and flexible electronics, high-performance stretchable tactile sensors play an increasingly important role in a variety of applications including human motion detection, stretchable smart robots, human-machine interaction, and wearable medical devices [1–4].

Numerous studies have reported on the development and fabrication of highly stretchable and sensitive tactile sensors. According to their working mechanism, tactile sensors include resistance [5], capacitance [6,7], piezoelectric, and triboelectric-type sensors [8]. To improve stretchable tactile sensor performance, researchers have enhanced their structures and morphologies [9–12], and prepared stretchable tactile sensors or sensor arrays [13–15] via complex microelectronic processes [16–18] and bionic methods [19,20]. For example, Chen et al. created a graphene-based resistive strain sensor with a sensitivity of 20.1 [5], and Gao et al. fabricated a capacitance-type sensor based on conductive silicone rubber and pure PDMS that can detect dropping water, feet lifting, and walking [6]. Pyo et al. fabricated a pressure sensor with a multi-layered structure and high sensitivity (26.13 kPa^{-1}) over a wide pressure range (0.2–982 kPa) [10]. Jian et al. also fabricated a pressure sensor with high sensitivity (19.8 kPa^{-1}, <0.3 kPa), a low detection limit (0.6 Pa), and a fast response time (<16.7 ms) due to its bionic hierarchical structures [19].

Tactile properties require a combination of roughness, hardness, thermal conductivity, temperature, humidity, sharpness, vibration, force, and other parameters in human skin through contact with surface objects [21–23], thus the development of multifunctional or multimodal tactile sensors has gained interest worldwide [24–28]. Unlike human skin, most stretchable sensors can only effectively sense one parameter, and researchers are investigating stretchable tactile sensors with improved stretchability, ductility, and sensitivity and measurement ranges. In addition, many conductive composite materials used as stretchable tactile sensors are sensitive to one type of tactile stimulus (mostly pressure or strain), as well as other parameters such as temperature and humidity [29–31]. Efforts were already made to engineer stretchable sensors that can detect various parameters simultaneously. For example, Liu et al. reported a stretchable multimodal sensor that can detect multiple stimuli with only one device by spraying a mixture of carbon black (CB) and reduced graphene oxide (rGO) on a paper substrate [32]. However, it was troublesome for the sensors in this report to distinguish different stimuli. Jung et al. also proposed a stretchable device containing pressure, temperature, and piezoresistive hair-type flow sensors, the latter of which was fabricated with a mixture of carbon nanotubes and polydimethylsiloxane piezoresistive materials [27]. However, the sensor manufacturing process in the study was complicated because each sensitive layer was prepared separately, and the output signals were diverse. Current multimodal sensors are limited by complex manufacturing processes, high cost, and complex signal processing. Therefore, challenges remain to implementing high performance multimodal sensors.

In this study, we developed a new stretchable tactile sensor consisting of conductive rubber composites with improved sensitivity, measurement range, and measurement functionalities. Due to its unique advantages, such as good conductivity, high chemical and thermal stability and low toxicity, carbon materials have great application potential in the field of stretchable and flexible sensors. For example, CNT has good conductivity, high aspect ratio and excellent flexibility. In addition, GP also has excellent flexibility and good conductivity, while CB has the advantages of low cost and good conductivity. Therefore, different conductive rubber composites were prepared with these carbon nanomaterials as conductive fillers in this work. Because rubber materials have good stretchability and biocompatibility, we constructed stretchable tactile sensors with silicone rubber materials and carbon nanomaterials [33–35]. The conductive rubber composites were prepared with carbon nanomaterials (multiwalled carbon nanotubes (MWCNTs), carbon black (CB), and graphene (GP)) incorporated into room temperature vulcanized silicone rubber (RTV). After testing the reinforcement of the conductive fillers on the mechanical and electrical properties of the conductive rubber composites, the stretchable tactile sensors were fabricated with a conductive rubber composite film as the sensitive layer. Then, an appropriate material ratio was selected according to the experimental data to properly integrate the stretchable multimodal tactile sensor. The fabrication method used in this study was simple and inexpensive. Based on the pressure-sensitive and temperature-sensitive effects of the conductive rubber composites, a final stretchable multimodal tactile sensor with a dual-sensitive layer was designed and fabricated. This sensor, with a simple structure and manufacturing process can simultaneously measure pressure and temperature. Since there are two signal outputs, the signal processing of this sensor was simple and did not interfere with each other. In addition, the stretchable multimodal tactile sensor developed in the study showed good sensitivity when exposed to compression at different temperatures.

2. Experimental Detail

2.1. Materials

Superconducting carbon black (CB) powder (CABOT BP2000) was purchased from Hefei Saibo New Materials Co., Ltd., Hefei, China. Multilayer graphene (GP) (5–10 layers, 95% purity) and multi-wall carbon nanotubes (MWCNTs) (TF-25001, inner diameter 3–5 nm, outer diameter 8–18 nm, length 3–12 μm, 95% purity) were obtained from Suzhou carbon graphene Technology Co., Ltd., Suzhou, China and were used as conductive fillers to

fabricate the conductive rubber composites. Room temperature vulcanized silicone rubber (RTV) (viscosity: 10,000 mps) and its curing agent were purchased from Jinan Guobang Chemical Co., Ltd., GB-107, Jinan, China. The RTV was subsequently used as the matrix material. A conductive paint pen (6 mL) whose volume resistance is 2.5 $m\Omega/mm^2$ and curing time is 24 h was purchased from Shenzhen Xinwei New Material Co., Ltd., Shenzhen, China. PET tape which was used as a stretchable electrode was purchased from Shenzhen Ausbond Co, Ltd., Shenzhen, China. High temperature resistant PET tape (thickness 60 μm) was used as a substrate to carry the sensors, and fiberglass adhesive tape was used as an insulating material to encapsulate the sensors.

2.2. Equipment

An analytical balance (ME104E/02, Mettler Toledo instruments (Shanghai) Co., Ltd., Shanghai, China) was used to weigh the experimental materials. The conductive fillers were dispersed in anhydrous ethanol using an ultrasonic disperser (FS-100t, Shanghai Shengxi ultrasonic Co., Ltd., Shanghai, China), and the conductive fillers, curing agent, and rubber matrix were evenly mixed with a digital display electric mixer (JB300-SH, Shanghai Specimen and Model Factory, Shanghai, China). After mixing, the conductive rubber composites were vacuumed with a vacuum pump (V-I140SV, Zhejiang Value Mechanical and Electrical Products Co., Ltd., Wenling, China). Then, the conductive rubber composites were spin-coated on the surface of a culture dish with a spin coater (12 A, Zhangqiu Guanpai Electronics Co., Ltd., Zhangqiu, China). A vacuum drying oven (DZF6050, Shanghai YIHENG Technical Co., Ltd., Shanghai, China) was used to provide a curing temperature environment for the conductive rubber composites. A DC power supply (IT6411, Taiwan ADEX Electronics Co., Ltd., Nanjing, China) was used to test the volt-ampere characteristics of the conductive rubber composites. In addition, a desktop digital multimeter (34465 A, Keysight Technologies Co., Ltd., Beijing, China) was used to test the electrical signals of the conductive rubber composites. An electronic universal testing machine (ZQ-990, Zhiqu Precision Instruments Co., Ltd., Dongguan, China) was used for the pressure and stretch test (Supplementary Materials), and a constant temperature heating table with a double digital display (JF-965S, Dongguan Jinfeng Electronics Co., Ltd., Dongguan, China) was used to provide the proper temperature environment. Lastly, a scanning electron microscope (SEM) (S-4800, Hitachi, Ltd., Tokyo, Japan) was used to observe the microstructures of the conductive rubber composites.

2.3. Preparation of the Conductive Rubber Composites

The fabrication process of conductive rubber composite film was shown in Figure 1a. The materials were prepared according to the following steps. First, the weighed conductive fillers were stirred and dispersed in ethanol with a glass rod, the volume of ethanol was 30% of that of the rubber matrix material. Then the conductive fillers were dispersed in an ultrasonic disperser for 1 h. Next, RTV matrix proportional to the conductive filler was added to the beaker and the mixed material was stirred at 300 rpm using an electric stirrer for 30 min. Subsequently, a curing agent with a mass fraction of 5% of the RTV matrix was added and stirred with an electric stirrer at 500 rpm for 30 min. Next, a vacuum pump was used to continuously remove any bubbles at a vacuum degree of −0.09 MPa for 30 min. Then, the liquid mixture was removed with a needle tube and injected into a polytetrafluoroethylene mold or PS culture dish, and then the mixed liquid materials were spin-coated at a speed of 200 rpm for 120 s. Finally, the mixtures were placed in a vacuum drying oven and maintained at 60 °C for 24 h.

Three types of carbon nanomaterials, including zero-dimensional (0-D) CB, 1-D CNT, and 2-D GP, were used as the conductive fillers. Combining various conductive fillers was advantageous, as the percolation threshold of the composite conductive fillers could be effectively reduced [36]. A pre-experiment was conducted to determine the mass ratio of the series of conductive rubber composites, and the quality of conductive filler is 8% of that of RTV matrix. For the conductive rubber composites containing hybrid fillers of CB/GP or

CB/CNT, the mass ratio of total fillers remained unchanged, and the selected mass ratio of CB were: CNT or GP = 1:1, CB: CNT or GP = 2:1, CB: CNT or GP = 3:1. Lastly, seven groups of conductive rubber composites were successfully prepared and tested.

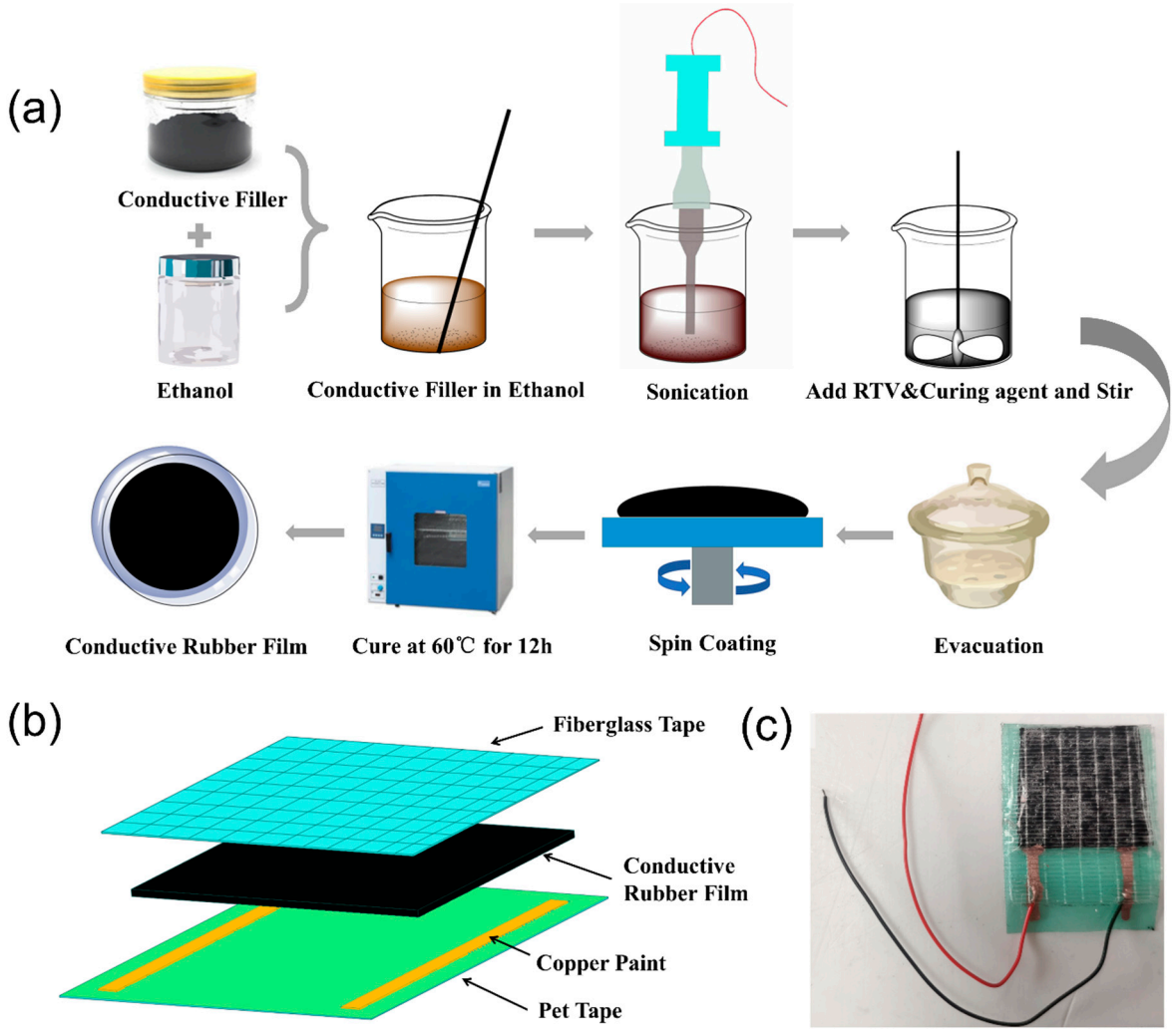

Figure 1. (**a**) Schematic of the conductive rubber composite fabrication process, (**b**) structure of the fabricated stretchable tactile sensor, and (**c**) photograph of the fabricated stretchable tactile sensor.

2.4. Preparation of the Stretchable Tactile Sensor

The stretchable compression and temperature-sensitive sensor developed in this study was assembled layer by layer, and the structure of the stretchable tactile sensor is shown in Figure 1b, while Figure 1c shows a photograph of the sensor. The preparation process of the stretchable compression-sensitive and temperature-sensitive sensor was as follows. First, two parallel conductive paths were drawn on the sticky side of the PET tape using a conductive copper paint pen. Second, 30 × 30 mm conductive composite films were cut and transferred to the side of the PET substrates coated with electrodes. Thirdly, the unfinished sensors were cured in a vacuum oven at 60 °C for 2 h, and then the electronic wires were welded on the cured electrode for testing. Finally, surface packaging was fabricated with fiberglass tape. The stretchable stretch-sensitive sensor was assembled in a similar manner. However, to prevent any effects on the stretch test, the PET tape was only used as the substrate in sections containing electrodes. In addition, the shape of the conductive composite film that was applied to stretch-sensitive sensor was modified, from 30 × 30 × 1 mm to 10 × 50 × 1 mm to obtain a wider deformation range during stretch test. After testing different conductive rubber composites, a stretchable multimodal tactile

sensor with a dual-sensitive layer was assembled. The two conductive rubber composites with temperature and compression sensitivity properties were stacked together to provide mutual insulation and an orthogonal arrangement of the electrodes. This uncomplicated method guaranteed that the input signals were unified while the output signals were processed separately.

2.5. Characterization of the Stretchable Tactile Sensor

The volt-ampere characteristics of sevens conductive composite films with the same shape (10 × 50 × 1 mm) were tested from 0 to 9 V with a DC power supply. The conductivities of conductive rubber composites can be calculated from the volt-ampere characteristic curves.

The mechanical properties were tested using an electronic universal testing machine using dog-bone conductive rubber composites. These samples were prepared with NC machined polytetrafluoroethylene mold to meet the testing standards, and elastic modulus, tensile strength, and elongation at break were measured. Following the GB/T528-2009 standard, the cross-sectional area of the specimens was 4 × 2 mm, with a gauge distance of 25 mm [37–39]. The moving speed of the fixture in the universal testing machine was 50 mm/min until the specimens broke. During the stretch test, three specimens of each conductive rubber composite type were used to ensure the repeatability of the test results. The test devices mainly included loading equipment, a desktop digital multimeter, and a PC. The loading equipment consisted of an electronic universal testing machine and a constant temperature heating table with a double digital display. The electronic universal testing machine was used to obtain the stretch and compressive test results, by replacing the fixture, and the performance of the stretch-sensitive and the compression-sensitive sensor was tested with a desktop digital multimeter and the electronic universal testing machine. To study the response of the stretchable tactile sensor to pulling and pressures, the probes of the digital multimeter were fixed on the universal testing machine fixture, so that they could move synchronously. In the stretch test, both ends of the stretchable tactile sensor were clamped in the jaws of the upper and lower fixtures. In the compression test, the sensor was fixed on the lower round flat top portion of the electronic universal testing machine fixture. The electronic wires welded on the electrodes were then connected with the probes from a digital multimeter. The four-wire resistance method was used to eliminate the effects of contact resistance. When applying compression or stretch to the sensor, the resistance changes in the sensor were recorded by the digital multimeter. During the stretch test, the loading speed of the stretch stroke was 2 mm/min [37], and when the strain approached the elongation at break, the fixture returned automatically at a speed of 5 mm/min. During compression testing, the loading speed of the compression stroke was 0.5 mm/min [38], and when the pressure was greater than 110 kPa, the fixture returned automatically at a speed of 100 mm/min. The sampling interval of the desktop digital multimeter was 0.01 s.

For the temperature-sensitive property measurements, the sensor was fixed to the surface of the constant temperature heating table, and sensor resistance changes were recorded by the digital multimeter. Starting from 30 °C, the temperature varied at intervals of 5 °C [32]. The resistance was tested three times and the average resistance was recorded, and the sampling interval of the desktop digital multimeter was 0.01 s. The cross-sectional morphologies of the conductive rubber composites were observed with a scanning electron microscope. To inspect the dispersion quality of the conductive fillers, the cross-sections of the conductive composites were magnified by 20,000× and 50,000× at 3–5 kV accelerating voltage.

3. Results and Discussion

3.1. Morphology of Conductive Rubber Composites

Figure 2 depicts the cross-section scanning electron microscopy (SEM) micrographs of the conductive rubber composites, showing that the conductive fillers were well-dispersed

in the RTV matrix and formed conductive pathways which, indicated by blue arrows in the Figure 2a,b, show the SEM micrographs of the pure silicone rubber and conductive silicone rubber filled with CB, respectively. Figure 2c,d shows the SEM micrographs of the conductive rubber composites containing the CB/CNT and CB/GP hybrid fillers, respectively.

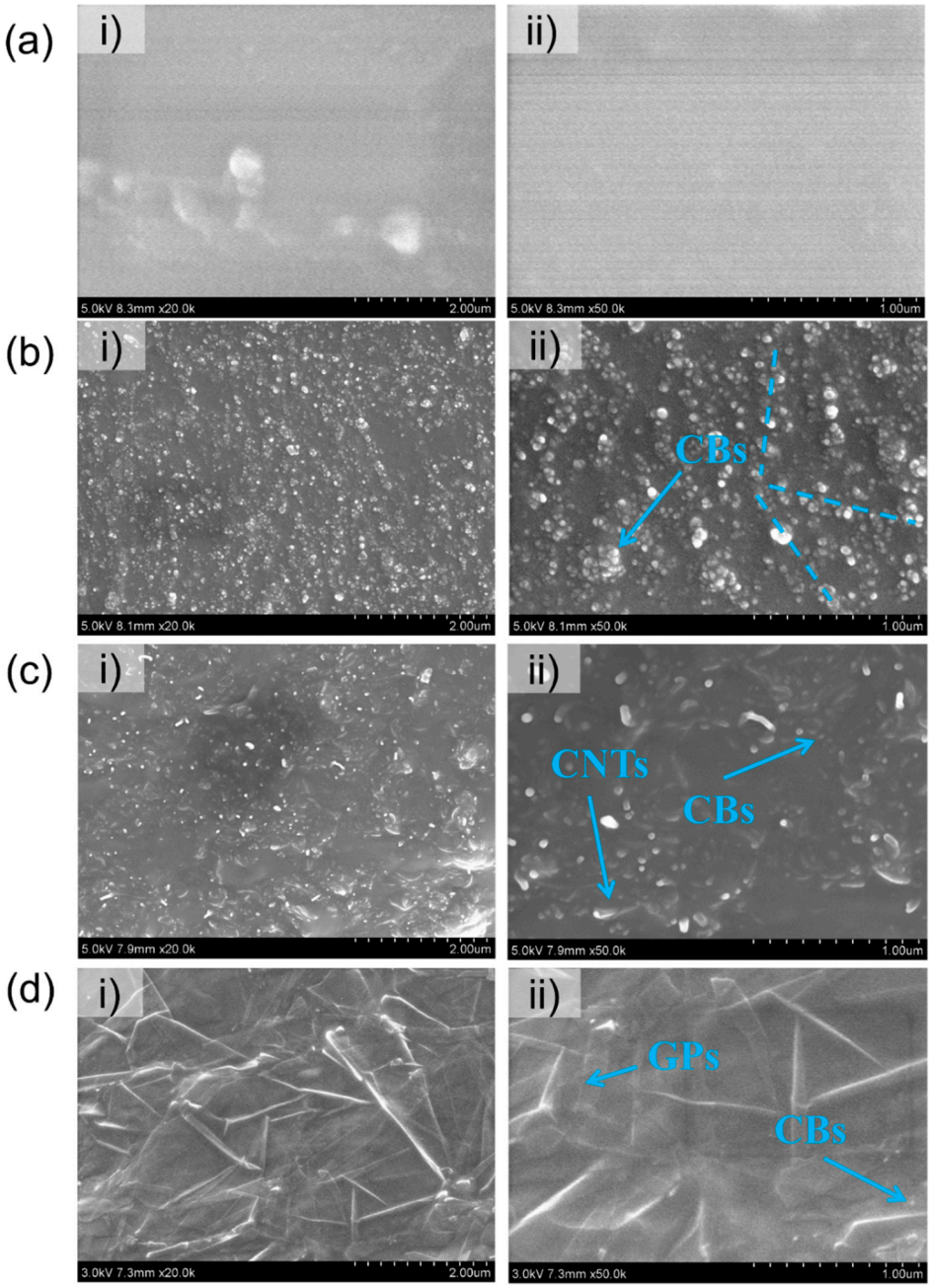

Figure 2. (**a**) SEM micrographs of RTV films of 20,000× (**i**) and 50,000× (**ii**) magnification, (**b**) SEM micrographs of CB-embedded composites films at 20,000× (**i**) and 50,000× (**ii**) magnification, (**c**) SEM micrographs of the CB/CNT-embedded composites films at 20,000× (**i**) and 50,000× (**ii**) magnification, (**d**) SEM micrographs of the CB/GP-embedded composites films at 20,000× (**i**) and 50,000× (**ii**) magnification.

3.2. Mechanical Properties and Conductivities of Conductive Rubber Composites

The volt-ampere characteristics of the seven conductive rubber composites are shown in Figure 3a. According to a previous study [36], the percolation threshold of the carbon-based conductive filler was approximately 5–8 wt%. The rubber transformed into the

conductive rubber composites when the conductive filler concentration exceeded the percolation threshold, and the conductive fillers overlapped and made contact with each other throughout the matrix [40–42].

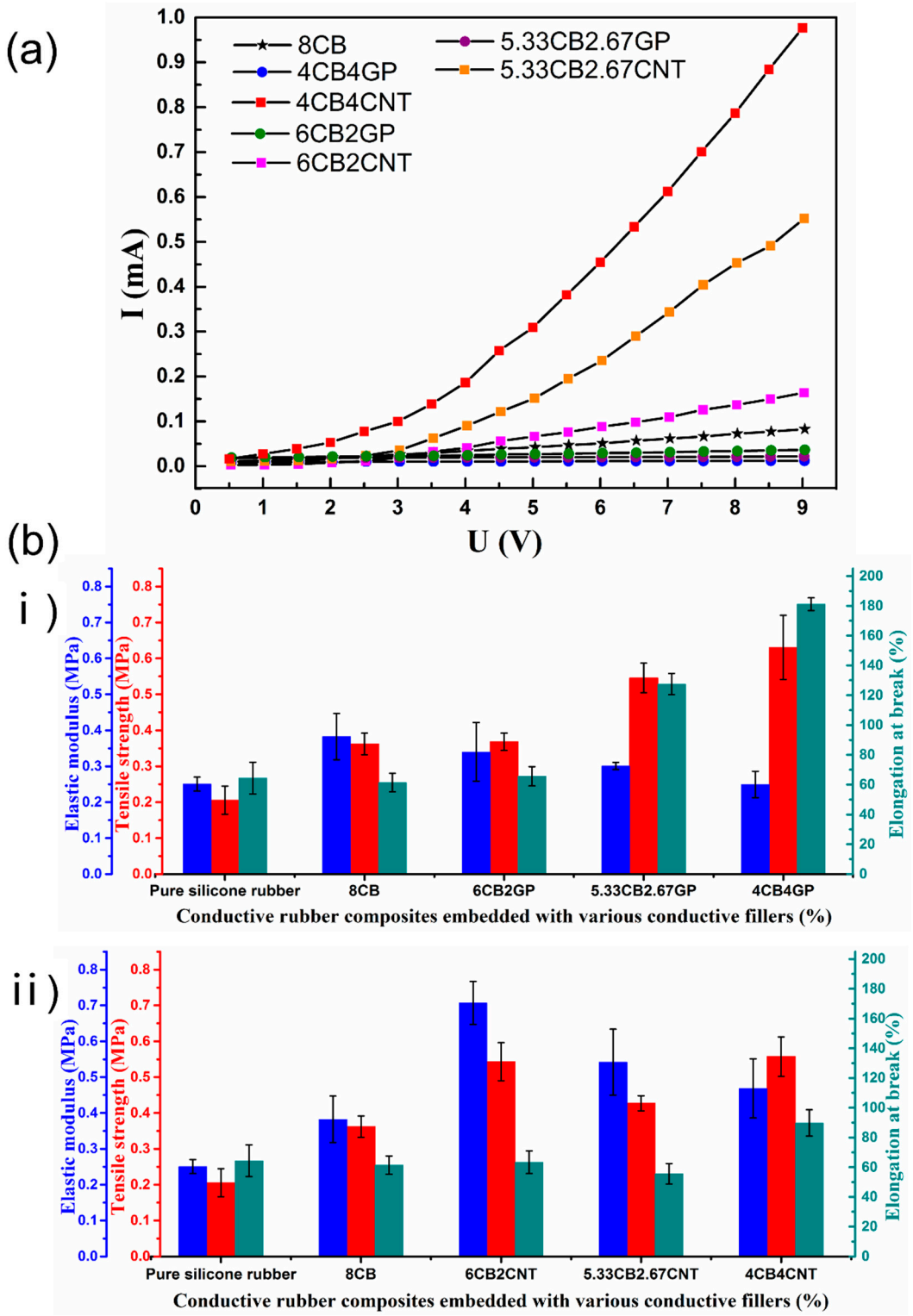

Figure 3. (**a**) Volt-ampere characteristics of the conductive rubber composites embedded with various conductive fillers, and (**b**) mechanical properties including the elastic modulus, tensile strength, and elongation at break of the conductive rubber composites embedded with CB/GP (**i**) and CB/CNT (**ii**).

The experimental results showed that CNT greatly improved the conductivity of the CB-embedded composites. When the mass ratio of CB and CNT was 1:1, the conductivity was more than 20 times that of the non-CNT-embedded composites. This was due to the high aspect ratio of CNT, which could effectively form overlapping conductive paths, and led to the synergistic effect of high conductivity at a low mass fraction of conductive fillers [41]. However, the embedded GP did not significantly affect the conductivity of the CB-embedded composites, which was possibly caused by the poor conductivity of GP embedded in the RTV matrix, and it is less able to disperse in the material compared with CNT [42].

The elastic modulus, tensile strength, and elongation at break of the conductive rubber composites with various mass ratios are shown in Figure 3b. Compared with the original rubber material, the tensile strength and elastic modulus of the conductive rubber composites increased with the introduction of CB. In addition, the tensile strength and elastic modulus of the conductive rubber composites further improved with the continuous addition of CNT. The tensile strength and elastic modulus increased by about 50% at the peak (CB:CNT = 3:1), and the elongation at break of the CB-embedded composites increased by 50% when the mass ratio of CNT and CB was 1:1. With continuous addition of GP, the elastic modulus decreased by 35% (CB:GP = 1:1); however, the tensile strength and elongation at break increased by 75% and 200% at the peak (CB:GP = 3:1), respectively. The high tensile strength was attributed to the reinforcement of the conductive fillers, which effectively transferred the load between the carbon nanomaterials.

L. Valentini et al. prepared ethylene-propylene-diene terpolymer rubber (EPDM)-based nanocomposites containing carbon black (CB), graphene nanoplatelets (GNPs), and mixtures of the two fillers [43]. They found that CB or silica when added to elastomers create a modulus that increases with strain. Besides, the sample EPDM-6 (i.e., 2 wt% of GNPs and 24 wt% of CB) showed a higher increment of the maximum strength along with a higher elongation at break with respect to the EPDM/CB blends. Unlike this study, the elongation at break of the sample EPDM-6 (i.e., 2 wt% of GNPs and 24 wt% of CB) is less than the sample EPDM without any fillers. This may relate to the fact that too much filler affects the good flexibility of EPDM. In another study, Md Najib Alam et al. explored the dispersion and reinforcement performance of binary fillers in natural rubber [44]. They found that binary fillers with a 1:1 ratio of silica to graphite powder provide excellent mechanical performance. Moreover, thermal oxidative aging resistance properties compared with single fillers and the binary filler system at only 20 phr of filler content shows an improved modulus and stress-at-break of approximately 110% and 15%, respectively, compared with the unfilled rubber vulcanizate. Their study also shows that the synergistic effect brought by various fillers is worthy of attention.

3.3. Characterization of Stretchable Tactile Sensors

3.3.1. Stretch and Compression-Sensitive Properties

Lastly, the stretch-sensitive and compression-sensitive characteristics of the materials were tested. Relative changes in resistance ($\Delta R/R_0$) were obtained as the output signal of the sensor, and the stimulus was the pressure or strain provided by the universal testing machine. The gauge factor (GF) was used to evaluate the sensitivity, as it is considered one of the most important sensor performance parameters. The GF of stretch-sensitive characteristic was defined as: GF = $(\Delta R/R_0)/\Delta\varepsilon$, and the GF of compression -sensitive characteristic was defined as: GF = $(\Delta R/R_0)/\Delta P$, where $\Delta R/R_0$ is the real-time relative change in resistance, R_0 is the initial resistance, R is the real-time resistance, ε is the strain, and P is the pressure [5]. The experimental stretch and compression sensitivity results of the fabricated sensors are shown in Figure 4.

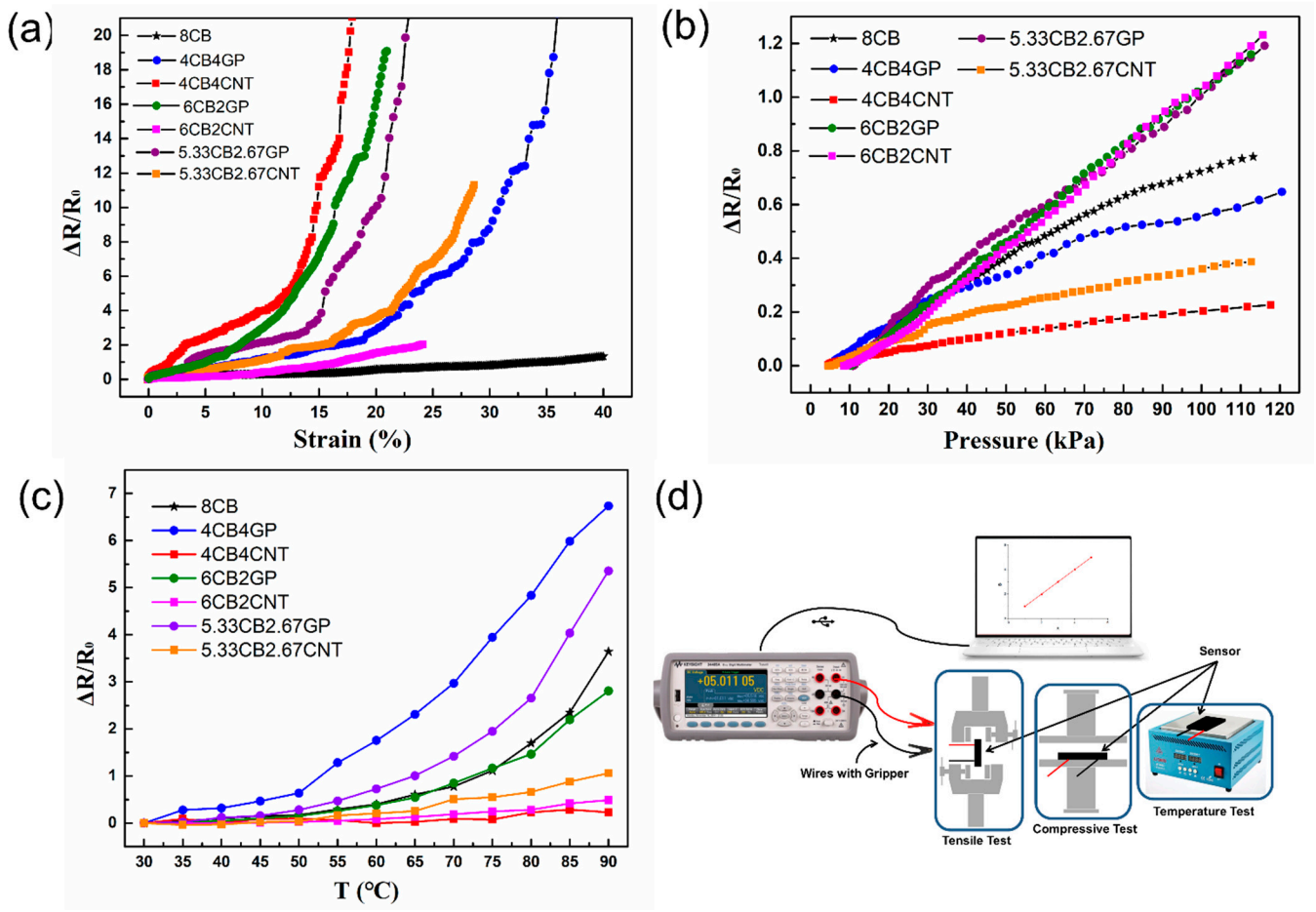

Figure 4. The test results and schematic of the test devices, showing the relative resistance changes in the conductive rubber composite stretchable tactile sensors with various material mass ratios as a function of strain (**a**) and pressure (**b**), and (**c**) relative changes in the resistance of the stretchable tactile sensors as a function of temperature, and (**d**) schematic of the test devices.

Figure 4a shows the relative resistance changes due to stretch. According to the stretch test results, GF showed a sharp increase with increased strain, which indicated that the sensitivity was dependent on strain. It is found that the sensitivity was higher when the strain was higher. This was attributed to the conductive paths, which were significantly reduced with maximum strain and when cracks appeared in the material [45]. With increased strain, the possibility of irreversible damage also increased. Therefore, GF was calculated in different strain ranges with good linearity. For example, the GF of 4CB4CNT-RTV was 37.45 (0–12%) and 247.54 (12–20%), and the linear fitting results of 4CB4GP-RTV showed that the GF in the linear range was 12.03 (0–20%) and 81.68 (20–35%). The GF of 5.33CB2.67CNT-RTV was 14.73 (0–20%) and 84.56 (20–30%), and the GF of 5.33CB2.67GP-RTV was 20.39 (0–15%) and 115.99 (15–20%). The GF of 6CB2CNT-RTV was 4.54 (0–15%) and 13.65 (15–25%), the GF of 6CB2GP-RTV was 25.11 (0–10%) and 129.81 (10–20%), and the GF of 8CB-RTV was 2.63 (0–40%). In conclusion, the GF values of the stretchable tactile sensors prepared in this study were 2–40 under low strain and 80–250 under high strain, and these values were similar to the reported results [45,46].

Figure 4b shows the pressure response curves of the sensors. The results of the compression test showed that most sensors exhibited excellent linearity. As shown in Figure 4b, the relative change in sensor resistance increased when exposed to pressure. According to the test results, the fabricated sensors exhibited excellent linearity for most samples. The GF of sensors based on different materials was also calculated. The data of 4CB4CNT-RTV showed that the GF in the linear range was 0.00204 kPa^{-1}. The GF of

4CB4GP-RTV was 0.00577 kPa^{-1}. The GF of 5.33CB2.67CNT-RTV was 0.00 401 kPa^{-1}, and the GF of 5.33CB2.67GP-RTV was 0.01097 kPa^{-1}. In addition, the GF of 6CB2CNT-RTV was 0.01171 kPa^{-1}, the GF of 6CB2GP-RTV was 0.01161 kPa^{-1}, and the GF of 8CB-RTV was 0.00803 kPa^{-1}. In conclusion, the GF values of the conductive rubber composite stretchable tactile sensors under compression were 0.00204–0.01171 kPa^{-1}, and these values were higher than the reported results [47,48].

3.3.2. Temperature-Sensitive Properties

Temperature is also important in tactile property and temperature-sensing is essential for many systems. The temperature test results from this study are shown in Figure 4c. Similarly, the GF for temperature sensitivity was defined as the ratio of relative change in resistance to the temperature: GF = $(\Delta R/R_0)/\Delta T$, where $\Delta R/R_0$ is the relative change in resistance, R_0 is the initial resistance, R is the real-time resistance, and T is the temperature [49,50]. The resistance of the stretchable tactile sensor changed with increasing temperature according to the temperature resistance data. In this study, 4CB4GP-RTV and 5.33CB2.67GP-RTV exhibited higher sensitivities according to the test results. The GF of 4CB4GP-RTV was 2.92%/°C (30–50 °C), 11.39%/°C (50–70 °C), and 19.14%/°C (70–90 °C). The GF of 5.33CB2.67GP-RTV was 1.39%/°C (30–50 °C), 5.62%/°C (50–70 °C) and 19.91%/°C (70–90 °C), which was higher than commercial platinum temperature sensors (0.39%/°C). The test results showed that the temperature sensors fabricated in this study had excellent temperature-sensitive characteristics, and the GF values of the CB-embedded conductive rubber composite were 0.89%/°C (30–50 °C), 3.06%/°C (50–70 °C), and 13.92%/°C (70–90 °C). In contrast, the temperature sensitivity of the conductive rubber composites containing hybrid CNT/CB fillers was low. These results showed that the temperature sensitivity of the conductive rubber composites with synergistic effects should be considered according to different situations. Thus, embedded CNTs can inhibit the positive temperature effect of conductive rubber composites, and an increasing quantity of CNTs causes a more obvious effect. However, embedded GP can enhance the positive temperature effect of the conductive rubber composites. Thus, with increasing GP mass ratio, the positive temperature effect of the conductive rubber composites significantly improved.

This work showed that the sensitive characteristics of the conductive rubber composites embedded with hybrid conductive fillers differed from those only embedded with CB. In addition, compared with the CB-embedded conductive rubber composites, the CNT/CB-embedded and GP/CB-embedded conductive rubber composites had higher GF values and a wider linear range in stretch and compression tests. The excellent sensitive characteristics of the conductive rubber composites containing hybrid conductive fillers may thus be related to the improved mechanical properties and observed synergistic effects.

In general, the results showed that the synergistic effect significantly impacted the sensitive characteristics of the conductive rubber composites, which can benefit the design and preparation of stretchable multimodal tactile sensors. The results also showed that the sensitivity and linearity of 5.33CB2.67GP-RTV were excellent, especially in the stretch, compression, and temperature tests. However, 6CB2CNT-RTV only exhibited better sensitivity characteristics in compression. To differentiate the functionalities of the two sensitive layers, these two materials were further studied in subsequent experiments.

The tensile, compression and temperature sensitivities of conductive rubber composites with different material ratios in the work are summarized in Table 1.

Table 1. Sensitivities of conductive rubber composites with different material ratios.

Conductive Rubber Composites	Temperature Sensitivity	Stretch Sensitivity	Compression Sensitivity
8CB-RTV	0.89%/°C (30–50 °C) 3.06%/°C (50–70 °C) 13.92%/°C (70–90 °C)	2.63 (0–40%)	0.803% kPa^{-1}
6CB2CNT-RTV		4.54 (0–15%) 13.65 (15–25%)	1.171% kPa^{-1}
6CB2GP-RTV		25.11 (0–10%) 129.81 (10–20%)	1.161% kPa^{-1}
5.33CB2.67CNT-RTV		14.73 (0–20%) 84.56 (20–30%)	0.401% kPa^{-1}
5.33CB2.67GP-RTV	1.39%/°C (30–50 °C) 5.62%/°C (50–70 °C) 19.91%/°C (70–90 °C)	20.39 (0–15%) 115.99 (15–20%)	1.097% kPa^{-1}
4CB4CNT-RTV		37.45 (0–12%) 247.54 (12–20%)	0.204% kPa^{-1}
4CB4GP-RTV	2.92%/°C (30–50 °C) 11.39%/°C (50–70 °C) 19.14%/°C (70–90 °C)	12.03 (0–20%) 81.68 (20–35%)	0.577% kPa^{-1}

3.3.3. Sensing Properties Stability

The repeatability and reproducibility of stretchable tactile sensors are important factors that need to be considered for practical use. As shown in Figure 5, the stretchable 5.33CB2.67GP-RTV and 6CB2CNT-RTV tactile sensors were tested 500 times under stretch and 1500 times under compression cyclic loading-unloading [51,52]. The maximum strain load was 30% and the maximum pressure load was 50 kPa. Additionally, the speed of the stretch and compression strokes were 50 and 5 mm/min, respectively, and the output signal was the resistance of the sensors. When subjected to cyclic loading-unloading, the stretchable tactile sensors showed a drift in electrical signals. Specifically, the average resistance of sensors decreased with an increasing number of stretch loading-unloading cycles, and increased with increasing compressive loading-unloading cycling. This phenomenon was more noticeable in the curves for the 5.33CB2.67GP-RTV-based sensors. The results also indicated that the fatigue properties of the CNT-embedded conductive rubber composites were better than the GP-embedded conductive rubber composites. Thus, the sensors showed good repeatability and few variations after 1000 loading-unloading cycles.

3.3.4. Sensing Mechanism

The cause of conductive rubber composites resistance changes under external stimuli has been studied by researchers [53–55], and resistance increases with loading and decreases with unloading proportionally, which is known as the positive force effect. The positive force effect occurs due to the disassembly and reassembly of the conductive paths. When an external force is applied, the conductive paths is destroyed due to the deformation of the conductive rubber composites. However, when the applied load is removed, the conductive rubber composites recover their shape and the conductive paths reassemble. We observed that the resistance of the sensors fabricated in this work increased with increasing stretch and compression, indicating that the results of the study followed this principle.

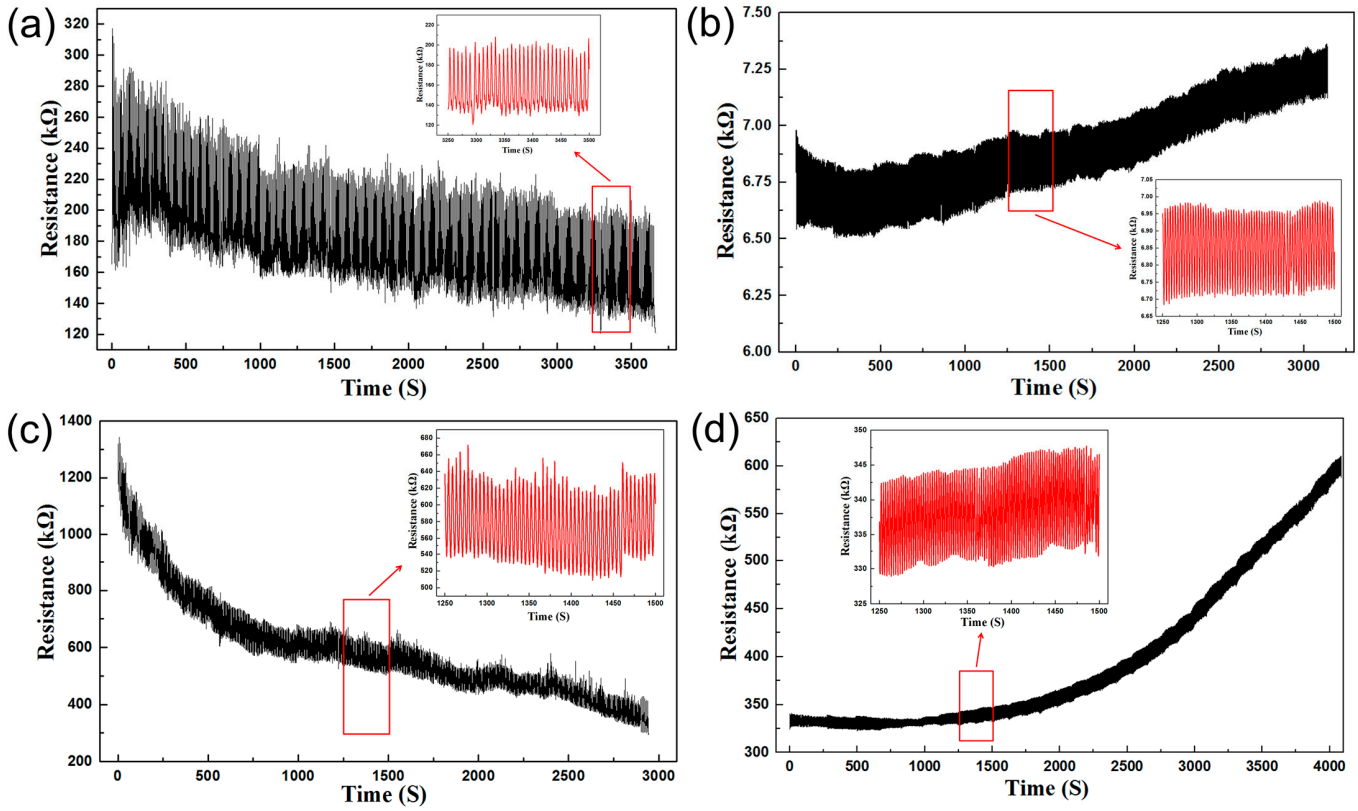

Figure 5. Repeatability tests of the stretchable tactile sensors based on 6CB2CNT-RTV under stretch (500 times) (**a**) and compression (1500 times) (**b**) cyclic loading-unloading. Repeatability testing of the stretchable tactile sensors based on 5.33CB2.67GP-RTV was conducted 500 times stretch (**c**) and 1500 times for compression (**d**) cyclic loading-unloading.

The influence of temperature on the conductive rubber composites was divided into positive temperature and negative temperature effects. The phenomenon where conductive rubber composites resistance increases with rising temperature is called the positive temperature effect. This is in contrast to the phenomenon known as the negative temperature effect. The mechanism of the positive temperature effect is due to the increase in temperature, where the polymer crystalline phase melts and expands, which increases the distance between the conductive filler particles. Hence, the resistance of the conductive rubber composites increased. The negative temperature effect occurred due to the increase in electron transitions with increasing temperature. According to the literature, the type and quantity of conductive fillers will significantly affect the dominant temperature effect in the conductive rubber composites [55]. Most sensors fabricated in this paper exhibited the positive temperature effect, which may be due to the high concentration of conductive particles. Moreover, adding GP to CB-embedded rubber composites leads to a more obvious temperature effect, while adding CNT to CB-embedded rubber composites leads to the opposite result. The experimental results in this paper verify the principle of temperature effect.

3.4. Preparation and Testing of the Stretchable Multimodal Tactile Sensor

According to the experimental results, the mass ratio of the material affects the sensitive characteristics of the conductive rubber composites. In this study, 5.33CB2.67GP-RTV and 6CB2CNT-RTV were used to fabricate the stretchable multimodal tactile sensors. Multimodal stretchable tactile sensors with dual-sensitive layers were fabricated by stacking the composites films, and the signals from the sensor units were sent out and analyzed separately. The stretchable multimodal tactile sensor in this study can simultaneously measure pressure and temperature.

As shown in Figure 6, the sensitive characteristics of the two sensor units were tested and recorded simultaneously. As shown in Figure 6a,b, the test was carried out under different temperature gradients, and the results showed that with increasing temperature, the sensitivity of 5.33CB2.67GP-RTV increased. The positive temperature effect of 5.33CB2.67GP-RTV was more noticeable than 6CB2CNT-RTV. The seven resistance-pressure curves of 6CB2CNT-RTV between 30 and 80 °C crossed each other in the low temperature range, while the resistance of 5.33CB2.67GP-RTV increased steadily with increasing temperature. No cross phenomenon was observed in the resistance-pressure curves of 5.33CB2.67GP-RTV. In addition, the curve for 90 °C was far from the other curves because the resistance increased sharply with increasing temperature.

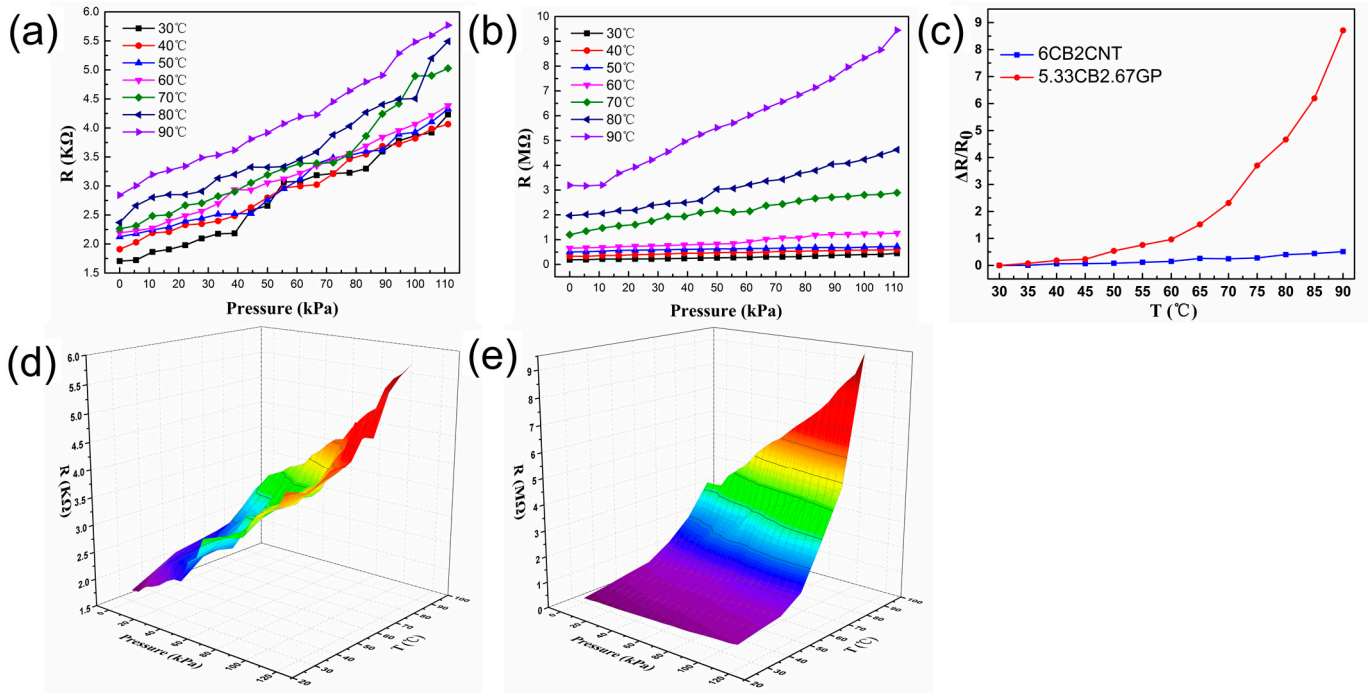

Figure 6. Changes in resistance of the 5.33CB2.67GP-RTV (**a**) and 6CB2CNT-RTV (**b**) sensor units as a function of pressure under different temperature gradients, (**c**) relative changes in resistance of the stretchable multimodal tactile sensor based on 5.33CB2.67GP-RTV and 6CB2CNT-RTV as a function of temperature, where the 3D surfaces were used to comprehensively illustrate the changes in resistance of the sensor units based on 5.33CB2.67GP-RTV (**d**) and 6CB2CNT-RTV (**e**).

As shown in Figure 6a, the GF values of the curves were 0.0198–0.0252 kPa^{-1}, and the GF values of the curves shown in Figure 6b were 0.0018–0.0549 kPa^{-1}. Compared with the stretchable tactile sensors with a single sensitive layer, the sensitivity of the 6CB2CNT-RTV sensor improved, while the GF of the 5.33CB2.67GP-RTV sensor fluctuated more than the 6CB2CNT-RTV sensor. This was due to the multilayer structure of the stretchable multimodal tactile sensor and the asymmetrical upper and lower arrangement of the electrodes. To observe the resistance changes in the stretchable multimodal tactile sensor under different stimuli, the 3D surfaces were used to illustrate the sensitivity characteristics of the stretchable multimodal tactile sensor, as shown in Figure 6d,e.

The temperature test results are shown in Figure 6c, which indicated better temperature sensitivity of 5.33CB2.67GP-RTV compared with 6CB2CNT-RTV. The GF values of 5.33CB2.67GP-RTV were 2.46%/°C (30–50 °C), 8.62%/°C (50–70 °C), 30.56%/°C (70–90 °C). The temperature sensitivity improved in each temperature range, which was possibly due to the multilayer structure, reduced heat loss. Additionally, 5.33CB2.67GP-RTV was located in the lower layer and thus closer to the heating table.

We found that the resistance of the stretchable multimodal tactile sensor was affected by both pressure and temperature, and the stretchable multimodal tactile sensor can effectively monitor pressure and temperature simultaneously. Thus, similar methods may be used to prepare stretchable tactile multimodal sensors that sense stretch and temperature simultaneously.

4. Signal Processing Circuit and Sensing Test

To further validate the compression and temperature monitoring functionality of the multimodal tactile sensors, a scene verification experiment was conducted. In this experiment, an Arduino UNO board was used to convert the resistance of the sensor units into a voltage signal, according to the voltage division principle. Afterward, resistance was calculated and output in real-time from the Arduino IDE to the PC, using a serial plotter. In the resistance test program, an Arduino IDE multithreading library scoop was used to establish the two-child thread algorithms to complete the simultaneous testing of the two sensor units. The formula for the voltage division principle was: $U_{out} = (U_{in} \times R_2)/(R_1 + R_2)$, where U_{in} is the input voltage, U_{out} is the output voltage, R_1 is the reference resistance, and R_2 is the resistance to be tested. The input voltage U_{in} was set to 5 V and R_2 was calculated based on the output voltage U_{out} and the known R_1. Therefore, R_2 was the real-time resistance of the sensor unit.

Figure 7a shows a photograph of the signal processing circuit of the stretchable multimodal tactile sensor, and Figure 7b shows the measured resistance based on the voltage division principle. The experimental signals were input into the PC through a USB cable, and then the electric signal curves were displayed on the PC in real-time. As shown in Figure 7c, the two real-time curves of the sensor units were observed in the window of the Arduino IDE serial plotter. The first peak was the change in the signal due to pressing of the sensor with a finger and then releasing it quickly. The second peak was the change in the signal when a cup filled with 90 °C hot water was placed on the surface of the sensor for 30 s and then moved away. The response amplitude of the two sensing units caused by temperature and pressure stimulation is different, and the response time of the two signals is significantly different. These measurement results further showed that our stretchable multimodal tactile sensor can simultaneously measure pressure and temperature and distinguish different stimuli. Therefore, this sensor holds potential for multi tactile parameters perception applications.

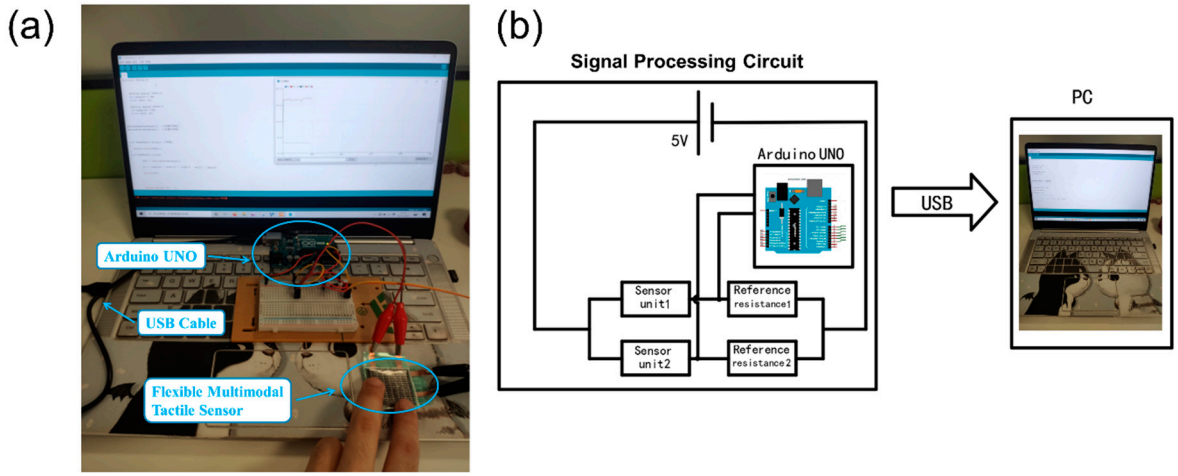

Figure 7. *Cont.*

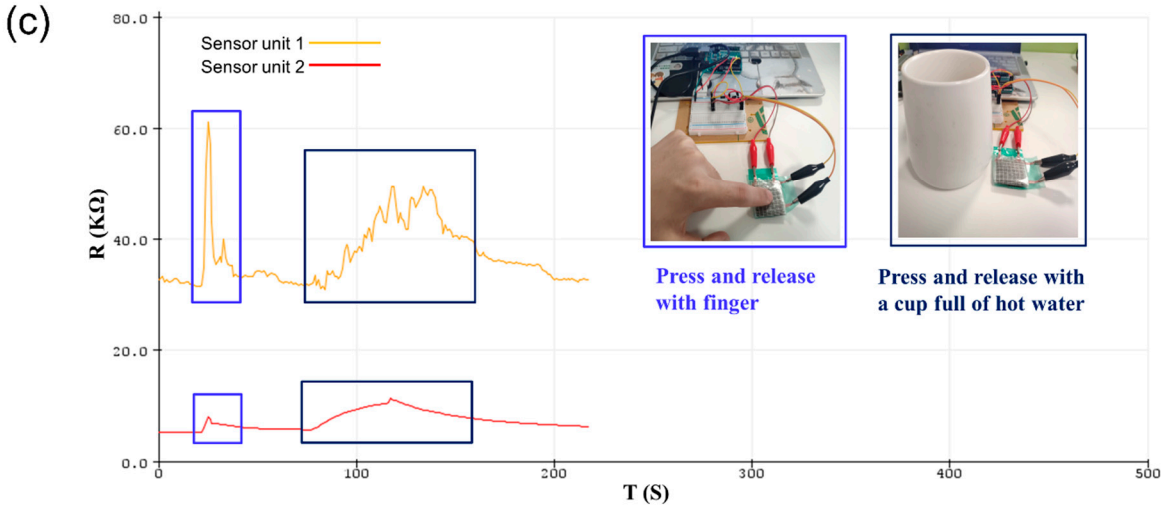

Figure 7. (**a**) Photograph of the signal processing circuit of the stretchable multimodal tactile sensor, (**b**) schematic of the signal processing circuit, and (**c**) real-time relative changes in resistance of the stretchable multimodal tactile sensor for monitoring finger pressing and pressing by a cup filled with hot water.

5. Conclusions

In this work, stretchable and flexible conductive rubber composites with force-sensitive and temperature-sensitive properties were fabricated, and we studied the mechanical and electrical properties of the conductive filler embedded with conductive rubber composites. The elastic modulus of the conductive rubber composites improved by 184% after embedding with conductive fillers, and the elongation at break and tensile strength both improved by 182% and 206%, respectively. Thus, our conductive rubber composites have potential for academic research and industrial applications as stretchable and flexible stretch, compression, and temperature sensors. Finally, a stretchable multimodal tactile sensor with high sensitivity and a large measurement range was manufactured.

The developed stretchable tactile sensor exhibited compression sensitivity values of 0.00204–0.01171 kPa^{-1} and stretch sensitivity of 2.63–37.45. The best temperature sensitivity values of the conductive rubber composites were 2.92%/°C (30–50 °C), 11.39%/°C (50–70 °C), and 19.14%/°C (70–90 °C). The test results of the stretchable multimodal tactile sensor showed that the temperature sensitivity results of the sensor unit with the best performance were 2.46%/°C (30–50 °C), 8.62%/°C (50–70 °C), and 30.56%/°C (70–90 °C). The results thus showed that the stretchable multimodal tactile sensor fabricated in this study can simultaneously monitor pressure and temperature. In addition, the signals were stable and did not interfere with each other, and the fabricated stretchable multimodal tactile sensor in the study did not require complex signal processing or a transmission circuit system.

In summary, conductive rubber composites were prepared by embedding hybrid conductive fillers, and a stretchable multimodal tactile sensor based on conductive rubber composites was developed via a simple fabrication process. The sensitive characteristics of the conductive rubber composites were tuned by embedding different carbon nanomaterials. The conductive composite stretchable multimodal tactile sensor exhibited high sensitivity and a wide measurement range for sensing pressure and temperature. Furthermore, the cyclic loading-unloading tests showed that the tactile sensor was reliable and durable. Therefore, this material can be used in various fields such as human-machine interfaces in intelligent automobiles, stretchable smart robots, and wearable medical devices.

Supplementary Materials: The following supporting information can be downloaded at: https://www.mdpi.com/article/10.3390/polym14071294/s1, Video S1: Pressure Test; Video S2: Stretch Test.

Author Contributions: Conceptualization, B.Z. and Z.Q.; methodology, C.M.; software, C.M.; validation, B.Z., Z.Q. and L.R.; formal analysis, Z.Q.; investigation, C.M.; resources, Z.Q.; data curation, C.M.; writing—original draft preparation, C.M.; writing—review and editing, Z.Q.; visualization, H.Y.; supervision, L.R.; project administration, Z.Q.; funding acquisition, B.Z. All authors have read and agreed to the published version of the manuscript.

Funding: This work was supported by the project of National Natural Science Foundation of China (No. 52175270, 91848204, 52172386, 51775235).

Institutional Review Board Statement: Not applicable.

Informed Consent Statement: Not applicable.

Data Availability Statement: The data used to support the findings of this study are available from the corresponding author upon request.

Acknowledgments: We also thank Suqian Ma for the discussion and advice of the experiment.

Conflicts of Interest: The authors declare that they have no known competing financial interest or personal relationships that could have appeared to influence the work reported in this paper.

References

1. Yang, J.C.; Mun, J.; Kwon, S.Y.; Park, S.; Bao, Z.; Park, S. Electronic Skin: Recent Progress and Future Prospects for Skin-Attachable Devices for Health Monitoring, Robotics, and Prosthetics. *Adv. Mater.* **2019**, *31*, e1904765. [CrossRef] [PubMed]
2. Yetisen, A.K.; Martinez-Hurtado, J.L.; Ünal, B.; Khademhosseini, A.; Butt, H. Wearables in Medicine. *Adv. Mater.* **2018**, *30*, 1706910. [CrossRef] [PubMed]
3. Gao, Y.; Yu, L.; Yeo, J.C.; Lim, C.T. Stretchable Hybrid Sensors for Health Monitoring: Materials and Mechanisms to Render Wearability. *Adv. Mater.* **2020**, *32*, e1902133. [CrossRef] [PubMed]
4. Noh, J.S. Conductive Elastomers for Stretchable Electronics, Sensors and Energy Harvesters. *Polymer* **2016**, *8*, 123. [CrossRef] [PubMed]
5. Chen, H.; Lv, L.; Zhang, J.; Zhang, S.; Xu, P.; Li, C.; Zhang, Z.; Li, Y.; Xu, Y.; Wang, J. Enhanced Stretchable and Sensitive Strain Sensor via Controlled Strain Distribution. *Nanomaterials* **2020**, *10*, 218. [CrossRef]
6. Gao, M.; Xia, Z.; Wang, X.; Wang, J.; Huang, P. Fabrication of a stretchable capacitor sensor with surface-fabric-structured conductive silicon rubber. *Sens. Actuators A* **2019**, *295*, 141–150. [CrossRef]
7. Kou, H.; Zhang, L.; Tan, Q.; Liu, G.; Lv, W.; Lu, F.; Dong, H.; Xiong, J. Wireless stretchable pressure sensor based on micro-patterned Graphene/PDMS composite. *Sens. Actuators A* **2018**, *277*, 150–156. [CrossRef]
8. Yamashita, T.; Takamatsu, S.; Okada, H.; Itoh, T.; Kobayashi, T. Development of Stretchable Piezoelectric Strain Sensor Array. *Electr. Eng. Jpn.* **2018**, *204*, 52–58. [CrossRef]
9. Wu, S.; Peng, S.; Wang, C.H. Stretchable strain sensors based on PDMS composites with cellulose sponges containing one- and two-dimensional nanocarbons. *Sens. Actuators A* **2018**, *279*, 90–100. [CrossRef]
10. Pyo, S.; Lee, J.; Kim, W.; Jo, E.; Kim, J. Multi-Layered, Hierarchical Fabric-Based Tactile Sensors with High Sensitivity and Linearity in Ultrawide Pressure Range. *Adv. Funct. Mater.* **2019**, *29*, 1902484. [CrossRef]
11. Huang, Z.; Gao, M.; Yan, Z.; Pan, T.; Khan, S.A.; Zhang, Y.; Zhang, H.; Lin, Y. Pyramid microstructure with single walled carbon nanotubes for stretchable and transparent micro-pressure sensor with ultra-high sensitivity. *Sens. Actuators A* **2017**, *266*, 345–351. [CrossRef]
12. Liu, Y.; Tao, L.-Q.; Wang, D.-Y.; Zhang, T.-Y.; Yang, Y.; Ren, T.-L. Stretchable, highly sensitive pressure sensor with a wide range based on graphene-silk network structure. *Appl. Phys. Lett.* **2017**, *110*, 123508. [CrossRef]
13. Fu, Y.F.; Yi, F.L.; Liu, J.R.; Li, Y.Q.; Wang, Z.Y.; Yang, G.; Huang, P.; Hu, N.; Fu, S.Y. Super soft but strong E-Skin based on carbon fiber/carbon black/silicone composite: Truly mimicking tactile sensing and mechanical behavior of human skin. *Compos. Sci. Technol.* **2020**, *186*, 107910. [CrossRef]
14. Kim, H.-J.; Thukral, A.; Yu, C. Highly Sensitive and Very Stretchable Strain Sensor Based on a Rubbery Semiconductor. *ACS Appl. Mater. Interfaces* **2018**, *10*, 5000–5006. [CrossRef]
15. Oh, J.H.; Woo, J.Y.; Jo, S.; Han, C.-S. Pressure-conductive rubber sensor based on liquid-metal-PDMS composite. *Sens. Actuators A* **2019**, *299*, 111610. [CrossRef]
16. Wang, S.; Zhang, X.; Wu, X.; Lu, C. Tailoring percolating conductive networks of natural rubber composites for stretchable strain sensors via a cellulose nanocrystal templated assembly. *Soft Matter* **2016**, *12*, 845–852. [CrossRef] [PubMed]
17. Tas, M.O.; Baker, M.A.; Masteghin, M.G.; Bentz, J.; Boxshal, K.; Stolojan, V. Highly Stretchable, Directionally Oriented Carbon Nanotube/PDMS Conductive Films with Enhanced Sensitivity as Wearable Strain Sensors. *ACS Appl. Mater. Interfaces* **2019**, *11*, 39560–39573. [CrossRef] [PubMed]

18. Jeon, D.-Y.; Kim, H.; Lee, M.W.; Park, S.J.; Kim, G.-T. Piezo-impedance response of carbon nanotube/polydimethylsiloxane nanocomposites. *APL Mater.* **2019**, *7*, 041118. [CrossRef]
19. Jian, M.; Xia, K.; Wang, Q.; Yin, Z.; Wang, H.; Wang, C.; Xie, H.; Zhang, M.; Zhang, Y. Stretchable and Highly Sensitive Pressure Sensors Based on Bionic Hierarchical Structures. *Adv. Funct. Mater.* **2017**, *27*, 1606066. [CrossRef]
20. Kang, D.; Pikhitsa, P.V.; Choi, Y.W.; Lee, C.; Shin, S.S.; Piao, L.; Park, B.; Suh, K.Y.; Kim, T.I.; Choi, M. Ultrasensitive mechanical crack-based sensor inspired by the spider sensory system. *Nature* **2014**, *516*, 222–226. [CrossRef]
21. Yang, T.; Xie, D.; Li, Z.; Zhu, H. Recent advances in wearable tactile sensors: Materials, sensing mechanisms, and device performance. *Mater. Sci. Eng. R* **2017**, *115*, 1–37. [CrossRef]
22. Lipomi, D.J.; Dhong, C.; Carpenter, C.W.; Root, N.B.; Ramachandran, V.S. Organic Haptics: Intersection of Materials Chemistry and Tactile Perception. *Adv. Funct. Mater.* **2020**, *30*, 1906850. [CrossRef] [PubMed]
23. Mu, C.; Song, Y.; Huang, W.; Ran, A.; Sun, R.; Xie, W.; Zhang, H. Stretchable Normal-Tangential Force Sensor with Opposite Resistance Responding for Highly Sensitive Artificial Skin. *Adv. Funct. Mater.* **2018**, *28*, 1707503. [CrossRef]
24. Zou, Z.; Zhu, C.; Li, Y.; Lei, X.; Zhang, W.; Xiao, J. Rehealable, fully recyclable, and malleable electronic skin enabled by dynamic covalent thermoset nanocomposite. *Sci. Adv.* **2018**, *4*, eaaq0508. [CrossRef]
25. Wang, S.; Gong, L.; Shang, Z.; Ding, L.; Yin, G.; Jiang, W.; Gong, X.; Xuan, S. Novel Safeguarding Tactile e-Skins for Monitoring Human Motion Based on SST/PDMS-AgNW-PET Hybrid Structures. *Adv. Funct. Mater.* **2018**, *28*, 1707538. [CrossRef]
26. Hong, S.Y.; Oh, J.H.; Park, H.; Yun, J.Y.; Jin, S.W.; Sun, L.; Zi, G.; Ha, J.S. Polyurethane foam coated with a multi-walled carbon nanotube/polyaniline nanocomposite for a skin-like stretchable array of multi-functional sensors. *NPG Asia Mater.* **2017**, *9*, e448. [CrossRef]
27. Jung, M.; Lee, J.; Vishwanath, S.K.; Kwon, O.S.; Ahn, C.W.; Shin, K.; Jeon, S. Stretchable multimodal sensor inspired by human skin based on hair-type flow, temperature, and pressure. *Stretchable Print. Electron.* **2020**, *5*, 025003. [CrossRef]
28. Kim, S.Y.; Park, S.; Park, H.W.; Park, D.H.; Jeong, Y.; Kim, D.H. Highly Sensitive and Multimodal All-Carbon Skin Sensors Capable of Simultaneously Detecting Tactile and Biological Stimuli. *Adv. Mater.* **2015**, *27*, 4178–4185. [CrossRef]
29. Lee, J.S.; Shin, K.-Y.; Cheong, O.J.; Kim, J.H.; Jang, J. Highly Sensitive and Multifunctional Tactile Sensor Using Free-standing ZnO/PVDF Thin Film with Graphene Electrodes for Pressure and Temperature Monitoring. *Sci. Rep.* **2015**, *5*, 7887. [CrossRef]
30. Han, S.; Kim, J.; Won, S.M.; Ma, Y.; Kang, D.; Xie, Z.; Lee, K.T.; Chung, H.U.; Banks, A.; Min, S.; et al. Battery-free, wireless sensors for full-body pressure and temperature mapping. *Sci. Transl. Med.* **2018**, *10*, eaan4950. [CrossRef]
31. Wang, C.; Xia, K.; Zhang, M.; Jian, M.; Zhang, Y. An All-Silk-Derived Dual-Mode E-skin for Simultaneous Temperature-Pressure Detection. *ACS Appl. Mater. Interfaces* **2017**, *9*, 39484–39492. [CrossRef] [PubMed]
32. Liu, H.; Xiang, H.; Wang, Y.; Li, Z.; Qian, L.; Li, P.; Ma, Y.; Zhou, H.; Huang, W. A Stretchable Multimodal Sensor That Detects Strain, Humidity, Temperature, and Pressure with Carbon Black and Reduced Graphene Oxide Hierarchical Composite on Paper. *ACS Appl. Mater. Interfaces* **2019**, *11*, 40613–40619. [CrossRef] [PubMed]
33. Kurian, A.S.; Souri, H.; Mohan, V.B.; Bhattacharyya, D. Highly stretchable strain sensors based on polypyrrole-silicone rubber composites for human motion detection. *Sens. Actuators A* **2020**, *312*, 112131. [CrossRef]
34. Kim, H.-J.; Sim, K.; Thukral, A.; Yu, C. Rubbery electronics and sensors from intrinsically stretchable elastomeric composites of semiconductors and conductors. *Sci. Adv.* **2017**, *3*, e1701114. [CrossRef] [PubMed]
35. Sim, K.; Rao, Z.; Ershad, F.; Yu, C. Rubbery Electronics Fully Made of Stretchable Elastomeric Electronic Materials. *Adv. Mater.* **2020**, *32*, e1902417. [CrossRef]
36. Paszkiewicz, S.; Szymczyk, A.; Zubkiewicz, A.; Subocz, J.; Stanik, R.; Szczepaniak, J. Enhanced Functional Properties of Low-Density Polyethylene Nanocomposites Containing Hybrid Fillers of Multi-Walled Carbon Nanotubes and Nano Carbon Black. *Polymers* **2020**, *12*, 1356. [CrossRef]
37. Tang, Y.; Witt, N.; Ye, L. Conductive rubber nanocomposites as tensile and pressure sensors. *Appl. Mech. Mater.* **2012**, *217*, 130–133. [CrossRef]
38. Meng, Q.; Kenelak, V.; Chand, A.; Kang, H.; Han, S.; Liu, T. A highly stretchable, electrically conductive, and mechanically robust graphene/epoxy composite film for its self-damage detection. *J. Appl. Polym. Sci.* **2020**, *137*, 48991. [CrossRef]
39. Yang, H.; Gong, L.H.; Zheng, Z.; Yao, X.F. Highly stretchable and sensitive conductive rubber composites with tunable piezoresistivity for motion detection and stretchable electrodes. *Carbon* **2020**, *158*, 893–903. [CrossRef]
40. Kumar, V.; Wu, R.-R.; Lee, D.-J. Morphological aspects of carbon nanofillers and their hybrids for actuators and sensors. *Polym. Compos.* **2019**, *40*, E373–E382. [CrossRef]
41. Kumar, V.; Lee, J.-Y.; Lee, D.-J. Synergistic effects of hybrid carbon nanomaterials in room-temperature-vulcanized silicone rubber. *Polym. Int.* **2017**, *66*, 450–458. [CrossRef]
42. Ke, K.; Yue, L.; Shao, H.; Yang, M.B.; Yang, W.; Manas-Zloczower, I. Boosting electrical and piezoresistive properties of polymer nanocomposites via hybrid carbon fillers: A review. *Carbon* **2021**, *173*, 1020–1040. [CrossRef]
43. Valentini, L.; Bon, S.B.; Lopez-Manchado, M.A.; Verdejo, R.; Pappalardo, L.; Bolognini, A.; Alvino, A.; Borsini, S.; Berardo, A.; Pugno, N.M. Synergistic effect of graphene nanoplatelets and carbon black in multifunctional EPDM nanocomposites. *Compos. Sci. Technol.* **2016**, *128*, 123–130. [CrossRef]
44. Alam, M.N.; Kumar, V.; Potiyaraj, P.; Lee, D.; Choi, J. Mutual dispersion of graphite–silica binary fillers and its effects on curing, mechanical, and aging properties of natural rubber composites. *Polym. Bull.* **2021**, *78*, 1–18. [CrossRef]

45. Zhang, Y.; He, P.; Luo, M.; Xu, X.; Dai, G.; Yang, J. Highly stretchable polymer/silver nanowires composite sensor for human health monitoring. *Nano Res.* **2020**, *13*, 919–926. [CrossRef]
46. Kumar, V.; Alam, M.N.; Manikkavel, A.; Choi, J.; Lee, D.-J. Investigation of silicone rubber composites reinforced with carbon nanotube, nanographite, their hybrid and applications for stretchable devices. *J. Vinyl Addit. Technol.* **2020**, *27*, 254–263. [CrossRef]
47. Ke, K.; McMaster, M.; Christopherson, W.; Singer, K.D.; Manas-Zloczower, I. Highly sensitive capacitive pressure sensors based on elastomer composites with carbon filler hybrids. *Compos. Part A* **2019**, *126*, 105614. [CrossRef]
48. Ruth, S.R.A.; Feig, V.R.; Tran, H.; Bao, Z. Microengineering Pressure Sensor Active Layers for Improved Performance. *Adv. Funct. Mater.* **2020**, *30*, 2003491. [CrossRef]
49. Wu, L.; Qian, J.; Peng, J.; Wang, K.; Liu, Z.; Ma, T.; Zhou, Y.; Wang, G.; Ye, S. Screen-printed stretchable temperature sensor based on FG/CNT/PDMS composite with constant TCR. *J. Mater. Sci.-Mater. Electron.* **2019**, *30*, 9593–9601. [CrossRef]
50. Han, S.; Chand, A.; Araby, S.; Cai, R.; Chen, S.; Kang, H.; Cheng, R.; Meng, Q. Thermally and electrically conductive multifunctional sensor based on epoxy/graphene composite. *Nanotechnology* **2020**, *31*, 075702. [CrossRef]
51. Wang, Y.; Wu, H.; Xu, L.; Zhang, H.; Yang, Y.; Wang, Z.L. Hierarchically patterned self-powered sensors for multifunctional tactile sensing. *Sci. Adv.* **2020**, *6*, eabb9083. [CrossRef] [PubMed]
52. Zhang, R.; Lv, A.; Ying, C.; Hu, Z.; Hu, H.; Chen, H.; Liu, Q.; Fu, X.; Hu, S.; Wong, C.P. Facile one-step preparation of laminated PDMS based stretchable strain sensors with high conductivity and sensitivity via filler sedimentation. *Compos. Sci. Technol.* **2020**, *186*, 107933. [CrossRef]
53. Sanchez-Gonzalez, C.-M.; Soriano-Pena, J.-F.; Rubio-Avalos, J.-C.; Pacheco-Ibarra, J.J. Fabrication of stretchable piezoresistive sensors based on RTV-silicone and milled carbon fibers and the temperature's effect on their electric resistance. *Sens. Actuators A* **2020**, *302*, 111811. [CrossRef]
54. Kim, H.; Hong, S.-K.; Ryu, J.-K.; Park, S.-H. Effect of Filler Alignment on Piezo-Resistive and Mechanical Properties of Carbon Nanotube Composites. *Materials* **2020**, *13*, 2598. [CrossRef] [PubMed]
55. Zhang, C.; Ma, C.A.; Wang, P.; Sumita, M. Temperature dependence of electrical resistivity for carbon black filled ultra-high molecular weight polyethylene composites prepared by hot compaction. *Carbon* **2005**, *43*, 2544–2553. [CrossRef]

Highly Stretchable and Sensitive Multimodal Tactile Sensor Based on Conductive Rubber Composites to Monitor Pressure and Temperature

作者 Zhu, B (Zhu, Bing) [1] ; Ma, C (Ma, Chi) [1] ; Qian, ZH (Qian, Zhihui) [2] ; Ren, L (Ren, Lei) [2] , [3] ; Yuan, HY (Yuan, Hengyi) [2]

查看 Web of Science ResearcherID 和 ORCID （由 Clarivate 提供）

来源出版物 POLYMERS

卷: 14 期: 7

DOI: 10.3390/polym14071294

文献号 1294

出版时间 APR 2022

已索引 2022-04-24

文献类型 Article

跳转至 ↓被引参考文献深度分析

摘要 Stretchable and flexible tactile sensors have been extensively investigated for a variety of applications due to their outstanding sensitivity, flexibility, and biocompatibility compared with conventional tactile sensors. However, implementing stretchable multimodal sensors with high performance is still a challenge. In this study, a stretchable multimodal tactile sensor based on conductive rubber composites was fabricated. Because of the pressure-sensitive and temperature-sensitive effects of the conductive rubber composites, the developed sensor can simultaneously measure pressure and temperature, and the sensor presented high sensitivity (0.01171 kPa(-1) and 2.46-30.56%/degrees C) over a wide sensing range (0-110 kPa and 30-90 degrees C). The sensor also exhibited outstanding performance in terms of processability, stretchability, and repeatability. Furthermore, the fabricated stretchable multimodal tactile sensor did not require complex signal processing or a transmission circuit system. The strategy for stacking and layering conductive rubber composites of this work may supply a new idea for building multifunctional sensor-based electronics.

关键词 **作者关键词:** multimodal sensors; stretchable tactile sensors; resistance-type sensors; conductive rubber; carbon nanomaterials

Keywords Plus: STRAIN SENSORS; CARBON-BLACK; NANOCOMPOSITES; SKIN

作者信息 通讯作者地址: Qian, Zhihui; Ren, Lei (通讯作者)

- Jilin Univ, Key Lab Bion Engn, Changchun 130025, Peoples R China

通讯作者地址: Ren, Lei (通讯作者)

- Univ Manchester, Sch Mech Aerosp & Civil Engn, Manchester M13 9PL, Lancs, England

电子邮件地址 : zhqian@jlu.edu

地址 :

- [1] Jilin Univ, State Key Lab Automot Simulat & Control, Changchun 130025, Peoples R China:
- [2] Jilin Univ, Key Lab Bion Engn, Changchun 130025, Peoples R China:
- [3] Univ Manchester, Sch Mech Aerosp & Civil Engn, Manchester M13 9PL, Lancs, England:

电子邮件地址 : zhubing@jlu.edu.cn; machi20@mails.jlu.edu.cn; zhqian@jlu.edu; lei.ren@manchester.ac.uk; yuanhy18@mails.jlu.edu.cn

类别/分类 研究方向: Polymer Science

引文主题: 2 Chemistry › 2.114 Organic Semiconductors › 2.114.914 Stretchable Electronics

可持续发展目标: 03 Good Health and Well-being

Web of Science 类别 Polymer Science

基金资助

查看资金资助信息

基金资助机构	授权号	显示所有详细信息
National Natural Science Foundation of China (NSFC)	52175270	显示详情
	91848204	显示详情
	52172386	显示详情
	51775235	显示详情

+ 查看更多数据字段

Find It 出版商处的免费全文 全文链接 导出 添加到标记结果列表 1 / 1

POLYMERS

eISSN 2073-4360

当前出版商 MDPI, ST ALBAN-ANLAGE 66, CH-4052 BASEL, SWITZERLAND

目录 Current Contents Connect

研究方向 Polymer Science

Web of Science 类别 Polymer Science

4.7 期刊影响因子™ (2023)

0.93 Journal Citation Indicator™ (2023)

引文网络

来自 Web of Science 核心合集

10 被引频次 创建引文跟踪

10 被引频次 所有数据库 + 查看更多的被引频次

55 篇引用的参考文献 → 查看相关记录

与同行文献相比，该文献的引用表现如何?

← 打开比较指标面板

数据来自 InCites Benchmarking & Analytics

按分类引用项目

根据可用的引文上下文数据和 3 条引用项目中的摘录，对此文献的提及方式进行细分。

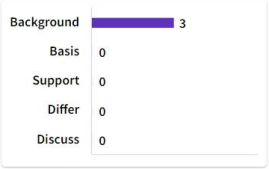

您可能也想要...

Zhang, PX; Zhu, B; Sun, YH; et al.
Performance Evaluation Method for Automated Driving System in Logical Scenario
AUTOMOTIVE INNOVATION

Zhu, B; Sun, YH; Song, DJ; et al.
Millimeter-Wave Radar in-the-Loop Testing for Intelligent Vehicles
IEEE TRANSACTIONS ON INTELLIGENT TRANSPORTATION SYSTEMS

Seok, H; Son, S; Kim, HU; et al.
Chromism-Integrated Sensors and Devices for Visual Indicators
SENSORS

Elanjeitsenni, VP; Vadivu, KS; Prasanth, BM;
A review on thin films, conducting polymers as sensor devices
MATERIALS RESEARCH EXPRESS

Johnson, MK; Cole, F; Adelson, EH; et al.
Microgeometry Capture using an Elastomeric Sensor
ACM TRANSACTIONS ON GRAPHICS

全部查看 →

最近被以下文献引用:

He, Y; Xu, XX; Liu, H; et al.
Research Progress and Application of Multimodal Flexible Sensors for Electronic Skin
ACS SENSORS

Guo, YW; Li, YN; Deng, T; et al.
Status, Applications, and Challenges of Flexible Pressure Sensors Based on 2-D Materials: A Review
IEEE SENSORS JOURNAL

Web of Science 中的使用情况

22 最近 180 天

166 2013 年至今

进一步了解 →

Journal of Manufacturing Processes 87 (2023) 1–10

Contents lists available at ScienceDirect

Journal of Manufacturing Processes

journal homepage: www.elsevier.com/locate/manpro

3D-printing of conductive inks based flexible tactile sensor for monitoring of temperature, strain and pressure

Chi Ma [a], Bing Zhu [a,*], Zhihui Qian [b,**], Lei Ren [b,c,**], Hengyi Yuan [b], Yunhao Meng [a]

[a] State Key Laboratory of Automotive Simulation and Control, Jilin University, Changchun 130025, PR China
[b] Key Laboratory of Bionic Engineering, Jilin University, Changchun 130025, PR China
[c] School of Mechanical, Aerospace and Civil Engineering, University of Manchester, Manchester M13 9PL, United Kingdom

ARTICLE INFO

Keywords:
3D printed sensor
Flexible tactile sensor
Direct ink writing
Conductive inks
Carbon nanomaterials

ABSTRACT

Flexible multimodal tactile sensors have been widely used in health monitoring devices, flexible smart robots, and human–machine interfaces in intelligent automobiles. In the present work, conductive inks embedded with carbon fillers were optimized to fabricate flexible multimodal tactile sensors by a direct ink writing process. Results showed that rheological properties and printing speed were key factors to print conductive paths with controllable shape and good conductivity. Flexible multimodal tactile sensors were fabricated at different printing speeds, and the effects of printing speed on sensing characteristics were observed. The flexible multimodal tactile sensors printed with conductive inks exhibited excellent sensitivities for temperature (up to 0.172 $°C^{-1}$), strain (1918.4), and pressure (610.208 kPa^{-1}). Furthermore, cyclic loading–unloading tests revealed that the as-fabricated flexible multimodal tactile sensors were reliable and durable. Finally, the application potential of these sensors for multimodal perception was verified by detecting their responses to finger flexion and extension, finger pressing, and hot air flow. The as-designed flexible multimodal tactile sensors manifested excellent potentialities in health monitoring devices, flexible smart robots, and human–machine interfaces in intelligent automobiles.

1. Introduction

Flexible tactile sensors, such as strain sensors, pressure sensors, temperature sensors, are widely used in electrical skin (e-skin), flexible robots, health monitoring devices, and intelligent human–computer interaction systems [1–3]. Due to the development of advanced materials and manufacturing processes in recent years, the fabrication of flexible tactile sensors with high sensitivity and excellent flexibility has become feasible. Flexible tactile sensors can be divided into capacitive, piezoelectric, and piezoresistive sensors according to their conversion mechanisms [4–6]. Especially, piezoresistive sensors are widely used because of their simple structure and wide detection range. Flexible tactile sensors are generally fabricated by three-dimensional (3D) printing, layer-by-layer assembly, lithography, and impregnation [7,8]. Among these methods, 3D printing has attracted considerable interest and effort because of its advantages of low material waste and high preparation efficiency [9–11].

Generally, 3D printing technologies include fused deposition modeling (FDM), digital light processing (DLP), selected laser sintering (SLS), and direct ink writing (DIW) [12,13]. Dong Xiang et al. [14] prepared flexible strain sensors with high-performance based on carbon nanotubes (CNTs) and thermoplastic polyurethane (TPU) composites embedded with graphene nanoplatelet (GNP) by the fused filament fabrication (FFF) method and noticed that the printed CNT/GNP (3:1)/TPU sensor had high sensitivity (maximum GF = 136,327.4), a large perception range (0–250 % strain), and good durability (3000 cycles). Pei Huang et al. [15] fabricated CF-filled conductive silicon rubbers (CSRs) in an extrusion device and observed that the resultant CSRs had good durability in cycling loading. Luyu Zhou et al. [16] reported an integrated multimaterial 3D printing process consisting of the direct ink writing of sealing silicone elastomer and a liquid mental-silicone (LMS) ink to manufacture a high-performance LMS-based flexible sensor. Yi-Fei Wang et al. [17] printed a flexible temperature sensor using cross-linked poly (3, 4-ethylenedioxythiophene):poly (styrenesulfonate) (PEDOT:PSS) and asserted that the introduction of (3-glycidyloxypropyl) trimethoxysilane (GOPS) and fluorinated polymer passivation

* Corresponding author.
** Corresponding authors at: Key Laboratory of Bionic Engineering, Jilin University, Changchun 130025, PR China.
E-mail addresses: zhubing@jlu.edu.cn (B. Zhu), zhqian@jlu.edu.cn (Z. Qian), lei.ren@manchester.ac.uk (L. Ren).

https://doi.org/10.1016/j.jmapro.2023.01.008
Received 20 October 2022; Received in revised form 29 December 2022; Accepted 5 January 2023
Available online 12 January 2023

(CYTOP) significantly enhanced the humidity stability and temperature sensitivity of the PEDOT:PSS-based film. Yancheng Wang et al. [18] fabricated a tactile sensor based on liquid metal by 3D printing for multimodal tactile perception applications. They designed a digital light processing-based printing method to engineer the tactile sensor with a force sensitivity of 0.29 N^{-1} and temperature sensitivities of 0.55 %°C^{-1} at 20–50 °C and 0.21 %°C^{-1} at 50–80 °C.

Although these sensors have strong potential as flexible tactile sensors, their fabrication methods are not facile [19–21]. The use of conductive inks with optimized rheological behavior in DIW can be an effective approach to fabricating flexible tactile sensors with complex shapes.

In comparison to other 3D printing technologies, DIW uses a wide range of printable materials, such as electrical, biological, and structural materials. In previous research [22–26], colloidal suspensions, hydrogels, thermosetting polymers, and escape inks have been used as ink materials. The main parameters affecting the applicability of sensors prepared by DIW include printing speed, ink viscosity, and nozzle diameter. To print flexible sensors by DIW, different conductive ink materials have been investigated [27–30].

Conductive printing inks generally contain matrix materials, conductive materials, and diluents [31,32]. Silicone rubber and TPU are common matrix materials. Carbon nanomaterials, metal nanowires, and PEDOT/PSS are generally used as conductive materials. Naphtha and ethanol are the most frequently used diluents [33–35]. Silicone rubber has the advantages of good biocompatibility and flexibility; thus, it is widely applied to flexible electronics [36–38]. Furthermore, carbon nanomaterials, such as CNTs, CB, and GPs, are widely used to fabricate flexible sensors. Carbon nanomaterials exhibit good conductivity and high stability [39–42]. In the present work, conductive inks based on silicon rubber and carbon nanomaterials were printed by DIW.

Flexible tactile sensors were prepared by DIW. Several groups of conductive inks with different viscosity were prepared, and the influences of the rheological behavior of the inks and printing speed on printed samples were analyzed. Sensors were fabricated at different printing speeds using the conductive inks with optimized viscosity, and the effects of printing speed on sensing characteristics were observed. The printed flexible tactile sensors were tested under cyclic loading to study their response stability. Finally, the potential application scenarios of the as-fabricated flexible tactile sensors were presented.

2. Experimental details

2.1. Materials

Conductive carbon black (CB) powder (CABOT BP2000) was supplied by Hefei Saibo New Materials Co. Ltd., Hefei, China. Multilayered graphene (GP; 95 % purity) and multi-walled carbon nanotubes (MWCNTs; TF-25001, 95 % purity) were provided by Suzhou Carbon Graphene Technology Co. Ltd., Suzhou, China. CB, GP and CNT were used as conductive components to prepare conductive inks. Room temperature-vulcanized silicone rubber (RTV; GB-107, viscosity = 10,000 mp•s) was supplied by Jinan Guobang Chemical Co. Ltd., Jinan, China. RTV was used as the matrix material of conductive inks. Anhydrous ethanol (concentration ≥ 99.7 %) was obtained from Tianjin Yifang Technology Co. Ltd., Tianjin, China, and used as the thinner of conductive inks. The electrodes of the sensor were copper foils, and they (thickness = 0.05 mm) were supplied by Taizhou Lingbang Hardware Technology Co. Ltd., Taizhou, China. Polydimethylsiloxane (PDMS; Sylgard 184 Silicone, Dow Corning) was provided by Wuxi Fites Electronic Technology Co. Ltd., Wuxi, China, and PDMS films were used as the flexible substrates.

2.2. Equipment

The conductive components, the curing agent, and the rubber matrix were evenly mixed in an electric mixer (JB300-SH, Shanghai Specimen and Model Factory, Shanghai, China). The rheological properties of the conductive inks were determined with a rheometer (MCR92, Anton Paar Shanghai Trading Co. Ltd., Shanghai, China). A vacuum pump (V-I140SV, Zhejiang Value Mechanical and Electrical Products Co. Ltd., Wenling, China) was used to defoam the conductive inks. A drying oven (DZF6050, Shanghai Yiheng Technical Co. Ltd., Shanghai, China) provided the curing environment for the conductive inks. A digital multimeter (34,465 A, Keysight Technologies Co. Ltd., Beijing, China) was employed to measure electrical signals generated from the sensors. Pressure and stretching tests (Supplementary Materials) were conducted with a universal testing machine (ZQ-990, Zhiqu Precision Instruments Co. Ltd., Dongguan, China), and a constant temperature heater (JF-965S, Dongguan Jinfeng Electronics Co. Ltd., Dongguan, China) was used to supply temperature stimulation. A scanning electron microscope (SEM; S-4800, Hitachi, Ltd., Tokyo, Japan) was employed to inspect the microstructure of the conductive inks.

2.3. Conductive inks preparation

The fabrication process of conductive inks is displayed in Fig. 1a. First, the conductive fillers were evenly distributed in the RTV with an electric stirrer at 500 rpm for 10 min. The curing agent with a mass fraction of 5 % of the RTV and ethanol with a certain proportion of the volume of the RTV were then added to the mixture and stirred at 500 rpm for 20 min. A vacuum pump was used to remove bubbles from the mixture at a vacuum degree of 0.01 MPa for 20 min.

Carbon nanomaterials, including CB, CNTs, and GPs were used as conductive fillers. CB has the advantage of good conductivity and low price, so all the ink in this study was embedded with CB. CNT and GP have different microstructures from CB, and the multiple nanofillers will bring synergistic effects. Therefore, this study also prepared two inks which were further filled with CNT and GP based on CB ink to study the influence of hybrid fillers on materials. The combination of different conductive fillers can effectively reduce the percolation threshold of the resultant conductive inks, which means conductive inks can obtain high conductivity without too much embedded conductive filler [43,44]. A pre-experiment was conducted to determine the mass ratios of the resultant conductive inks, and 8 wt% of carbon black was embedded to prepare CB ink. The mass ratio of CB:CNT/GP was 1:1 for the conductive inks containing hybrid fillers. In this experiment, 18 types of conductive inks with different carbon fillers and rheological properties were successfully prepared and tested.

2.4. Preparation of flexible tactile sensors

2.4.1. Direct ink writing process

The conductive inks were printed by a DIW process. The conductive inks were extruded by a pneumatic extrusion system. The movements of each axis were controlled by a motion controller, and patterns to be printed were set in the controller in advance. The basic printing parameters were set based on the pre-experimental results (Table 1).

As the rheological properties of inks have a significant effect on printed samples, conductive inks with different rheological properties were prepared and applied to DIW. Six groups of conductive inks were printed according to pre-experimental results. The quality of printed samples was evaluated by measuring their conductivity and width. Samples with poor conductivity could not output electrical signals; thus, they were not used to develop sensors. Moreover, when the printed sample width was too large, it was difficult to control the shape. Fine and complex patterns were printed by optimizing the rheological properties of the inks.

2.4.2. Sensor fabrication

The preparation process of a flexible tactile sensor is presented in Fig. 1b. First, the PDMS and the cross-linker were uniformly mixed and

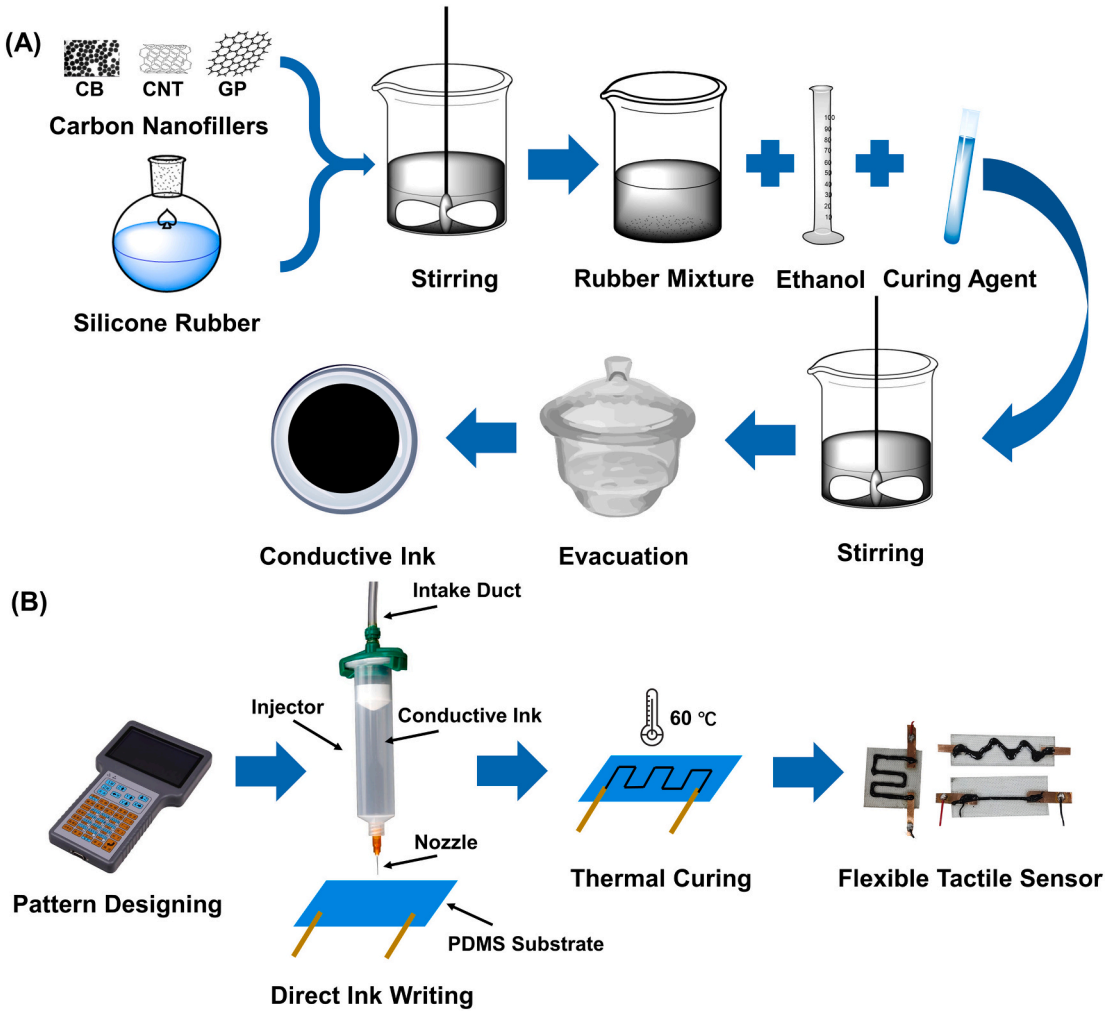

Fig. 1. (A) Conductive inks synthesis route and (B) preparation of flexible multimodal tactile sensors by DIW.

Table 1
Parameters for the DIW process of conductive inks.

Printing pressure (MPa)	Printing height (mm)	Printing speed (mm·min^{-1})	Inner diameter of nozzle (mm)
0.3	5 ± 0.5	60/70/80/90/100	1.4

cast on a Polytetrafluoroethylene (PTFE) mold and then annealed. The resultant PDMS membrane was cut into the desired shape and used as the flexible sensor substrate. The conductive inks with optimized rheological characteristics were then put into the syringe of the DIW printer. The conductive inks were printed on the PDMS substrate after setting the printing parameters and the printing path on the controller. The printing parameters are listed in Table 1. The printed sensor was cured at 60 °C for 24 h in the vacuum drying oven. In this experiment, 15 types of sensors with simple patterns and several sensors with complex patterns were successfully fabricated.

2.5. Characterization

2.5.1. Rheological property characterization

Five conductive inks with different rheological properties (Volume ratio of ethanol to the rubber matrix = 10 %, 20 %, 30 %, 40 %, 50 %) were prepared. The rheometer was used to determine the rheology of the conductive inks at 25 °C.

2.5.2. Conductivity measurement

The conductivity of the printed conductive inks was tested by the desktop digital multimeter, and conductive path widths were measured by a vernier caliper. In addition, 10 mm resistance was used as an index to represent conductivity, and the maximum conductive path width was taken as the result of shape characterization.

2.5.3. Sensitivity characterization

The as-fabricated flexible multimodal tactile sensors were sensitive to tactile parameters (temperature, strain, and pressure); thus, their sensitivity characterization was divided into three experiments. Pressure and strain sensitivity tests were conducted on the universal testing machine, and temperature sensitivity tests were executed by the heating table equipped. Electrical signals were collected by the digital multimeter.

The temperature of the heating table was set to 20 °C, 30 °C, 40 °C, 50 °C, 60 °C, 70 °C, and 80 °C. The heating table was kept at each temperature for 1 min, and the average value of three tests was recorded to ensure the validity of the results. During strain sensitivity tests, the clip of the universal testing machine stretched the sensors and loaded the strain at an interval of 0.04. The maximum strain was 0.2. During pressure tests, the clip of the universal testing machine pressed the sensors and applied pressure at an interval of 25 kPa. The maximum pressure was 250 kPa. When the test sensors were more sensitive, the

pressure was applied at an interval of 5 kPa and the maximum pressure was 25 kPa. The sampling frequency of the digital multicenter was 100 Hz during all tests. The loading and unloading speeds of the clip of the universal testing machine were 5 mm/min and 10 mm/min, respectively [45,46].

2.5.4. Morphological observation

The cross-sectional morphologies of the printed conductive inks were observed by the scanning electron microscope to examine the dispersion state of the conductive fillers. The cross-sections of the printed conductive inks were magnified by 10,000–50,000× at 3–5 kV.

3. Results and discussion

3.1. Rheological properties of conductive inks

The rheological behaviors of different conductive inks are presented in Fig. 2. The percolation threshold of the conductive composites embedded with carbon nanomaterials was 5–10 %. The insulating material was transformed into the conductive elastomer when the conductive filler concentration exceeded the percolation threshold; subsequently, the conductive fillers overlapped and made contacts with each other in the matrix. The mass fraction of the carbon fillers was 8 %, and each filler accounted for 4 wt% of the conductive inks. Furthermore, different volume fractions of ethanol were used to adjust the conductive ink viscosity.

With the increase in the shear rate, the conductive ink viscosity first decreased sharply and then gradually became stabilized. Moreover, the conductive ink viscosity decreased with the increase in the volume fraction of absolute ethanol. Little difference was noticed between the viscosity of the conductive inks filled with CB and the conductive inks filled with CB/CNTs, whereas the viscosity of the conductive inks filled with CB/GPs was smaller than that of the other two groups. The addition of 50 % ethanol (by volume) to the same ink material reduced the conductive ink viscosity by 65–70 %.

3.2. SEM characterization results and sensitive mechanism

Fig. 3 displays the cross-sectional morphologies of the conductive inks. It is noticeable that the carbon nanomaterials were well dispersed in the RTV and created conductive pathways (marked by blue arrows). Fig. 3a, b, and c present the SEM micrographs of the conductive inks filled with CB, CB/CNTs, and CB/GPs, respectively.

When an external pressure or strain was applied, the conductive networks were destroyed due to the deformation of the conductive inks. When the pressure was removed, the conductive networks were reassembled with the recovery of their shapes. The conductive inks manifested a positive temperature effect; thus, resistance increased with the rising temperature. With the rise of temperature, the polymer crystalline phase melted and expanded; hence, the distance between conductive filler particles increased, causing the positive temperature effect [39–42].

3.3. Effects of rheological properties

Six types of conductive inks were selected for DIW to study the influence of rheological properties on the printing process. The volume fraction of ethanol and the parameters of DIW printing were determined by a pre-experiment. In the pre-experiment, the conductive inks did not block the nozzle during the printing process or flowed out of the needle tube when there was no air pressure. All conductive inks were printed on plastic Petri dishes. Linear conductive paths with complex patterns were printed and tested.

The photographs and test results of the printed conductive paths are presented in Fig. 4. It is noticeable from Fig. 4a and b that the forming ability of conductive ink is better. When 30 vol% of ethanol was added, whereas the conductive inks had better conductivity when the ethanol content was 40 vol%. A small difference was detected in the conductive path widths of the inks filled with CB and the inks filled with CB/CNTs, whereas the conductive path width of the inks filled with CB/GPs was larger than those of the other two groups. Spiral and folding line patterns were printed with the conductive inks filled with CB added with 40 vol% of ethanol (Fig. 4c). To sum up, rheological properties mainly affected the shape and conductivity of the conductive inks.

3.4. Effects of printing speed

Three types of conductive inks (CB inks with 40 vol% of ethanol, CB/CNTs inks with 35 vol% of ethanol, and CB/GPs inks with 25 vol% of ethanol) were selected for DIW to analyze the influences of printing speeds (60 mm/min, 70 mm/min, 80 mm/min, 90 mm/min, and 100 mm/min) on the printing process. The conductive inks were printed on soft PDMS substrates, and the width and resistance of the printed conductive paths were tested.

The photographs and test results of the printed conductive paths on PDMS substrates are displayed in Fig. 5. It is noticeable from Fig. 5a–c that the conductive inks path width decreased with the increasing printing speed, whereas the conductivity of the inks got worse as the printing speed increased. Although the rheological properties of the conductive inks and the inner diameter of the nozzle were definite, printing speed still had an influence on the shape and conductivity of the printed conductive paths. The conductive path width at the printing speed of 100 mm/min was reduced by 24–30 % as compared with that at 60 mm/min. The 10 mm resistance of the conductive path at 100 mm/min increased by 70–140 % as compared with that at 60 mm/min. The faster the printing speed, the higher the preparation efficiency.

3.5. Sensitivity

The sensitivity test results of the printed flexible tactile multimodal

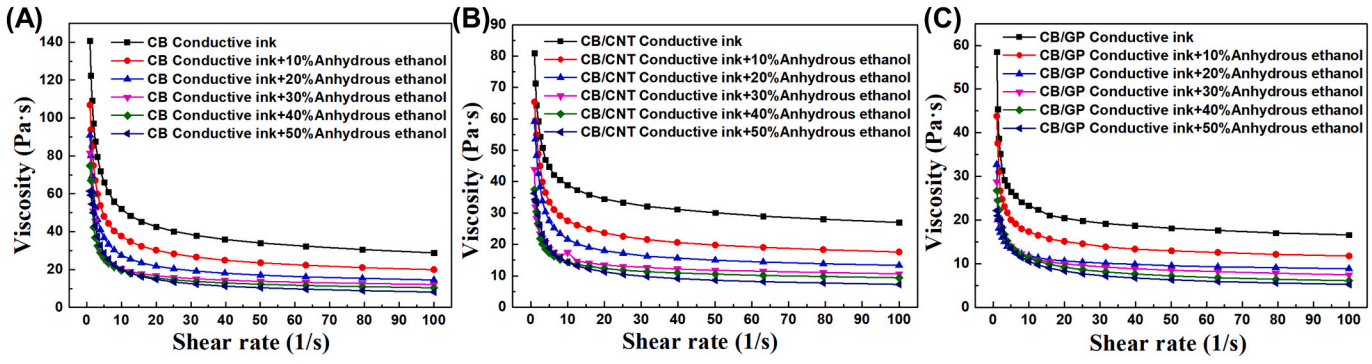

Fig. 2. Rheological properties of the conductive inks filled with (A) CB, (B) CB/CNTs, and (C) CB/GPs.

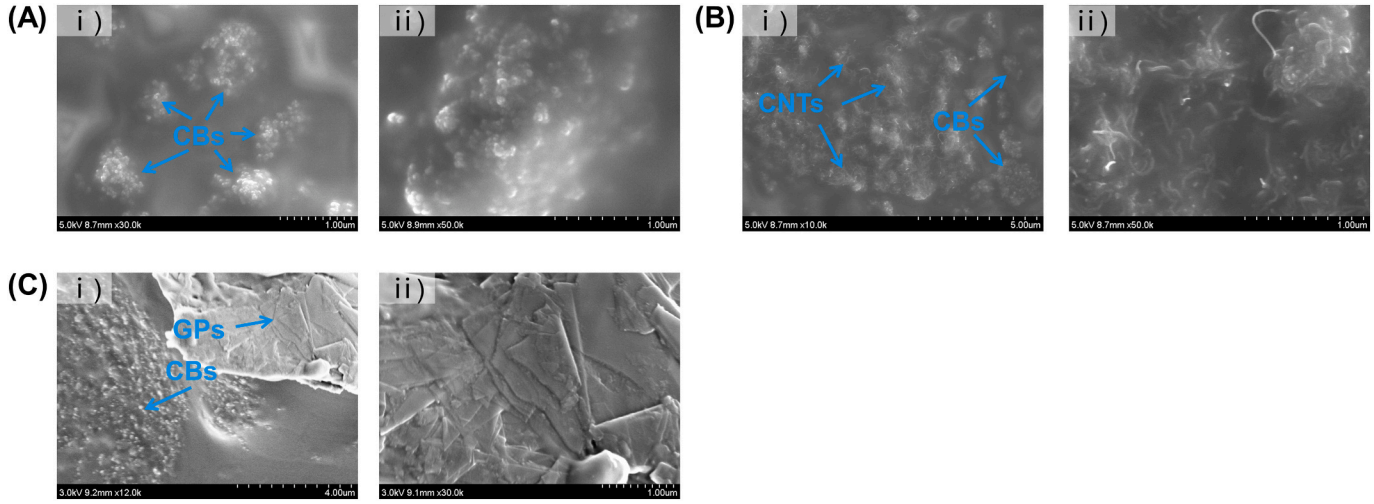

Fig. 3. SEM micrographs of the conductive inks filled with (A) CB, (B) CB/CNTs, and (C) CB/GPs.

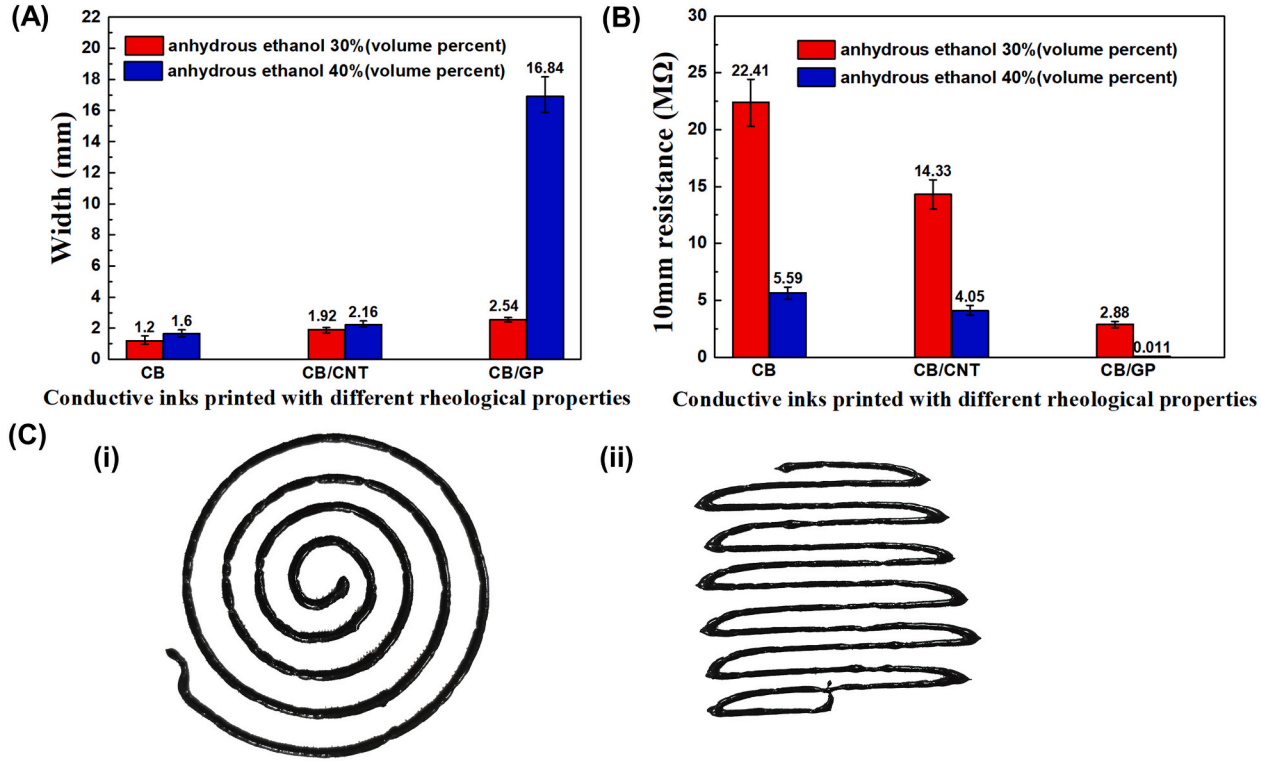

Fig. 4. (A) Printed conductive path widths, (B) 10 mm resistance to printed conductive paths, and (C) Photographs of conductive paths with complex patterns.

sensors are presented in Fig. 6. Three types of conductive inks (CB inks with 40 vol% of ethanol, CB/CNTs inks with 35 vol% of ethanol, and CB/GPs inks with 25 vol% of ethanol) and five different printing speeds (60 mm/min, 70 mm/min, 80 mm/min, 90 mm/min, and 100 mm/min) were selected. The temperature, strain, and pressure sensitivities of flexible tactile multimodal sensors are presented in Fig. 6a, b, and c, respectively.

The sensitivity was used to analyze the sensitive characteristics of the as-fabricated sensors. The temperature sensitivity was defined as the ratio of the relative change in resistance to temperature; therefore, S_temp (temperature sensitivity) = $(\Delta R/R_0)/\Delta T$, where R_0 is the initial resistance, ΔR is the resistance change, and ΔT is temperature change. It was found that with the rising temperature, the resistance of the flexible tactile multimodal sensors increased monotonously. The sensors printed with the CB/GPs inks had the best sensitivity ranging from 0.017 $°C^{-1}$ to 0.172 $°C^{-1}$, whereas the sensors printed with the CB inks and the CB/CNTs inks had the best sensitivities of 0.027 $°C^{-1}$ and 0.07 $°C^{-1}$, respectively. Moreover, printing speed yielded different impacts on the sensors printed by different types of conductive inks. Printing speed had little impact on the sensitivity of the sensor printed with the CB inks. However, for the sensor printed with the CB/GPs inks, the higher the printing speed, the lower the sensitivity. On the contrary, for the sensor printed with the CB/CNTs inks, the higher the printing speed, the greater the sensitivity.

The strain sensitivity was defined as S_strain (strain sensitivity) = $(\Delta R / R_0) / \Delta\varepsilon$, where R_0 is the initial resistance, ΔR is the resistance change, and $\Delta\varepsilon$ is the strain change. With the increasing strain, the resistance of the flexible tactile multimodal sensors increased greatly.

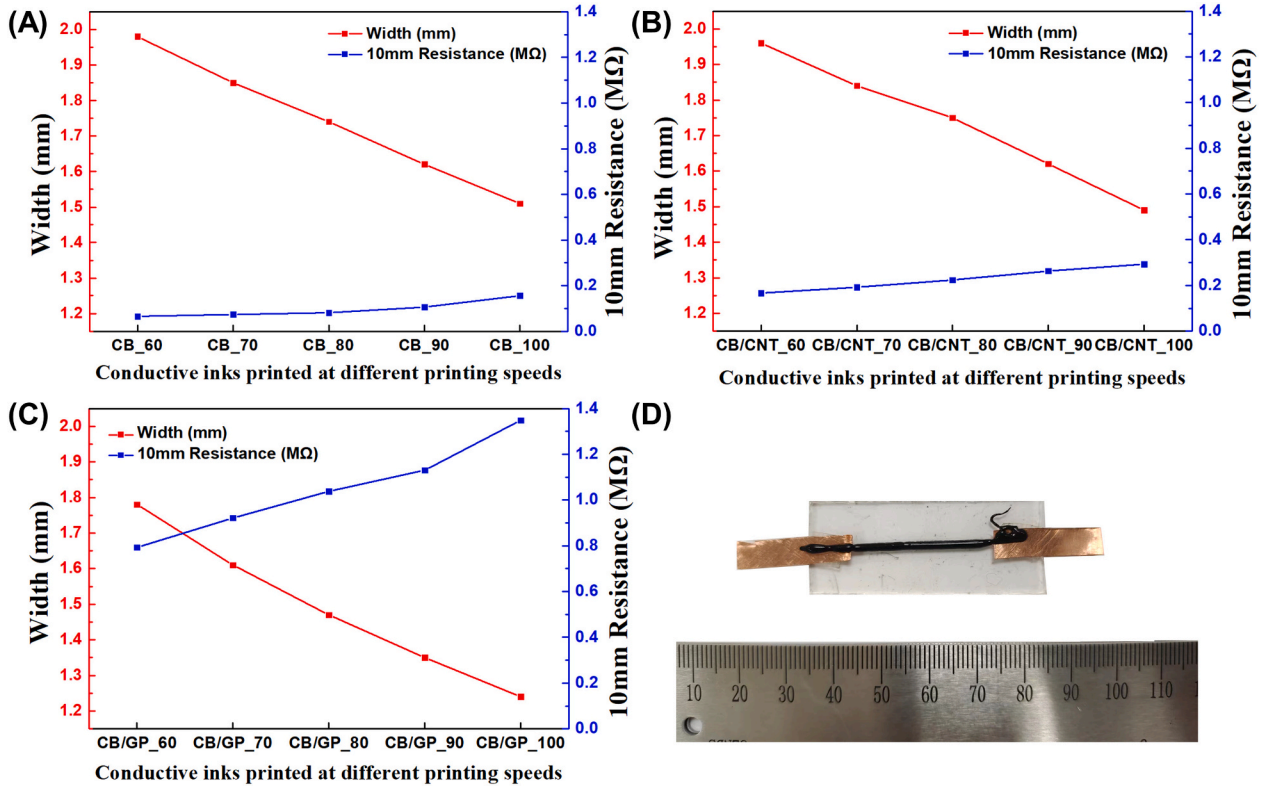

Fig. 5. (A–C) Width and 10 mm resistance of the printed conductive paths with (A) CB inks, (B) CB/CNTs inks, and (C) CB/GP inks, and (D) Photographs of conductive paths printed on PDMS substrates.

The fabricated sensors exhibited excellent linearity under the applied strain. The sensors printed with the CB/GPs inks had the best sensitivity ranging from 297.4 to 1918.4. The sensitivities of the sensors printed with the CB inks and the CB/CNTs inks were 9.1–41.3 and 48.2–488.8, respectively. Moreover, printing speed yielded the same impact on the sensors printed by different types of conductive inks—the higher the printing speed, the greater the sensitivity.

The pressure sensitivity was defined as S_pressure (pressure sensitivity) = $(\Delta R / R_0) / \Delta P$, where R_0 is the initial resistance, ΔR is the resistance change, and ΔP is the pressure change. With the increasing pressure, the resistance of the flexible tactile multimodal sensors increased sharply. When an external pressure was applied, the conductive networks were destroyed due to the deformation of the conductive inks. The sensor printed with the CB/GPs inks had the best sensitivity of 610.208 kPa^{-1}; however, its detection range was smaller than those of the other sensors. The sensitivity of the sensor printed with the CB/CNTs inks ranged from 0.717 kPa^{-1} to 90.885 kPa^{-1}. The sensor printed with the CB inks yielded the lowest sensitivity (ranging from 0.204 kPa^{-1} to 0.919 kPa^{-1}). Moreover, printing speed had a similar impact on the sensitivity of the sensors printed with different types of conductive inks. When the printing speed was 70–80 mm/min, the sensitivity of the sensors was larger than those of the sensors printed at a higher or lower speed. The results indicated that there is an optimum printing speed for sensitivity to some extent.

Therefore, the flexible multimodal tactile sensors printed with conductive inks exhibited excellent sensitivities for temperature (up to 0.172 $°C^{-1}$), strain (1918.4), and pressure (610.208 kPa^{-1}). For comparison, Jinhua Wu et al. [47] calculated the temperature and pressure sensitivities of the flexible multimodal tactile sensor as −10.0 $°C^{-1}$ and 777 kPa^{-1}, respectively. Liangren Chen et al. [48] found that the temperature and strain sensitivities of the flexible multimodal tactile sensor were −0.076 $°C^{-1}$ and 1.6, respectively. Hanbin Liu et al. [49] prepared a flexible multimodal tactile sensor with temperature and pressure sensitivities of 0.006 $°C^{-1}$ and 0.0059 kPa^{-1}, respectively. Young Kim et al. [50] designed a flexible multimodal tactile sensor with temperature and pressure sensitivities of 0.0024 $°C^{-1}$ and 0.034–0.05 kPa^{-1}, respectively.

Hence, the flexible multimodal tactile sensors printed by DIW had good sensitivity for multifunctional tactile parameters. Printing speed and carbon fillers affected the sensitivity and detection range of the sensors. In addition to sensitivity, the lowest detection pressure limit and resolution of the sensor need detailed experimental research in the future with more sophisticated loading equipment.

3.6. Dynamic performance

The cyclic test results of the printed flexible tactile multimodal sensors are presented in Fig. 7. Repeatability and reproducibility are the two main factors for flexible tactile sensors. The sensor printed with the CB inks at a printing speed of 60 mm/min was selected for the dynamic test. The flexible multi-mode tactile sensors were tested at 1000 cycles of strain and 2000 cycles of pressure [51–53]. The strain and pressure for the dynamic test were 0.1 and 10 kPa, respectively. The speed of the loading and unloading strokes was 20 mm/min, and output signals were the real-time resistances of the sensor.

It can be seen from Fig. 7 that the R of the sensor decreases and increases in varying degrees at the beginning of the cycle, and then tends to be stable. This can be attributed to that the electrical connection between the electrode and the conductive ink requires a certain pressure stimulation to activate and the internal conductive path of the conductive composites needs some stimuli to form. Under cyclic loading and unloading, the flexible tactile sensor yielded multiple signal peaks. Overall, the sensors had good repeatability and small variations after 1000 and 2000 loading–unloading cycles.

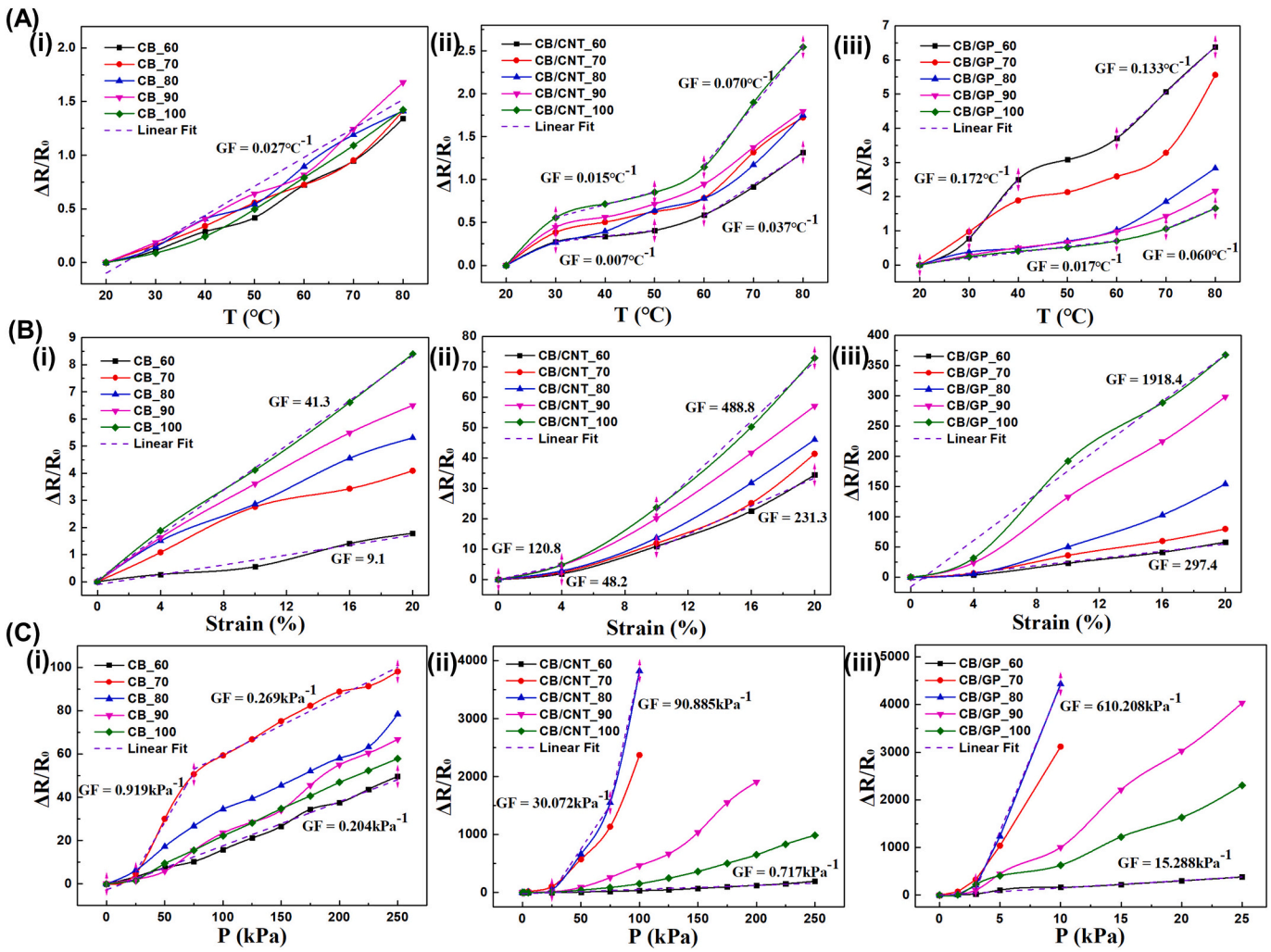

Fig. 6. Sensing characteristics of the printed flexible multimodal tactile sensors for (A) temperature, (B) strain, and (C) pressure.

3.7. Applications

To validate the multimodal monitoring functionalities of the flexible multimodal tactile sensors, some application verification experiments of the developed sensor were conducted. Fig. 8a displays the photograph and test result of the sensor worn on the finger to detect finger flexion and extension. Fig. 8b presents the photograph and test result of the sensor under finger pressing stimulation. Fig. 8c exhibits the photograph and test result of the sensor blown by hot air flow. Fig. 8d displays the photograph and test result of the sensors installed at the heel and knee joint to detect plantar pressure and knee joint motion during walking. It is evident that sensor signal responses caused by pressure or strain stimulation were faster than those caused by temperature, and it happened because the speed of thermal expansion for the sensitive materials was less than the speed of deformation caused by an external force. Therefore, this sensor could detect mechanical and temperature stimuli at the same time, and categories of stimuli can be distinguished by the signal response time of the sensor to some extent. Fig. 8 manifests the application potentials of the as-fabricated sensors as wearable devices and electronic skins, and it is clear that the sensors had good flexibility and stretchability. These results further showed that the flexible multimodal tactile sensor could detect various stimuli. Therefore, this sensor has the potential to be applied in the field of multimodal tactile perception.

4. Conclusions

Conductive inks were prepared by mixing silicone rubber, carbon nanomaterials, and anhydrous ethanol, and flexible multimodal tactile sensors were fabricated by DIW. The influences of the rheological behaviors of the conductive inks and printing speed on the printed conductive paths were investigated. The best diluent volume fraction was determined, and full shape conductive paths with complex patterns were successfully printed. The impacts of printing speed on the characteristics of the printed sensors were analyzed.

Experimental results indicated that printing speed and the carbon fillers greatly affected the sensitivities of the sensors. The flexible multimodal tactile sensors printed with conductive inks exhibited excellent sensitivities for temperature (up to 0.172 $°C^{-1}$), strain (1918.4), and pressure (610.208 kPa^{-1}). Furthermore, durability tests revealed that the flexible multimodal tactile sensors were reliable.

Finally, the application potentials of these sensors for multimodal perception were verified by detecting their responses to finger flexion and extension, finger pressing, and hot air flow. The as-designed flexible multimodal tactile sensors manifested excellent potentialities in health monitoring devices, flexible smart robots, and human–machine interfaces in intelligent automobiles.

Supplementary data to this article can be found online at https://doi.org/10.1016/j.jmapro.2023.01.008.

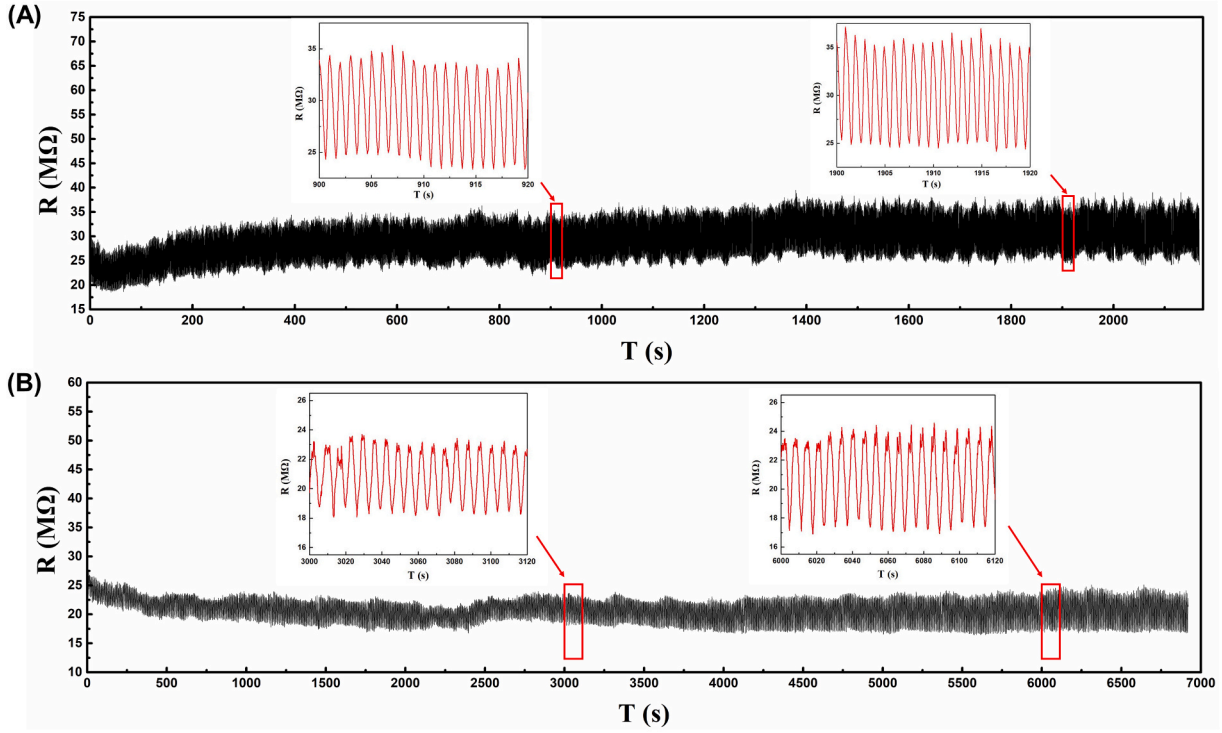

Fig. 7. Variation of R under (A) cyclic pressure and (B) stretching.

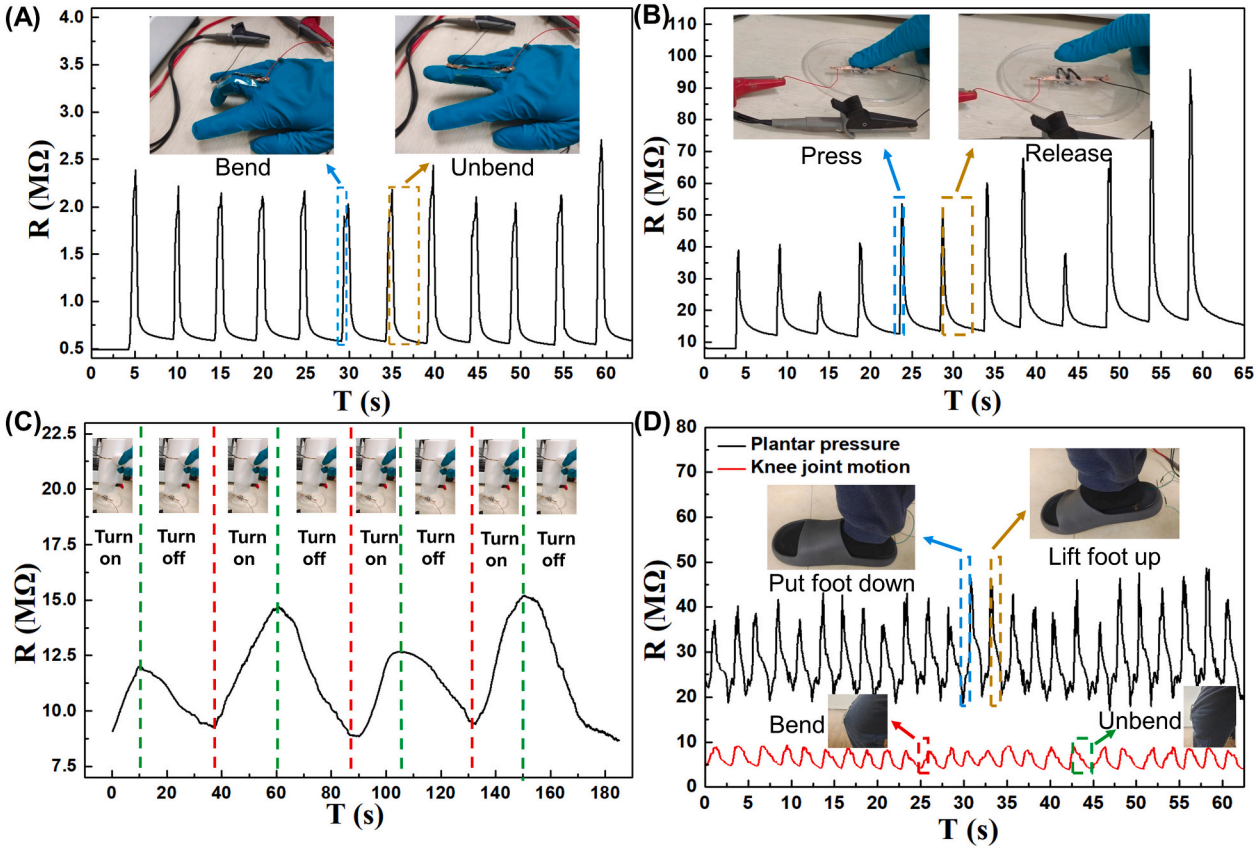

Fig. 8. Responses of the flexible tactile multimodal sensors to (A) finger flexion and extension, (B) finger pressing, (C) hot air flow and (D) plantar pressure and knee joint motion.

Declaration of competing interest

The authors declare that they have no known competing financial interests or personal relationships that could have appeared to influence the work reported in this paper.

Data availability

The data used to support the findings of this study are available from the corresponding author upon request.

Acknowledgements

This research was supported by the projects of National Natural Science Foundation of China (No. 52175270, No. 52172386), and the Project of Scientific and Technological Development Plan of Jilin Province (No.20220508130RC).

References

[1] Park M, Bok B-G, Ahn J-H, Kim M-S. Recent advances in tactile sensing technology. Micromachines 2018;9:321.
[2] Pyo S, Lee J, Bae K, Sim S, Kim J. Recent Progress in flexible tactile sensors for human-interactive systems: from sensors to advanced applications. Adv Mater 2021;33:e2005902.
[3] Yang JC, Mun J, Kwon SY, Park S, Park S. Electronic skin: recent Progress and future prospects for skin-attachable devices for health monitoring, robotics, and prosthetics. Adv Mater 2019;31:e1904765.
[4] Chen H, Lv L, Zhang J, Zhang S, Xu P, Li C, Zhang Z, Li Y, Xu Y, Wang J. Enhanced stretchable and sensitive strain sensor via controlled strain distribution. Nanomaterials 2020;10:218.
[5] Kou, Hairong, Zhang, Lei, Tan, Qiulin, Liu, Guanyu, Lv. Wen wireless flexible pressure sensor based on micro-patterned Graphene/PDMS composite. Sensors Actuators A Phys 2018;277:150–6.
[6] Kim MO, Pyo S, Oh Y, Kang Y, Kim J. Flexible and multi-directional piezoelectric energy harvester for self-powered human motion sensor. Smart Mater Struct 2018; 27:035001.
[7] Nasiri S, Khosravani MR. Progress and challenges in fabrication of wearable sensors for health monitoring. Sensors Actuators A Phys 2020;312:112105.
[8] Khosravani MR, Reinicke T. Applications of additive manufacturing in fabrication of sensors - a review. Sensors Actuators A Phys 2020;305:111916.
[9] Hisham HH, Arifin SS, Aya A, Anil PB. 3D printable conductive materials for the fabrication of electrochemical sensors: a mini review. Electrochem Commun 2018; 96:27–31.
[10] Liu H, Zhang H, Han W, Lin H, Li R, Zhu J, Huang W. 3D printed flexible strain sensors: from printing to devices and signals. Adv Mater 2021;33:2004782.
[11] Barmpakos D, Kaltsas G. A review on humidity, temperature and strain printed sensors—current trends and future perspectives. Sensors 2021;21:1–24.
[12] Han T, Kundu S, Nag A, Xu Y. 3D printed sensors for biomedical applications: a review. Sensors 2019;19:1706.
[13] Park S, Kim H, Kim J-H, Yeo W-H. Advanced nanomaterials, printing processes, and applications for flexible hybrid electronics. Materials 2020;13:3587.
[14] Xiang D, Zhang X, Han Z, Zhang Z, Zhou Z, Harkin-Jones E, Zhang J, Luo X, Wang P, Zhao C. 3D printed high-performance flexible strain sensors based on carbon nanotube and graphene nanoplatelet filled polymer composites. JMatS 2020;55:15769–86.
[15] Huang P, Xia Z, Cui S. 3D printing of carbon fiber-filled conductive silicon rubber. Mater Des 2018;142:11–21.
[16] Zhou LY, Fu JZ, Gao Q, Zhao P, He Y. All-printed flexible and stretchable electronics with pressing or freezing activatable liquid-metal–silicone inks. Adv. Funct. Mater. 2020;30:1906683.
[17] Wang Y-F, Sekine T, Takeda Y, Yokosawa K, Matsui H, Kumaki D, Shiba T, Nishikawa T, Tokito S. Fully printed PEDOT: PSS-based temperature sensor with high humidity stability for wireless healthcare monitoring. Sci Rep 2020;10:1–8.
[18] Wang Y, Jin J, Lu Y, Mei D. 3D printing of liquid metal based tactile sensor for simultaneously sensing of temperature and forces. Int J Smart Nano Mater 2021; 12:269–85.
[19] Xiang D, Zhang X, Harkin-Jones E, Zhu W, Zhou Z, Shen Y, Li Y, Zhao C, Wang P. Synergistic effects of hybrid conductive nanofillers on the performance of 3D printed highly elastic strain sensors. Composites, Part A 2020;129:105730.
[20] Guo SZ, Qiu K, Meng F, Park SH, McAlpine MC. 3D printed stretchable tactile sensors. Adv Mater 2017;29:1701218.
[21] Wu L, Qian J, Peng J, Wang K, Liu Z, Ma T, Zhou Y, Wang G, Ye S. Screen-printed flexible temperature sensor based on FG/CNT/PDMS composite with constant TCR. J Mater Sci Mater Electron 2019;30:9593–601.
[22] Hassan K, Tung TT, Stanley N, Yap PL, Farivar F, Rastin H, Nine MJ, Losic D. Graphene ink for 3D extrusion micro printing of chemo-resistive sensing devices for volatile organic compound detection. Nanoscale 2021;13:5356–68.
[23] Fekiri C, Kim HC, Lee IH. 3D-printable carbon nanotubes-based composite for flexible piezoresistive sensors. Materials 2020;13:5482.
[24] Abshirini M, Charara M, Marashizadeh P, Saha MC, Altan MC, Liu Y. Functional nanocomposites for 3D printing of stretchable and wearable sensors. Appl Nanosci 2019;9:2071–83.
[25] Muth JT, Vogt DM, Truby RL, Mengüç Y, Kolesky DB, Wood RJ, Lewis JA. Embedded 3D printing of strain sensors within highly stretchable elastomers. Adv Mater 2014;26:6307–12.
[26] Saadi M, Maguire A, Pottackal NT, Thakur MSH, Ikram MM, Hart AJ, Ajayan PM, Rahman MM. Direct ink writing: a 3D printing technology for diverse materials. Adv Mater 2022;34:2108855.
[27] Dolganov A, Bishop MT, Chen GZ, Hu D. Rheological study and printability investigation of titania inks for direct ink writing process. Ceram Int 2021;47: 12020–7.
[28] Li S, Lu Z, Zhang H, Ai Z, Ran Y, Li Y, Deng X, Li D. Rheological behavior of multi-sized SiC inks containing polyelectrolyte complexes specifically for direct ink writing. J Eur Ceram Soc 2022;42:4810–6.
[29] Arlington SQ, Barron SC, DeLisio JB, Rodriguez JC, Vummidi Lakshman S, Weihs TP, Fritz GM. Multifunctional reactive nanocomposites via direct ink writing. Adv Mater Technol 2021;6:1–7.
[30] Mantelli A, Romani A, Suriano R, Levi M, Turri S. Direct ink writing of recycled composites with complex shapes: process parameters and ink optimization. Adv Eng Mater 2021;23:2100116.
[31] Qi X, Ha H, Hwang B, Lim S. Printability of the screen-printed strain sensor with carbon black/silver paste for sensitive wearable electronics. Appl Sci 2020;10: 6983.
[32] Loh HA, Graves AR, Stinespring CD, Sierros KA. Direct ink writing of graphene-based solutions for gas sensing. ACS Appl Nano Mater 2019;2:4104–12.
[33] Liang Z, Pei Y, Chen C, Jiang B, Yao Y, Xie H, Jiao M, Chen G, Li T, Yang B. General, vertical, three-dimensional printing of two-dimensional materials with multiscale alignment. ACS Nano 2019;13:12653–61.
[34] Shao Y, Han R, Quan X, Niu K. Study on ink flow of silicone rubber for direct ink writing. J Appl Polym Sci 2021;138:50819.
[35] Kim M, Choi J-W. Rubber ink formulations with high solid content for direct-ink write process. Addit Manuf 2021;44:102023.
[36] Sim K, Rao Z, Ershad F, Yu C. Rubbery electronics fully made of stretchable elastomeric electronic materials. Adv Mater 2020;32:e1902417.
[37] Kurian AS, Souri H, Mohan VB, Bhattacharyya D. Highly stretchable strain sensors based on polypyrrole-silicone rubber composites for human motion detection. Sensors Actuators A 2020;312:112131.
[38] Kim H-J, Sim K, Thukral A, Yu C. Rubbery electronics and sensors from intrinsically stretchable elastomeric composites of semiconductors and conductors. Sci Adv 2017;3:e1701114.
[39] Sánchez-González C-M, Soriano-Peña J-F, Rubio-Avalos J-C, Pacheco-Ibarra J-J. Fabrication of flexible piezoresistive sensors based on RTV-silicone and milled carbon fibers and the temperature´s effect on their electric resistance. Sensors Actuators A 2020;302:111811.
[40] Ma L-F, Bao R-Y, Dou R, Zheng S-D, Liu Z-Y, Zhang R-Y, Yang M-B, Yang W. Conductive thermoplastic vulcanizates (TPVs) based on polypropylene (PP)/ ethylene-propylene-diene rubber (EPDM) blend: from strain sensor to highly stretchable conductor. Compos Sci Technol 2016;128:176–84.
[41] Ke K, McMaster M, Christopherson W, Singer KD, Manas-Zloczower I. Highly sensitive capacitive pressure sensors based on elastomer composites with carbon filler hybrids. Composites, Part A 2019;126:105614.
[42] Zhu B, Ma C, Qian Z, Ren L, Yuan H. Highly stretchable and sensitive multimodal tactile sensor based on conductive rubber composites to monitor pressure and temperature. Polymers 2022;14:1294.
[43] Kumar V, Lee JY, Lee DJ. Synergistic effects of hybrid carbon nanomaterials in room-temperature-vulcanized silicone rubber. Polym Int 2017;66:450–8.
[44] Ke K, Yue L, Shao H, Yang M-B, Yang W, Manas-Zloczower I. Boosting electrical and piezoresistive properties of polymer nanocomposites via hybrid carbon fillers: a review. Carbon 2021;173:1020–40.
[45] Meng Q, Kenelak V, Chand A, Kang H, Han S, Liu T. A highly flexible, electrically conductive, and mechanically robust graphene/epoxy composite film for its self-damage detection. J Appl Polym Sci 2020;137:48991.
[46] Yang H, Gong LH, Zheng Z, Yao XF. Highly stretchable and sensitive conductive rubber composites with tunable piezoresistivity for motion detection and flexible electrodes. Carbon 2020;158:893–903.
[47] Wu J, Fan X, Liu X, Ji X, Shi X, Wu W, Yue Z, Liang J. Highly sensitive temperature-pressure bimodal aerogel with stimulus discriminability for human physiological monitoring. Nano Lett 2022;22:4459–67.
[48] Chen L, Chang X, Wang H, Chen J, Zhu Y. Stretchable and transparent multimodal electronic-skin sensors in detecting strain, temperature, and humidity. Nano Energy 2022;96:107077.
[49] Liu H, Xiang H, Wang Y, Li Z, Qian L, Li P, Ma Y, Zhou H, Huang W. A flexible multimodal sensor that detects strain, humidity, temperature, and pressure with carbon black and reduced graphene oxide hierarchical composite on paper. ACS Appl Mater Interfaces 2019;11:40613–9.
[50] Kim SY, Park S, Park HW, Park DH, Jeong Y, Kim DH. Highly sensitive and multimodal all-carbon skin sensors capable of simultaneously detecting tactile and biological stimuli. Adv Mater 2015;27:4178–85.
[51] Wang Y-F, Sekine T, Takeda Y, Hong J, Yoshida A, Matsui H, Kumaki D, Nishikawa T, Shiba T, Sunaga T. Printed strain sensor with high sensitivity and

wide working range using a novel brittle–stretchable conductive network. ACS Appl Mater Interfaces 2020;12:35282–90.
[52] Sekine T, Abe M, Muraki K, Tachibana S, Wang Y-F, Hong J, Takeda Y, Kumaki D, Tokito S. Microporous induced fully printed pressure sensor for wearable soft robotics machine interfaces. Adv Intell 2020;2:2000179.
[53] Guo Z, Yu P, Liu Y, Zhao J. High-precision resistance strain sensors of multilayer composite structure via direct ink writing: optimized layer flatness and interfacial strength. Compos Sci Technol 2021;201:108530.

3D-printing of conductive inks based flexible tactile sensor for monitoring of temperature, strain and pressure

作者 Ma, C (Ma, Chi) [1] ; Zhu, B (Zhu, Bing) [1] ; Qian, ZH (Qian, Zhihui) [2] ; Ren, L (Ren, Lei) [2] , [3] ; Yuan, HY (Yuan, Hengyi) [2] ; Meng, YH (Meng, Yunhao) [1]

来源出版物 JOURNAL OF MANUFACTURING PROCESSES
卷: 87 页: 1-10
DOI: 10.1016/j.jmapro.2023.01.008

出版时间 FEB 3 2023

在线发表 JAN 2023

已索引 2023-01-12

文献类型 Article

摘要 Flexible multimodal tactile sensors have been widely used in health monitoring devices, flexible smart robots, and human-machine interfaces in intelligent automobiles. In the present work, conductive inks embedded with carbon fillers were optimized to fabricate flexible multimodal tactile sensors by a direct ink writing process. Results showed that rheological properties and printing speed were key factors to print conductive paths with controllable shape and good conductivity. Flexible multimodal tactile sensors were fabricated at different printing speeds, and the effects of printing speed on sensing characteristics were observed. The flexible multi-modal tactile sensors printed with conductive inks exhibited excellent sensitivities for temperature (up to 0.172 degrees C-1), strain (1918.4), and pressure (610.208 kPa(-1)). Furthermore, cyclic loading-unloading tests revealed that the as-fabricated flexible multimodal tactile sensors were reliable and durable. Finally, the application potential of these sensors for multimodal perception was verified by detecting their responses to finger flexion and extension, finger pressing, and hot air flow. The as-designed flexible multimodal tactile sensors manifested excellent potentialities in health monitoring devices, flexible smart robots, and human-machine interfaces in intelligent automobiles.

关键词 **作者关键词:** 3D printed sensor; Flexible tactile sensor; Direct ink writing; Conductive inks; Carbon nanomaterials
Keywords Plus: CARBON; NANOCOMPOSITES; COMPOSITE

作者信息
通讯作者地址: Zhu, Bing (通讯作者)
Jilin Univ, State Key Lab Automot Simulat & Control, Changchun 130025, Peoples R China
所属机构
Jilin University
Jilin University College of Automotive Engineering
Jilin University State Key Laboratory of Automotive Simulation and Control
通讯作者地址: Qian, Zhihui; Ren, Lei (通讯作者)
Jilin Univ, Key Lab Bion Engn, Changchun 130025, Peoples R China
电子邮件地址 :
zhubing@jlu.edu.cn; zhqian@jlu.edu.cn
地址 :
[1] Jilin Univ, State Key Lab Automot Simulat & Control, Changchun 130025, Peoples R China:
所属机构
Jilin University
Jilin University College of Automotive Engineering
Jilin University State Key Laboratory of Automotive Simulation and Control
[2] Jilin Univ, Key Lab Bion Engn, Changchun 130025, Peoples R China:
[3] Univ Manchester, Sch Mech Aerosp & Civil Engn, Manchester M13 9PL, England:
所属机构
University of Manchester
The University of Manchester Faculty of Science and Engineering
The University of Manchester School of Mechanical Aerospace and Civil Engineering
电子邮件地址 :
zhubing@jlu.edu.cn; zhqian@jlu.edu.cn; lei.ren@manchester.ac.uk

类别/分类
研究方向: Engineering
引文主题: 2 Chemistry › 2.114 Organic Semiconductors › 2.114.914 Stretchable Electronics
可持续发展目标: 03 Good Health and Well-being

Web of Science 类别 Engineering, Manufacturing

基金资助

查看资金资助信息

基金资助机构	授权号	隐藏所有详细信息
National Natural Science Foundation of China (NSFC)	52175270	隐藏详情
在来源出版物中显示为: National Natural Science Foundation of China		
Project of Scientific and Technological Development Plan of Jilin Province	20220508130RC	

+ 查看更多数据字段

期刊信息

JOURNAL OF MANUFACTURING PROCESSES

ISSN	1526-6125
eISSN	2212-4616
当前出版商	ELSEVIER SCI LTD, 125 London Wall, London EC2Y 5AS, ENGLAND
目录	Current Contents Connect
期刊影响因子	Journal Citation Reports ™
研究方向	Engineering
Web of Science 类别	Engineering, Manufacturing

6.1
期刊影响因子 ™ (2023)

1.17
Journal Citation Indicator ™ (2023)

引文网络

来自 Web of Science 核心合集

21
被引频次
创建引文跟踪

22
被引频次 所有数据库
+ 查看更多的被引频次

53
篇引用的参考文献
→ 查看相关记录

与同行文献相比，该文献的引用表现如何?

← 打开比较指标面板

数据来自 InCites Benchmarking & Analytics

按分类引用项目

根据可用的引文上下文数据和 10 条引用项目中的摘录，对此文献的提及方式进行细分。

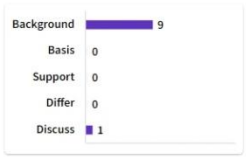

最近被以下文献引用:

Hu, SQ; Zhang, WX; Li, RW; et al.
A Highly Sensitive 3D-Printed Flexible Sensor for Sensing Small Pressures in Deep-Sea High-Pressure Environment
ACS APPLIED MATERIALS & INTERFACES

Kumar, S; Duvedi, RK; Batish, A; et al.
Navigating the frontier: Additive Manufacturing's role in synthesizing piezoelectric materials for flexible electronics
JOURNAL OF THERMOPLASTIC COMPOSITE MATERIALS

全部查看 →

Web of Science 中的使用情况

49
最近 180 天

54
2013 年至今

进一步了解 →

此记录来自:

Web of Science 核心合集

- Science Citation Index Expanded (SCI-Expanded)

证书号第6770657号

发明专利证书

发 明 名 称：一种新型仿生机械的行走机构

发 明 人：苑恒轶;邢进;吕恕位;张庆芳;李琳琳;刘书溢;邓鑫
王涵;赵彤彤;马驰

专 利 号：ZL 2019 1 0245645.4

专利申请日：2019年03月28日

专 利 权 人：吉林工程技术师范学院

地 址：130052 吉林省长春市宽城区凯旋路3050号

授权公告日：2024年03月08日　　授权公告号：CN 109850030 B

国家知识产权局依照中华人民共和国专利法进行审查，决定授予专利权，颁发发明专利证书并在专利登记簿上予以登记。专利权自授权公告之日起生效。专利权期限为二十年，自申请日起算。

专利证书记载专利权登记时的法律状况。专利权的转移、质押、无效、终止、恢复和专利权人的姓名或名称、国籍、地址变更等事项记载在专利登记簿上。

局长
申长雨

国家知识产权局
2024年03月08日

其他事项参见续页

证书号第6770657号

专利权人应当依照专利法及其实施细则规定缴纳年费。本专利的年费应当在每年03月28日前缴纳。未按照规定缴纳年费的，专利权自应当缴纳年费期满之日起终止。

申请日时本专利记载的申请人、发明人信息如下：

申请人：

吉林工程技术师范学院

发明人：

苑恒轶;邢进;吕恕位;张庆芳;李琳琳;刘书溢;邓鑫;王涵;赵彤彤;马驰

证书号第4776455号

发明专利证书

发明名称：一种仿生捕鱼器及其控制方法

发明人：苑恒轶;邢进;张庆芳;李琳琳;伦风艳;宋敏;王宏志;邓鑫
王璐;苑力鑫

专利号：ZL 2019 1 0043907.9

专利申请日：2019年01月17日

专利权人：吉林工程技术师范学院

地址：130000 吉林省长春市凯旋路3050号

授权公告日：2021年11月05日　　授权公告号：CN 109548762 B

国家知识产权局依照中华人民共和国专利法进行审查，决定授予专利权，颁发发明专利证书并在专利登记簿上予以登记。专利权自授权公告之日起生效。专利权期限为二十年，自申请日起算。

专利证书记载专利权登记时的法律状况。专利权的转移、质押、无效、终止、恢复和专利权人的姓名或名称、国籍、地址变更等事项记载在专利登记簿上。

局长
申长雨

国家知识产权局
2021年11月05日

其他事项参见续页

证 书 号 第 4776455 号

国家税务总局北京市海淀区税务局 印花税 代扣专用章 国家知识产权局

专利权人应当依照专利法及其实施细则规定缴纳年费。本专利的年费应当在每年 01 月 17 日前缴纳。未按照规定缴纳年费的，专利权自应当缴纳年费期满之日起终止。

申请日时本专利记载的申请人、发明人信息如下：

申请人：

吉林工程技术师范学院

发明人：

苑恒轶；邢进；张庆芳；李琳琳；伦风艳；宋敏；王宏志；邓鑫；王璐；苑力鑫

证书号第10565852号

实用新型专利证书

实用新型名称：一种可调节的仿生微纳柔性触觉传感器用固定装置

发　明　人：苑恒轶;邢进;于海跃;刘峰;邓俊;付蕙铭;付豪

专　利　号：ZL 2019 2 2165259.2

专利申请日：2019年12月06日

专 利 权 人：吉林工程技术师范学院

地　　址：130052 吉林省长春市宽城区凯旋路3050号

授权公告日：2020年05月22日　　授权公告号：CN 210603358 U

国家知识产权局依照中华人民共和国专利法经过初步审查，决定授予专利权，颁发实用新型专利证书并在专利登记簿上予以登记。专利权自授权公告之日起生效。专利权期限为十年，自申请日起算。

专利证书记载专利权登记时的法律状况。专利权的转移、质押、无效、终止、恢复和专利权人的姓名或名称、国籍、地址变更等事项记载在专利登记簿上。

局长
申长雨

国家知识产权局
2020年05月22日

其他事项参见背面